Bachelor's Thesis

Merger Timescales in Hierarchical Triple Black Hole Systems

Huibert het Lam
Student Number: 3662144
Utrecht University

Supervisors:

Daniel Caputo
Simon Portegies Zwart
Leiden University

Gerard Barkema
Utrecht University

Abstract

We examine the possibility that the three black holes in a hierarchical triple system all merge on a very small timescale with respect to the Hubble time. Hierarchical triples can be seen as an inner binary with a tertiary on a wide orbit around it. We find a formula that approximates the merger time of the inner binary. For certain initial conditions of the triple system this merger time can be strongly accelerated with respect to an isolated binary. This is caused by the Kozai effect: the tertiary induces oscillations in the eccentricity of the orbit of the inner binary. Using the approximation formula we examine the dependence of the Kozai effect on the initial conditions of the triple. When the inner binary merges, the remnant of the merger receives a kick due to conservation of linear momentum. We examine the influence of this kick on the merger time of the outer binary. A formula is derived for the changed merger time due to the kick in the limit that the tertiary is much more massive than the inner masses. We find distributions of the merger time assuming certain distributions for the initial parameters. It is found that it is possible that the merger time of the outer binary strongly decreases. Thus, it is possible that all three masses in a hierarchical triple black hole system merge on a small timescale.

Contents

1 Introduction **4**

2 Theory **6**
2.1 Hamiltonian and Lagrangian Formalism . . . 6
2.1.1 Uniqueness of the Lagrangian . . . 6
2.2 Trigonometric Identities . . . 6
2.3 Two Body System . . . 7
2.3.1 Orbital Elements . . . 7
2.3.2 Anomalies . . . 8
2.4 The Three-Body Hamiltonian . . . 9
2.4.1 Angular Momentum . . . 13
2.5 Secularizing the Hamiltonian . . . 14
2.5.1 Zeroth and First Order . . . 16
2.5.2 Quadrupole Order . . . 17
2.5.3 Octupole Order . . . 21
2.5.4 Secular Hamiltonian . . . 22
2.6 Equations of Motion . . . 22
2.7 Post-Newtonian Terms . . . 25
2.7.1 1PN Correction Term . . . 25
2.7.2 2.5PN Correction Term . . . 27

3 Simulation Equations of Motion **28**
3.1 Examples . . . 30

4 Merger Time Inner Binary **33**
4.1 Merger Time Isolated Binary . . . 33
4.2 Merger Time Inner Binary in Hierarchical Triples . . . 33
4.2.1 Maximum Eccentricity . . . 35
4.2.2 Minimum Eccentricity . . . 36
4.2.3 Approximations . . . 36
4.2.4 Newtonian Kozai Mechanism . . . 39
4.2.5 Gravitational Wave Term . . . 40
4.2.6 Criterion Importance Kozai Mechanism . . . 40
4.2.7 Correction Factor . . . 41
4.2.7.1 Quadrupole Case . . . 41
4.2.7.2 Octupole Case . . . 42
4.2.7.3 Snapshot Time Step Integrator . . . 43
4.3 Dependence Merger Time Inner Binary on the Initial Conditions . . . 44
4.3.1 Initial Inclination . . . 45
4.3.2 Inner Masses . . . 46
4.3.3 Initial Argument of Periastron Inner Binary . . . 46
4.3.4 Mass Tertiary Component . . . 47
4.3.5 Initial Eccentricity Inner Orbit . . . 48
4.3.6 Initial Eccentricity Outer Orbit . . . 48
4.3.7 Mass Space . . . 48

5 Merger Time Outer Binary **50**
5.1 Expressions Changed Semi-Major Axis and Eccentricity . . . 50
5.2 New Merger Time . . . 53
5.2.1 Necessary Velocity Kick for Merger within Time T . . . 55
5.2.2 Change Distribution Merger Times by Kick . . . 56
5.2.2.1 Simulation 1 . . . 59
5.2.2.2 Simulation 2 . . . 61
5.2.2.3 Simulation 3 . . . 61
5.3 Influence of the Kozai Effect on the Velocity Kick . . . 61

6 Discussion **62**
6.1 Assumptions . . . 62
6.2 Future Work . . . 62

7 Conclusion **64**

Bibliography **66**

Appendices **68**

A Derivation Octupole Term Averaged over l_1 **69**

B Octupole Equations of Motion **72**

Chapter 1

Introduction

A black hole is a region in space time where gravity prevents everything, even light, from escaping[1]. Black holes were first considered by John Michell and Piere-Simon Laplace in the 18th century. A few months after Einstein published his general theory of relativity in 1915, Karl Schwarzschild found a solution of the Einstein field equations which described the gravitational field of a point mass and a spherical mass which has neither angular momentum nor charge. This solution appeared to have the features of a black hole: it has a so called event horizon which is situated at the Schwarzschild radius beyond which nothing can escape. It also has a singularity at $r = 0$ and it can be shown that all of the mass of the black hole is in this singularity. This solution is called the Schwarzschild black hole. Everything that comes within the event horizon will be carried into the singularity. In the 1960s solutions were found that describe rotating black holes and, electrically charged and rotating black holes. They have similar features as the Schwarzschild black hole such as an event horizon and a singularity. There has been much discussion whether the solutions which describe black holes are real or rather pathological solutions to Einstein's field equations. By the end of the 1960s the majority of the physicists believed that it is possible to form an event horizon. Once an event horizon is formed, Penrose (1965) proved that a singularity will form somewhere inside the event horizon.

Spherical objects will form a black hole as soon as its radius is smaller than the Schwarzschild radius. When a star does not have enough fuel to maintain its temperature or when it receives too much extra matter, the star can gravitationally collapse, because the star's internal pressure is insufficient to resist its own gravitational force. This collapse can be stopped by the pressure of either electrons or neutrons, but if the mass of the remnant is too large (after the outer layers of the star are blown away by for instance a supernova explosion), even this pressure is not enough to stop the collapse. That happens for remnant masses that are larger than $3 - 4$ M_{Sun}, where M_{Sun} is the solar mass. Such an object will form a black hole. This mechanism is believed to be responsible for solar mass black holes; black holes up to 10^3 M_{Sun} can form this way.

Another mechanism that can cause black hole formation were density perturbations in the early universe. To form a black hole, a very high density is required and the early universe was very dense. A uniform density makes it impossible for mass to bunch up and form black holes, thus the density perturbations are necessary. Different theories predict different sizes of perturbations and black holes up to 10^5 M_{Sun} can be formed this way.

Once a black hole is created it can grow by absorbing matter such as surrounding gas and stars, but also by mergers with other black holes. The latter mechanism is a possibility to create super massive black holes which have masses ranging between 10^5 and 10^9 M_{Sun}.

Black holes may be observed indirectly via different mechanisms. The gas falling into a black hole will form a disk-like structure (accretion disk) because of angular momentum conservation. Due to friction within the disk angular momentum is transported outward, such that matter can fall to the black hole. This releases potential energy by which the temperature of the gas increases. The gas near the black hole can become so hot that it emits enough radiation to be detected by telescopes. Many of the more energetic phenomena in the universe are explained by accretion disks of black holes. The active galactic nuclei are such a phenomena. It is now widely accepted that nearly all galaxies have a super massive black hole at the center (e.g. Richstone et al. (1998)). Another such phenomenon are the X-ray binaries: binaries which are extreme X-ray sources. These systems are believed to be binaries consisting of a compact object such as a black hole and a star companion. The compact object accretes mass from the companion and this causes the X-rays.

If two galaxies merge, the two black holes at the center of these galaxies should form a binary (Begelman et al., 1980). Energy is extracted from such a binary by interactions with the surrounding matter, for instance

[1] Much of the information about black holes is taken from Carroll and Ostlie (2006).

by dynamical friction. This mechanism can be seen as follows. When for instance a star comes near a black hole it will gain momentum and kinetic energy by the gravitational pull of the black hole. Because of conservation of energy and momentum we can conclude that the black hole will slow down and that results in a tighter orbit. A classical work written on this mechanism is Chandrasekhar (1942). Eventually the orbit will become so tight that the orbits of surrounding matter come not close enough for this effect to be significant. In Newtonian mechanics the orbit would now be fixed: the orbital parameters, such as the eccentricity, would be constant. But from the theory of general relativity follows that orbiting masses radiate energy and this causes the orbit to become tighter until the masses merge. The timescale of this process can be much larger than the age of the universe, the Hubble time ($T_{\rm Hubble} \approx 4.35 \cdot 10^{17}$ s). If the timescale of the merger of the black hole binary is larger than the timescale of the merger of galaxies, it is possible that a triple black hole system forms. In this thesis we will consider isolated Schwarzschild black hole triples. In general a triple system is not stable, but if the third black hole, the tertiary, is on an orbit far enough from the orbit of the inner two black holes, this system is stable on timescales much longer than the periods of the separate orbits. These triples are called hierarchical and can be treated as two separate binaries: the inner binary consisting of the inner two black holes and the outer binary consisting of the tertiary and the inner binary. Of course, these binaries influence each other. If the angle between the orbital planes of both binaries is close enough to 90^o, the eccentricity of the inner orbit will oscillate and much larger eccentricities than the initial value can be reached while the semi-major axis does not change. This effect is known as the Kozai effect (Kozai, 1962). Due to this effect the distance between the bodies at periastron oscillates and can become much smaller than the initial value. The rate of radiation of gravitational radiation increases enormous when the distance between the bodies at periastron decreases (Peters, 1964). That causes the inner binary to merge much faster than it would do if it was isolated. The Kozai mechanism in triple black hole systems was first considered by Blaes et al. (2002) and Miller and Hamilton (2002).

Gravitational radiation also carries away linear momentum. Because of conservation of this momentum, the remnant of the merger of the inner binary receives a kick. There have been many calculations of the recoil velocity of this kick (e.g. Bekenstein (1973), Favata et al. (2004) and Lousto et al. (2010)). Due to this kick the orbital parameters of the outer orbit change and this influences its merger time.

The main goal of this thesis is to find if it is possible for all black holes in the triple to merge on a very short timescale with respect to the Hubble time. We divide this in two parts: first, we consider the merger of the inner binary and second, the merger of the outer binary.

For the merger of the inner binary, we consider the acceleration caused by the Kozai mechanism. We will first find expressions to calculate the merger time of the inner binary very fast. Using these expressions we will give a criterion for the importance of the Kozai effect. We will also show the dependence of the Kozai effect on the initial orbital parameters of the triple. The latter has already been done by Thompson (2011), but for stellar masses and only for a few parameters.

For the merger of the outer binary, we will examine the influence of the kick. We will derive expressions for the changed eccentricity and semi-major axis of the outer orbit, and the changed merger time of the outer binary due to the kick. The expression for the merger time only holds for triples in which the mass is dominated by the mass of the tertiary. Using this formula we will examine what merger times can be reached for the outer binary. We will also give distributions of the merger time, where we assume distributions for the initial parameters.

The thesis is organized as follows. In Chapter 2 we shortly discuss the binary system and after that, an extensive derivation is given of the (Newtonian) Hamiltonian equations of motion for a hierarchical triple system. We then consider the relativistic 1PN and 2.5PN corrections to the Newtonian theory. In Chapter 3 we describe the method by which the equations of motion of a triple are integrated. We will also treat two examples of black hole triples and consider the evolution of the orbital parameters of these systems. In Chapter 4 we will examine the influence of the Kozai mechanism on the merger time of the inner binary and in Chapter 5 we will examine the influence of the kick on the merger time of the outer binary. We discuss some of the assumptions made and possibilities for future work in Chapter 6, the discussion. Finally, we conclude in Chapter 7.

Chapter 2

Theory

2.1 Hamiltonian and Lagrangian Formalism

We briefly recall the Hamiltonian and Lagrangian formalism. n parameters $q_1, ..., q_n$ are called generalized coordinates for a system if every particle's position $\mathbf{r}_i$ can be expressed as a function of $q_1, ..., q_n, t$. We call a system holonomic if the number of degrees of freedom is equal tot the number of coordinates that can be independently varied. We define the Lagrangian for a conservative system as $\mathcal{L} = T - U$ where T is the kinetic energy and U is the potential energy of the system. Suppose the system passes through $\mathbf{q}_1$ at time t_1 and through $\mathbf{q}_2$ at time t_2 and it follows a path $\mathbf{q}(t)$ in the meantime. We define the action integral as $S = \int_{t_1}^{t_2} \mathcal{L}(\mathbf{q}(t), \dot{\mathbf{q}}(t), t)dt$. For a conservative, holonomic system, Newton's second law is equivalent to Hamilton's principle: the system follows the path $\mathbf{q}(t)$ such that the action integral S is stationary. This principle is in turn equivalent to the Lagrange equations: the system follows the path $\mathbf{q}(t)$ such that $\frac{\partial \mathcal{L}}{\partial q_i} = \frac{d}{dt}\frac{\partial \mathcal{L}}{\partial \dot{q}_i}$. We now define the general momentum as $p_i = \frac{\partial \mathcal{L}}{\partial \dot{q}_i}$ and the Hamiltonian as $\mathcal{H} = \mathbf{p} \cdot \mathbf{q} - \mathcal{L}$. For a Hamiltonian that is independent of the time, $\mathcal{H} = T + U$. The Lagrangian equations are equivalent to the Hamiltonian equations: a system follows a path $\mathbf{q}(t)$ such that: $\dot{q}_i = \frac{\partial \mathcal{H}}{\partial p_i}$ and $\dot{p}_i = -\frac{\partial \mathcal{H}}{\partial q_i}$.

2.1.1 Uniqueness of the Lagrangian

Although we introduced the Lagrangian as $\mathcal{L} = T - U$, there is a more general definition: a Lagrangian for a system is a function $\mathcal{L}$ such that the correct path $\mathbf{q}(t)$ follows from Hamilton's principle. Hence we can show that a function $\mathcal{L}' = \mathcal{L} + \frac{d}{dt}G(\mathbf{q}, \dot{\mathbf{q}}, t)$ is also a Lagrangian for a system. Indeed $S' = S + \int_{t_1}^{t_2} \frac{d}{dt}G(\mathbf{q}, \dot{\mathbf{q}}, t)dt = S + G(\mathbf{q}_2, \dot{\mathbf{q}}_2, t_2) - G(\mathbf{q}_1, \dot{\mathbf{q}}_1, t_1)$ and the paths for which an action integral is stationary do not change if we add a constant to S.

2.2 Trigonometric Identities

We recall here a few trigonometric identities that we will use a lot. These are valid for all values of α and β.

$$-\cos(\pi - \alpha) = \cos(\alpha) = \sin(\pi/2 - \alpha) \quad \text{(T.1)}$$

$$\sin(\pi - \alpha) = \sin(\alpha) = \cos(\pi/2 - \alpha) \quad \text{(T.2)}$$

$$\sin^2(\alpha) + \cos^2(\alpha) = 1 \quad \text{(T.3)}$$

$$\cos(2\alpha) = \cos^2(\alpha) - \sin^2(\alpha) \quad \text{(T.4)}$$

$$\cos(2\alpha) = 2\cos^2(\alpha) - 1 \quad \text{(T.5)}$$

$$\cos(2\alpha) = 1 - 2\sin^2(\alpha) \quad \text{(T.6)}$$

$$\sin(2\alpha) = 2\sin(\alpha)\cos(\alpha) \quad \text{(T.7)}$$

$$\cos(\alpha + \beta) = \cos(\alpha)\cos(\beta) - \sin(\alpha)\sin(\beta) \quad \text{(T.8)}$$

$$\sin(\alpha + \beta) = \cos(\alpha)\sin(\beta) + \sin(\alpha)\cos(\beta) \quad \text{(T.9)}$$

$$\cos(\alpha - \beta) = \sin(\alpha)\sin(\beta) + \cos(\alpha)\cos(\beta) \quad \text{(T.10)}$$

$$\sin(\alpha - \beta) = \sin(\alpha)\cos(\beta) - \cos(\alpha)\sin(\beta) \quad \text{(T.11)}$$

2.3 Two Body System

We will recall some basic facts of the two body system consisting of masses m_1 and m_2 in which gravity is the only force. The two masses move in a fixed plane which is called the orbital plane. There are no external forces, hence the center of mass frame is inertial; we will use this as our reference frame. The system is described by a vector $\mathbf{r}$ pointing from one mass toward the other. If we fix an x-as in the orbital plane, the following relation holds for the length of $\mathbf{r}$:

$$r = \frac{G^2(m_1+m_2)}{G_N m_1^2 m_2^2(1+e\cos(f-\delta))}, \tag{2.12}$$

where f is the true anomaly, the angle that $\mathbf{r}$ makes with the x-axis. G_N is the gravitational constant, $G = \mu r_0^2 \dot{f}_0$ is the angular momentum which is determined by the initial values of r and $\dot{f}$, and $\mu = \frac{m_1 m_2}{m_1+m_2}$, e is the eccentricity and δ is the constant that determines the position for $f = 0$. Using the fact that $G = \mu r^2 \dot{f}$, the motion is determined. Eq. 2.12 corresponds to three possible orbits: an ellipse, a parabola or a hyperbola. We will focus on the ellipse, because that orbit corresponds to a bound system.

An ellipse is described by the semi-major axis a and the eccentricity $e = \sqrt{1-\left(\frac{b}{a}\right)^2}$, where b is the semi-minor axis. The distance between a focus, F_1 or F_2, and the center is ea. The position of the mass is given by the true anomaly. The ellipse can be parametrized by

$$\begin{aligned} x &= a\cos(f-\delta); \\ y &= b\sin(f-\delta). \end{aligned} \tag{2.13}$$

If the orbit is an ellipse, we can write Eq. 2.12 as

$$r = \frac{a(1-e^2)}{1+e\cos(f-\delta)}. \tag{2.14}$$

The position with largest r, $r = a(1+e)$, is called the apastron, the position with smallest r, $r = a(1-e)$, is called the periastron. We will henceforth use the direction of the periastron as x-axis, hence $\delta = 0$.

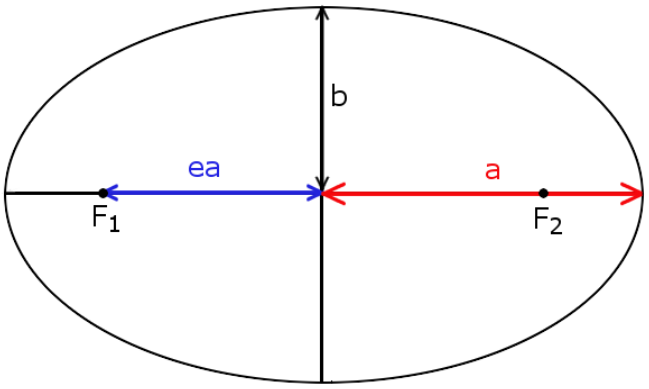

Figure 2.1: Ellipse with eccentricity e, semi-major axis a, semi-minor axis b, and foci F_1 and F_2.

The angular momentum can be expressed as

$$G = \frac{m_1 m_2}{\sqrt{m_1+m_2}}\sqrt{G_N a(1-e^2)}. \tag{2.15}$$

The energy is given by

$$E = \frac{1}{2}\mu r^2\dot{r}^2 - \frac{\gamma}{r} + \frac{G^2}{2\mu r^2} = \frac{\gamma^2\mu(e^2-1)}{2G^2} = -\frac{\gamma}{2a}, \tag{2.16}$$

where $\gamma = G_N m_1 m_2$. The second and third expressions in Eq. 2.16 follow from the first one by evaluating the energy at periastron.

2.3.1 Orbital Elements

Sometimes the system is described with respect to a reference plane. Natural elements in that case are the Keplerian elements; see Fig. 2.2 for an illustration of these elements. In the reference plane, a reference direction is specified which is called the Y-axis. The center of the orbit is C. The first two Keplerian elements are the already known eccentricity e and semi-major axis a which define the shape of the orbit. The point in the orbit in which the body moves upward through the plane of reference is called the ascending node. At this point the third element, the inclination i, is measured; this is the angle that the reference plane makes with the orbital plane. Thus, this is a value between 0 and π. The angle between the intersection of the orbital plane and plane of reference, and the reference direction is the longitude of ascending node h. The angle between the vector that points from C toward the periastron and the vector that points from C toward the ascending node is called the argument of periastron g. And the final Keplerian element is the mean anomaly l, which specifies the position of the masses in the orbit.

There is a bijection between l and f, the true anomaly. We will explain what l is and find the relation between l and f in the following section. As can be seen in Fig. 2.2, all the angles are measured counterclockwise. The six elements e, a, i, h, g and l uniquely define the system, this corresponds to the six degrees of freedom this system has.

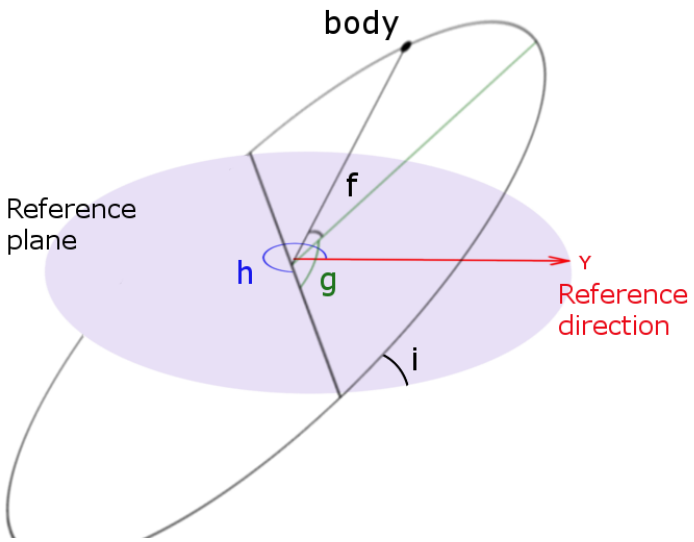

Figure 2.2: Keplerian elements. This figure is strongly based on `http://en.wikipedia.org/wiki/File:Orbit1.svg`.

2.3.2 Anomalies

Instead of the true anomaly, the eccentric anomaly E and the mean anomaly l can be used to describe the position of the mass. Relations between these anomalies, that will be used in Sec. 2.5, will be derived in this section. Fig. 2.3 is used as illustration for the true and eccentric anomaly. In this figure the ellipse is given with the position of the particle $P(x, y)$. Furthermore, the auxiliary circle (the circle with radius a and same center C, as the ellipse) and the minor circle (the circle with radius $b = a\sqrt{1-e^2}$ centered on C) are drawn. E can be found in the following way. Draw a line perpendicular to the major axis of the ellipse, through $P(x, y)$. Call the intersection of this line with the auxiliary circle P'. Then E is the angle between the radius of that circle passing through P', and the major axis of the ellipse. Using the trigonometric relations from section 2.2, one can find a relation between E and f. If we apply Pythagoras' theorem to the triangle in Fig. 2.3 with r as hypothenusa, we find that

$$\begin{aligned} r^2 &= b^2\sin^2(E) + (ae - a\cos(E))^2 \\ &= b^2\sin^2(E) + a^2e^2 + a^2\cos^2(E) - 2a^2e\cos(E). \end{aligned} \tag{2.17}$$

Using $b^2 = a^2(1-e^2)$ it follows that

$$\begin{aligned} r^2 &= a^2(1-e^2)(1-\cos^2(E)) + a^2e^2 + a^2\cos^2(E) - 2a^2e\cos(E) \\ &= a^2 - a^2e^2\cos^2(E) - 2a^2e\cos(E) \\ &= a^2(1-e\cos(E))^2. \end{aligned} \tag{2.18}$$

From Fig. 2.3 and Eq. 2.18 follows that

$$\cos(E) = \frac{x}{a} = \frac{ae - r\cos(\pi - f)}{a} = \frac{ae + r\cos(f)}{a} = e + (1 - e\cos(E))\cos(f), \tag{2.19}$$

hence

$$\cos(E) = \frac{e + \cos(f)}{1 + e\cos(f)}. \tag{2.20}$$

Inverting this relation, we find that

$$\cos(f) = \frac{e - \cos(E)}{e\cos(E) - 1}. \tag{2.21}$$

The derivative of the eccentric anomaly with respect to the true anomaly is:

$$\begin{aligned} \frac{dE}{df} &= \frac{-1}{\sqrt{1 - \left(\frac{e+\cos(f)}{1+e\cos(f)}\right)^2}} \frac{-(1+e\cos(f))\sin(f) + e\,(e+\cos(f))\sin(f)}{(1+e\cos(f))^2} \\ &= \frac{-(1+e\cos(f))}{\sqrt{(1-e^2)(1-\cos^2(f))}} \frac{(e^2-1)\sin(f)}{(1+e\cos(f))^2} = \frac{1}{\sqrt{1-e^2}}\frac{r}{a}, \end{aligned} \tag{2.22}$$

where we used Eq. 2.14.

The mean anomaly l relates position and time and is based on Kepler's second law: equal areas, defined by a line joining the particle and the focus, are swept in equal intervals of time. l is given by the formula:

$$l = \sqrt{\frac{G_N(m_1+m_2)}{a^3}}t, \tag{2.23}$$

where t is the time since the last periastron passage. It follows from Eq. 2.23 and Kepler's third law that l increases monotonically from 0 to 2π. Kepler's third law is an expression for the period T of an orbit:

$$T = \sqrt{\frac{4\pi^2 a^3}{G_N(m_1+m_2)}}. \tag{2.24}$$

From this relation follows that

$$\sqrt{\frac{G_N(m_1+m_2)}{a^3}} = \frac{2\pi}{T}, \tag{2.25}$$

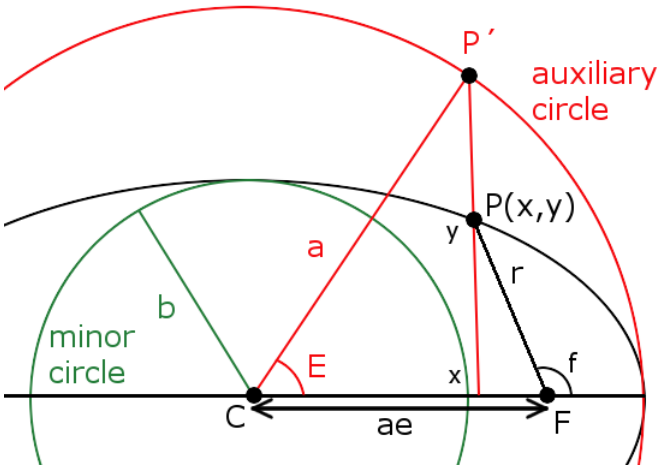

Figure 2.3: Ellipse with position of the mass $P(x, y)$, the semi-major axis a, the semi-minor axis b, the true anomaly f and the eccentric anomaly E. Also drawn are the auxiliary and minor circle, circles which have the same center as the ellipse C, and have radii a and b respectively.

such that $l = \frac{2\pi}{T}t$. One can derive a relation between l and E by calculating the time t, it takes to reach true anomaly f: $t = \int_0^t dt'$. Using $\dot{f} = \frac{G}{\mu r^2}$ we find that

$$t = \int_0^f \frac{\mu r^2}{G} df' \tag{2.26}$$

(r is a function of f). From Eq. 2.18 we find that

$$r = a(1 - e\cos(E)). \tag{2.27}$$

With this relation, Eq. 2.26 and the inverse of Eq. 2.22, one obtains

$$t = \int_0^E \frac{\mu a r}{G}\sqrt{1-e^2}dE' = \int_0^E \frac{\mu a^2}{G}\sqrt{1-e^2}(1-e\cos(E'))dE' = \frac{\mu a^2}{G}\sqrt{1-e^2}(E - e\sin(E)). \tag{2.28}$$

Substituting this in Eq. 2.23 and using Eq. 2.15 one finds that

$$l = \sqrt{\frac{G_N(m_1+m_2)}{a^3}}\frac{\mu a^2}{G}\sqrt{1-e^2}(E - e\sin(E)) = E - e\sin(E). \tag{2.29}$$

If we combine this relation with Eq. 2.21 we have found the bijection between l and f.

We will also use the derivative of the mean anomaly with respect to the eccentric anomaly which is equal to:

$$\frac{dl}{dE} = 1 - e\cos(E). \tag{2.30}$$

Using Eqs. 2.20, 2.22, 2.30 and 2.14 with $\delta = 0$, and the chain rule for differentiation, we are able to find the derivative of l with respect to f:

$$\frac{dl}{df} = \frac{dl}{dE}\frac{dE}{df} = \left(1 - e\frac{e+\cos(f)}{1+e\cos(f)}\right)\frac{1}{\sqrt{1-e^2}}\frac{r}{a} = \frac{1-e^2}{1+e\cos(f)}\frac{1}{\sqrt{1-e^2}}\frac{r}{a} = \frac{1}{\sqrt{1-e^2}}\left(\frac{r}{a}\right)^2. \tag{2.31}$$

2.4 The Three-Body Hamiltonian

In the following, we will derive the Hamiltonian for a system that consists of three masses (m_1, m_2 and m_3) in which the only force considered is gravity. As before, since there are no external forces, the center of mass frame is inertial, so we take this as our reference frame. In Cartesian coordinates the Hamiltonian is:

$$\mathcal{H} = \frac{1}{2}m_1{\dot{\mathbf{r}}_1}^2 + \frac{1}{2}m_2{\dot{\mathbf{r}}_2}^2 + \frac{1}{2}m_3{\dot{\mathbf{r}}_3}^2 - \frac{G_N m_1 m_2}{|\mathbf{r}_2 - \mathbf{r}_1|} - \frac{G_N m_1 m_3}{|\mathbf{r}_3 - \mathbf{r}_1|} - \frac{G_N m_2 m_3}{|\mathbf{r}_3 - \mathbf{r}_2|}, \tag{2.32}$$

where $\mathbf{r}_i$ and $\dot{\mathbf{r}}_i$ are the position and velocity of mass i . We now introduce three new coordinates: 1) $\mathbf{r} = \mathbf{r}_2 - \mathbf{r}_1$, the vector which points from m_1 toward m_2, 2) $\mathbf{R} = \frac{m_1\mathbf{r}_1 + m_2\mathbf{r}_2}{M}$ where $M = m_1 + m_2$, the position vector of the center of mass of m_1 and m_2 and 3) $\mathbf{r}' = \mathbf{r}_3 - \mathbf{R}$, the vector which points from $\mathbf{R}$ toward m_3. These are the Jacobian coordinates. We find that

$$\begin{aligned} \mathbf{r}_1 &= \mathbf{R} - \frac{m_2}{M}\mathbf{r}; \\ \mathbf{r}_2 &= \mathbf{R} + \frac{m_1}{M}\mathbf{r}; \\ \mathbf{r}_3 &= \mathbf{R} + \mathbf{r}'. \end{aligned} \tag{2.33}$$

In our reference frame the position vector of the center of mass is zero:

$$\frac{m_1\mathbf{r}_1 + m_2\mathbf{r}_2 + m_3\mathbf{r}_3}{M_\mathrm{t}} = \mathbf{0}, \tag{2.34}$$

where $M_\mathrm{t} = \sum_{i=1}^{3} m_i$. Using this, we find that $\mathbf{R} = \frac{m_1\mathbf{r}_1 + m_2\mathbf{r}_2}{M} = \frac{m_1\mathbf{r}_1 + m_2\mathbf{r}_2}{M_\mathrm{t}}\frac{M_t}{M} = -\frac{m_3\mathbf{r}_3}{M}$. Substituting this in our equation for $\mathbf{r}'$ yields: $\mathbf{r}' = \mathbf{r}_3(1 + \frac{m_3}{M})$, or $\mathbf{r}_3 = \frac{1}{1+\frac{m_3}{M}}\mathbf{r}' = \frac{M}{M_\mathrm{t}}\mathbf{r}'$. In the same way, we find that

$$\begin{aligned} \mathbf{r}_1 &= -\frac{m_3}{M_\mathrm{t}}\mathbf{r}' - \frac{m_2}{M}\mathbf{r}; \\ \mathbf{r}_2 &= -\frac{m_3}{M_\mathrm{t}}\mathbf{r}' + \frac{m_1}{M}\mathbf{r}; \\ \mathbf{r}_3 &= \frac{M}{M_\mathrm{t}}\mathbf{r}'. \end{aligned} \tag{2.35}$$

In these new coordinates Eq. 2.32 becomes:

$$\begin{aligned} \mathcal{H} &= \frac{1}{2}m_1\left(-\frac{m_3}{M_\mathrm{t}}\dot{\mathbf{r}}' - \frac{m_2}{M}\dot{\mathbf{r}}\right)^2 + \frac{1}{2}m_2\left(-\frac{m_3}{M_\mathrm{t}}\dot{\mathbf{r}}' + \frac{m_1}{M}\dot{\mathbf{r}}\right)^2 + \frac{1}{2}m_3\left(\frac{M}{M_\mathrm{t}}\dot{\mathbf{r}}'\right)^2 \\ &\quad -\frac{G_N m_1 m_2}{|\mathbf{r}|} - \frac{G_N m_1 m_3}{|\frac{m_2}{M}\mathbf{r} + (\frac{m_3}{M_\mathrm{t}} + \frac{M}{M_\mathrm{t}})\mathbf{r}'|} - \frac{G_N m_2 m_3}{|-\frac{m_1}{M}\mathbf{r} + (\frac{m_3}{M_\mathrm{t}} + \frac{M}{M_\mathrm{t}})\mathbf{r}'|} \\ &= \frac{1}{2}\frac{(m_1+m_2)m_3^2 + m_3M^2}{M_\mathrm{t}^2}\dot{\mathbf{r}}'^2 + \frac{1}{2}\frac{m_1m_2^2 + m_2m_1^2}{M^2}\dot{\mathbf{r}}^2 - \frac{G_N m_1 m_2}{|\mathbf{r}|} - \frac{G_N m_1 m_3}{|\frac{m_2}{M}\mathbf{r} + \mathbf{r}'|} - \frac{G_N m_2 m_3}{|-\frac{m_1}{M}\mathbf{r} + \mathbf{r}'|}. \end{aligned} \tag{2.36}$$

If we consider two arbitrary vectors $\mathbf{A}$ and $\mathbf{B}$ with an angle Φ between them, we can use the law of cosines (see Fig. 2.4 for an illustration) and apply a Taylor approximation to obtain

$$\begin{aligned} \frac{1}{|\mathbf{A} - \mathbf{B}|} &= \frac{1}{\sqrt{A^2 + B^2 - 2AB\cos(\Phi)}} = \frac{1}{A\sqrt{1 + \left(\frac{B}{A}\right)^2 - 2\left(\frac{B}{A}\right)\cos(\Phi)}} \\ &= \frac{1}{A}(1 - \frac{1}{2}\cdot -2\cos(\Phi)\frac{B}{A} + \frac{1}{2}\cdot -\frac{1}{2}\cdot(2 - 6\cos^2(\Phi))\left(\frac{B}{A}\right)^2 + ...) \\ &= \frac{1}{A} + \cos(\Phi)\frac{B}{A^2} + \frac{1}{2}(3\cos^2(\Phi) - 1))\frac{B^2}{A^3} + ... \\ &= \sum_{j=0}^{\infty}\frac{B^j}{A^{j+1}}P_j(\cos(\Phi)), \end{aligned} \tag{2.37}$$

where P_j are the Legendre polynomials and A, B are the lengths of $\mathbf{A}$ and $\mathbf{B}$ respectively. Applying this formula twice to Eq. 2.36 yields:

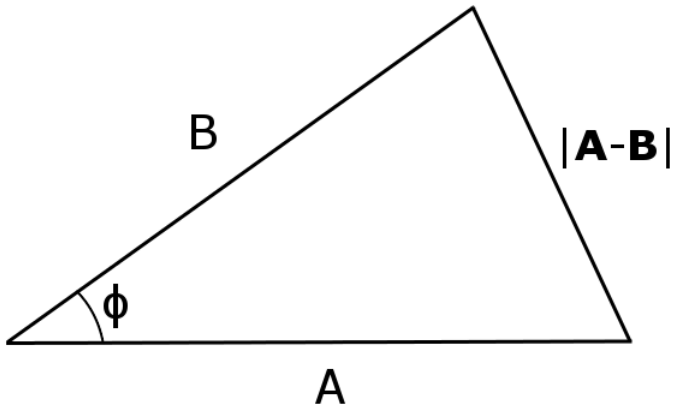

Figure 2.4: Law of cosines: $|\mathbf{A}-\mathbf{B}|^2 = A^2 + B^2 - 2AB\cos(\Phi)$.

$$
\begin{aligned}
\mathcal{H} &= \frac{1}{2}\frac{m_3(m_1+m_2)}{M_\mathrm{t}}\dot{\mathbf{r}}'^2 + \frac{1}{2}\frac{m_1 m_2}{M}\dot{\mathbf{r}}^2 - \frac{G_N m_1 m_2}{r} \\
&\quad - \sum_{j=0}^{\infty} \frac{G_N m_1 m_3 (-\frac{m_2}{M} r)^j}{r'^{j+1}} P_j(\cos(\Phi)) - \sum_{j=0}^{\infty} \frac{G_N m_2 m_3 (\frac{m_1}{M} r)^j}{r'^{j+1}} P_j(\cos(\Phi)) \\
&= \frac{1}{2} m_3 \frac{M}{M_\mathrm{t}}\dot{\mathbf{r}}'^2 + \frac{1}{2}\frac{m_1 m_2}{M}\dot{\mathbf{r}}^2 - \frac{G_N m_1 m_2}{r} - \frac{G_N (m_1+m_2) m_3}{r'} \\
&\quad - \frac{G_N}{r'} \sum_{j=2}^{\infty} \frac{m_3 m_2 (\frac{m_1}{M} r)^j + m_3 m_1 (-\frac{m_2}{M} r)^j}{r'^j} P_j(\cos(\Phi)).
\end{aligned}
\tag{2.38}
$$

To make this Hamiltonian more clear, we have to introduce another transformation of variables. We know from Sec. 2.3 that the coordinates of the 2 masses in a Keplerian orbit can be described by a vector $\mathbf{r}$. The differential equations that describe such a system are continuous differentiable for $\mathbf{r} \neq \mathbf{0}$ and therefore it follows from the theory of differential equations that for every set of initial conditions $(\mathbf{r}(t_0), \dot{\mathbf{r}}(t_0))$ (for $\mathbf{r}(t_0) \neq \mathbf{0}$) there exists one and only one solution. We know that that is a conic section. In Sec. 2.3.1 we defined the orbital elements to describe such a system and that is the transformation we will use for $(\mathbf{r}, \dot{\mathbf{r}})$ and $(\mathbf{r}', \dot{\mathbf{r}}')$. The Hamiltonian, Eq. 2.38, can then be interpreted as the Hamiltonian of two isolated binary systems. The inner binary has point masses m_1 and m_2 and the outer binary has point masses $m_1 + m_2$ and m_3. The summation in Eq. 2.38 consists of perturbation terms to the Keplerian orbits of both binaries. We will use subscript 1 and 2 for the orbital variables of the orbit of the inner and outer binary respectively.

The first and the fourth terms in Eq. 2.38 are the energy of the outer binary and with Eq. 2.16, this energy is equal to $-\frac{G_N M m_3}{2a_2}$. The same can be done for the second and third terms of Eq. 2.38. Therefore, we can write the Hamiltonian, Eq. 2.38, in the following way:

$$
\mathcal{H} = -\frac{G_N m_3 M}{2a_2} - \frac{G_N m_1 m_2}{2a_1} - \frac{G_N}{r'} \sum_{j=2}^{\infty} M_j \rho^j P_j(\cos(\Phi)),
\tag{2.39}
$$

where $M_j = m_3 m_2 (\frac{m_1}{M})^j + m_3 m_1 (-\frac{m_2}{M})^j = m_1 m_2 m_3 \frac{m_1^{j-1} - (-m_2)^{j-1}}{M^j}$ and $\rho = \frac{r}{r'}$. ρ, r' and Φ should be read as functions of e_j, a_j, i_j, l_j, h_j and g_j for $j = 1, 2$. The problem with this transformation is that both $\mathbf{r}$ and $\mathbf{r}'$, and $\dot{\mathbf{r}}$ and $\dot{\mathbf{r}}'$ are transformed. Therefore, it is not obvious that we will find the equations of motion for the system if we apply Hamilton's equations to this Hamiltonian. In particular, for this coordinate system we will not find them. A transformation where the Hamiltonian equations still hold after transforming is a so called canonical transformation. Such a transformation is given by the additional change to Delaunay's elements: l_j, g_j, and h_j stay the same, but we transform a_j, e_j and i_j into:

$$
\begin{aligned}
L_1 &= \frac{m_1 m_2}{M}\sqrt{G_N M a_1};\\
L_2 &= \frac{m_3(m_1+m_2)}{M_\mathrm{t}}\sqrt{G_N M_\mathrm{t} a_2};\\
G_j &= L_j\sqrt{1-e_j^2};\\
H_j &= G_j\cos(i_j).
\end{aligned}
\tag{2.40}
$$

A derivation of Delaunay's elements can be found in Valtonen and Karttunen (2006). Note that G_j is the angular momentum of orbit j. If we can write the three-body Hamiltonian only with these variables, we are able to formulate the equations of motion for our problem.

Consider the Hamiltonian, Eq. 2.39. Since we will be interested in systems where $\rho = \frac{r}{r'} \ll 1$, we only take the first three powers of ρ, such that

$$
\begin{aligned}
\mathcal{H} &= -\frac{G_N m_3 M}{2a_2} - \frac{G_N m_1 m_2}{2a_1} - \frac{G_N}{r'}M_2\rho^2 P_2(\cos(\Phi)) - \frac{G_N}{r'}M_3\rho^3 P_3(\cos(\Phi))\\
&= -\frac{G_N m_1 m_2}{2a_1} - \frac{G_N m_3 M}{2a_2} - \frac{1}{2}G_N M_2\frac{a_1^2}{a_2^3}\left(\frac{r_1}{a_1}\right)^2\left(\frac{a_2}{r'}\right)^3(3\cos^2(\Phi)-1)\\
&\quad -\frac{1}{2}G_N M_3\frac{a_1^3}{a_2^4}\left(\frac{r_1}{a_1}\right)^3\left(\frac{a_2}{r'}\right)^4(5\cos^3(\Phi)-3\cos(\Phi)).
\end{aligned}
\tag{2.41}
$$

To write this Hamiltonian in the new coordinates, we use the expression for the radius from the two-body problem, Eq. 2.14, with $\delta = 0$: $r = \frac{a_1(1-e_1^2)}{1+e_1\cos(f_1)}$ and $r' = \frac{a_2(1-e_2^2)}{1+e_2\cos(f_2)}$. We will also derive an expression for $\cos(\Phi)$ in i_j, f_j, g_j and h_j. f_j should be read as function of l_j via Eqs. 2.21 and 2.29, and the other coordinates not part of Delaunay's elements are transformed using the relations in 2.40.

To find an expression for $\cos(\Phi) = \frac{\mathbf{r}\cdot\mathbf{r}'}{rr'}$ we will first derive an expression for $\mathbf{r}$ and $\mathbf{r}'$ in the new variables. Let $\mathbf{r}_\mathrm{o} = r(\cos(f), \sin(f), 0)$ be a vector in an orbital coordinate system (x,y,z) and $\mathbf{r}_\mathrm{inv}$ the same vector in an invariant coordinate system (X,Y,Z). It follows from Fig. 2.2 that we can express $\mathbf{r}_\mathrm{inv}$ in $\mathbf{r}_\mathrm{o}$ by executing the following method. Rotate $\mathbf{r}_\mathrm{o}$ around the the z-axis by an angle g. Next, rotate around the X-axis by an angle i, and finally, rotate around the Z-axis by an angle h. So if we write $R_k(\alpha)$ for the rotation of angle α around axis k and use the sum formulas from Sec. 2.2, we find that

$$
\begin{aligned}
\mathbf{r}_\mathrm{inv} &= R_Z(h)R_X(i)R_z(g)\mathbf{r}_o\\
&= R_Z(h)R_X(i)r\begin{pmatrix}\cos(g) & -\sin(g) & 0\\ \sin(g) & \cos(g) & 0\\ 0 & 0 & 1\end{pmatrix}\begin{pmatrix}\cos(f)\\ \sin(f)\\ 0\end{pmatrix}\\
&= R_Z(h)R_X(i)r\begin{pmatrix}\cos(f)\cos(g)-\sin(f)\sin(g)\\ \cos(f)\sin(g)+\sin(f)\cos(g)\\ 0\end{pmatrix}\\
&= R_Z(h)r\begin{pmatrix}1 & 0 & 0\\ 0 & \cos(i) & -\sin(i)\\ 0 & \sin(i) & \cos(i)\end{pmatrix}\begin{pmatrix}\cos(f+g)\\ \sin(f+g)\\ 0\end{pmatrix}\\
&= r\begin{pmatrix}\cos(h) & -\sin(h) & 0\\ \sin(h) & \cos(h) & 0\\ 0 & 0 & 1\end{pmatrix}\begin{pmatrix}\cos(f+g)\\ \cos(i)\sin(f+g)\\ \sin(i)\sin(f+g)\end{pmatrix}\\
&= r\begin{pmatrix}\cos(h)\cos(f+g)-\sin(h)\cos(i)\sin(f+g)\\ \sin(h)\cos(f+g)+\cos(h)\cos(i)\sin(f+g)\\ \sin(i)\sin(f+g)\end{pmatrix}.
\end{aligned}
\tag{2.42}
$$

Applying Eq. 2.42 to $\mathbf{r}$ and $\mathbf{r}'$ and using the relations from Sec. 2.2, we calculate:

$$
\begin{aligned}
\cos(\Phi) &= \frac{\mathbf{r}\cdot\mathbf{r}'}{rr'} \\
&= \big[\cos(h_1)\cos(f_1+g_1)-\sin(h_1)\cos(i_1)\sin(f_1+g_1)\big]\big[\cos(h_2)\cos(f_2+g_2)-\sin(h_2)\cos(i_2)\sin(f_2+g_2)\big] \\
&\quad +\big[\sin(h_1)\cos(f_1+g_1)+\cos(h_1)\cos(i_1)\sin(f_1+g_1)\big]\big[\sin(h_2)\cos(f_2+g_2)+\cos(h_2)\cos(i_2)\sin(f_2+g_2)\big] \\
&\quad +\sin(i_1)\sin(f_1+g_1)\sin(i_2)\sin(f_2+g_2) \\
&= \big[\cos(f_1+g_1)\cos(f_2+g_2)+\sin(f_1+g_1)\sin(f_2+g_2)\cos(i_1)\cos(i_2)\big]\big[\sin(h_1)\sin(h_2)+\cos(h_1)\cos(h_2)\big] \\
&\quad +\big[\cos(f_1+g_1)\sin(f_2+g_2)\cos(i_2)-\sin(f_1+g_1)\cos(f_2+g_2)\cos(i_1)\big]\big[\sin(h_1)\cos(h_2)-\cos(h_1)\sin(h_2)\big] \\
&\quad +\sin(i_1)\sin(f_1+g_1)\sin(i_2)\sin(f_2+g_2) \\
&= \big[\cos(f_1+g_1)\cos(f_2+g_2)+\sin(f_1+g_1)\sin(f_2+g_2)\cos(i_1)\cos(i_2)\big]\cos(h_1-h_2) \\
&\quad +\big[\cos(f_1+g_1)\sin(f_2+g_2)\cos(i_2)-\sin(f_1+g_1)\cos(f_2+g_2)\cos(i_1)\big]\sin(h_1-h_2) \\
&\quad +\sin(i_1)\sin(f_1+g_1)\sin(i_2)\sin(f_2+g_2).
\end{aligned} \tag{2.43}
$$

2.4.1 Angular Momentum

Because we assume there is no external torque, the total angular momentum is conserved. We take the plane through the center of mass and perpendicular to the angular momentum as reference plane. As is commonly known, the angular momentum is equal to

$$
\begin{aligned}
\mathbf{L} &= m_1\mathbf{r}_1\times\dot{\mathbf{r}}_1+m_2\mathbf{r}_2\times\dot{\mathbf{r}}_2+m_3\mathbf{r}_3\times\dot{\mathbf{r}}_3 \\
&= m_1(-\frac{m_3}{M_\mathrm{t}}\mathbf{r}'-\frac{m_2}{M}\mathbf{r})\times(-\frac{m_3}{M_\mathrm{t}}\dot{\mathbf{r}}'-\frac{m_2}{M}\dot{\mathbf{r}})+m_2(-\frac{m_3}{M_\mathrm{t}}\mathbf{r}'+\frac{m_1}{M}\mathbf{r})\times(-\frac{m_3}{M_\mathrm{t}}\dot{\mathbf{r}}'+\frac{m_1}{M}\dot{\mathbf{r}})+m_3\frac{M}{M_\mathrm{t}}\mathbf{r}'\times\frac{M}{M_\mathrm{t}}\dot{\mathbf{r}}' \\
&= \frac{m_3M}{M_\mathrm{t}}\mathbf{r}'\times\dot{\mathbf{r}}'+\frac{m_1m_2}{M}\mathbf{r}\times\dot{\mathbf{r}} \\
&= \frac{m_3M}{M_\mathrm{t}}r'^2\widehat{\mathbf{r}}'\times\dot{\widehat{\mathbf{r}}}'+\frac{m_1m_2}{M}r^2\widehat{\mathbf{r}}\times\dot{\widehat{\mathbf{r}}},
\end{aligned} \tag{2.44}
$$

where we used $\mathbf{r}\times\dot{\mathbf{r}}=r\widehat{\mathbf{r}}\times(\dot{r}\widehat{\mathbf{r}}+r\dot{\widehat{\mathbf{r}}})=r^2\widehat{\mathbf{r}}\times\dot{\widehat{\mathbf{r}}}$ and Eqs. 2.35. We find that $\mathbf{L}$ is equal to the sum of the angular momenta of the two orbits. We can take some advantage out of our reference frame in the following way. The angular momenta of the two orbits and the total angular momentum are in the same plane and the angles between the momenta and the total angular momentum are the inclinations. See Fig. 2.5a for an illustration. If we assume that $\dot{g}_j=\dot{h}_j=\dot{i}_j=0$ for $j=1,2$ (we will assume that this is true for at least one orbital period of the binaries), it follows from Eq. 2.42 that $\dot{\widehat{\mathbf{r}}}$ and $\dot{\widehat{\mathbf{r}}}'$ are only determined by the time derivative of the true anomaly. This is exactly the situation of a two-body system described with respect to a plane of reference. We know that in the two-body case the angular momentum is perpendicular to the orbital plane. Thus, the angular momenta of the outer and inner binary system are perpendicular to the orbital planes of the outer and inner binary respectively.

Now G_j is the length of the angular momentum of orbit j, so H_j is the component of the angular momentum in the direction of the total angular momentum. Thus, $G=H_1+H_2$ is the length of the total angular momentum, so a constant. Because the component of the total angular momentum in the reference plane is zero, $G_1\sin(i_1)=G_2\sin(i_2)$. So $G_1^2(1-\cos^2(i_1))=G_2^2(1-\cos^2(i_2))$ or $G_1^2-H_1^2=G_2^2-H_2^2$. Hence, $G_1^2-H_1^2=G_2^2-(G-H_1)^2=G_2^2-G^2-H_1^2+2GH_1$. Thus,

$$
H_1=\frac{G_1^2-G_2^2+G^2}{2G}. \tag{2.45}
$$

In the same way, it follows that

$$
H_2=\frac{G_2^2-G_1^2+G^2}{2G}. \tag{2.46}
$$

Using these equations we can get rid of the dependence of the Hamiltonian on H_1 and H_2.

We can also find a relation between $\cos(i_\mathrm{tot})$ and the length of the angular momentum vectors ($i_\mathrm{tot}=i_1+i_2$). If one applies the law of cosines to the left triangle in Fig. 2.5a, one finds that $G^2=G_1^2+G_2^2-2G_1G_2\cos(\pi-i_\mathrm{tot})=G_1^2+G_2^2+2G_1G_2\cos(i_\mathrm{tot})$. Hence,

$$
\cos(i_\mathrm{tot})=\frac{G^2-G_1^2-G_2^2}{2G_1G_2}. \tag{2.47}
$$

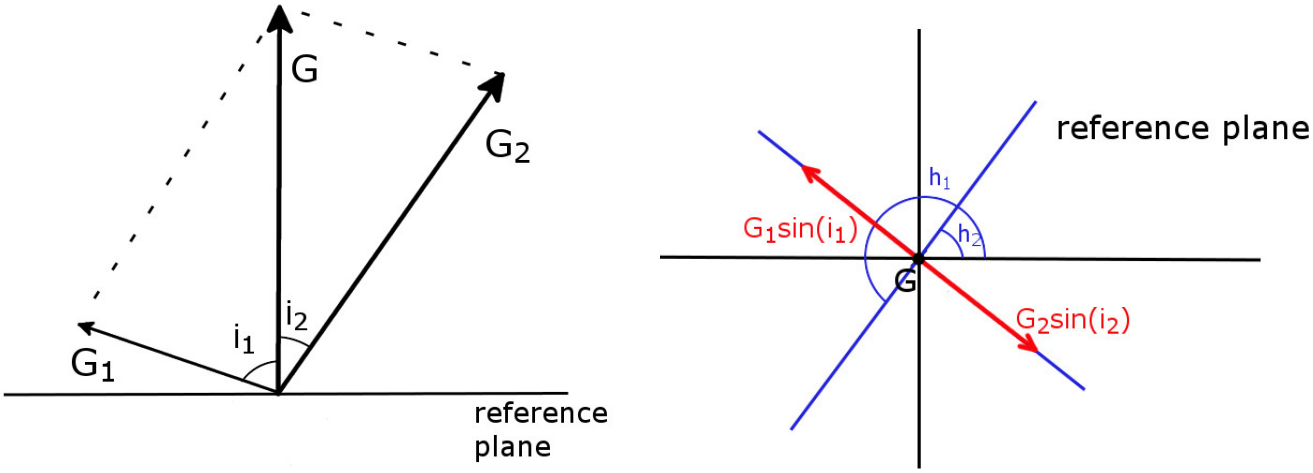

(a) Illustration of the different angular momentum vectors. The angle between G_1 and G is i_1 and the angle between G_2 and G is i_2.

(b) Illustration for the elimination of the nodes. It shows the reference plane and the component of G_1 and G_2 in this plane. Also the angles of the nodes are shown.

Figure 2.5: Illustrations of the different important planes.

For both orbits, the intersection of the orbital plane with the reference plane is a line perpendicular to the angular momentum of that orbit. This same line is also perpendicular to the total angular momentum, because the total angular momentum is perpendicular to the reference plane. So these lines are both perpendicular to the plane spanned by the angular momentum vectors (see also Fig. 2.5b). The ascending nodes of both orbits are on these lines, thus $h_1 - h_2$ is equal to 0 or to π. If we use that h is the angle where the orbit crosses upward the reference plane and use the right-hand rule to determine the direction of the angular momentum of both orbits, it follows that $h_1 - h_2 = \pi$.

Because our Hamiltonian is only dependent on h_1 and h_2 via $\cos(\Phi)$ in the combination $h_1 - h_2$, we can substitute the value found above. We can do this before we calculate the equations of motion, because we can find the equations of motion of H_j from Eqs. 2.45 and 2.46; the equations of motion of the other variables follow with partial derivatives, so $h_1 - h_2$ forms a constant which is not important. The expression for $\cos(\Phi)$, Eq. 2.43, changes in the following way:

$$\begin{aligned}\cos(\Phi) &= -\cos(f_1+g_1)\cos(f_2+g_2) - \sin(f_1+g_1)\sin(f_2+g_2)\cos(i_1)\cos i_2 \\ &\quad + \sin(i_1)\sin(i_2)\sin(f_1+g_1)\sin(f_2+g_2) \\ &= -\cos(f_1+g_1)\cos(f_2+g_2) - \sin(f_1+g_1)\sin(f_2+g_2)\cos(i_{\text{tot}}),\end{aligned} \tag{2.48}$$

where we used Eq. T.8. This process is commonly referred to as the elimination of the nodes (e.g. Naoz et al. (2011)).

2.5 Secularizing the Hamiltonian

In the following, we want to do a transformation to get rid of the dependency of the Hamiltonian on l_1 and l_2; this way we eliminate any short-term effects. The resulting Hamiltonian will be referred to as the secular Hamiltonian (secular means averaged over short-term effects). The transformation follows with the so called 'Von Zeipel method'. This method is explained in Ciacaglia (1964) and an application of this method to artificial-satellite theory, in which lots of details are given, can be found in Brouwer (1959). An application of this method to the three-body Hamiltonian can be found in e.g. Harrington (1968) and Naoz et al. (2011).

Consider our Hamiltonian $\mathcal{H}$ that is dependent on coordinates $\mathbf{q} = \{g_1, g_2, l_1, l_2, h_1, h_2\}$ and corresponding momenta $\mathbf{p} = \{G_1, G_2, L_1, L_2, H_1, H_2\}$. We also included the coordinates h_j and momenta H_j and will apply the results from Sec. 2.4.1 to the secular Hamiltonian.

We have the relations: $\dot{q}_i = \frac{\partial \mathcal{H}}{\partial p_i}$ and $\dot{p}_i = -\frac{\partial \mathcal{H}}{\partial q_i}$. The Lagrangian corresponding to $\mathcal{H}$ is $\mathcal{L} = \mathbf{p}\cdot\dot{\mathbf{q}} - \mathcal{H}(\mathbf{q},\mathbf{p})$. We want to apply a canonical transformation f to the coordinates $\mathbf{q}' = \{g_1', g_2', l_1', l_2', h_1', h_2'\}$ and conjugate momenta

$\mathbf{p}' = \{G_1', G_2', L_1', L_2', H_1', H_2'\}$ with Hamiltonian $\mathcal{H}'(g_1', g_2', h_1', h_2', \mathbf{p}')$ such that $(\mathbf{q}', \mathbf{p}') = f(\mathbf{q}, \mathbf{p})$. Notice that this new Hamiltonian is not dependent on l_1', l_2'. The corresponding Lagrangian is $\mathcal{L}' = \mathbf{p}' \cdot \dot{\mathbf{q}}' - \mathcal{H}'(\mathbf{q}', \mathbf{p}')$. Suppose that we can write $\mathbf{p}' \cdot \dot{\mathbf{q}}' - \mathcal{H}'(\mathbf{q}', \mathbf{p}') + \frac{dF'}{dt} = \mathbf{p} \cdot \dot{\mathbf{q}} - \mathcal{H}(\mathbf{q}, \mathbf{p})$, where $F' = -\mathbf{p}' \cdot \mathbf{q}' + F(\mathbf{q}, \mathbf{p}')$. F is called the generating function. We want to derive the transformation f between the two sets of coordinates and to that end, we expand the formula above:

$$\mathbf{p} \cdot \dot{\mathbf{q}} - \mathcal{H}(\mathbf{q}, \mathbf{p}) = \mathbf{p}' \cdot \dot{\mathbf{q}}' - \mathcal{H}'(\mathbf{q}', \mathbf{p}') + \frac{dF'}{dt} = -\dot{\mathbf{p}}' \cdot \mathbf{q}' - \mathcal{H}'(\mathbf{q}', \mathbf{p}') + \frac{\partial F}{\partial \mathbf{q}} \cdot \dot{\mathbf{q}} + \frac{\partial F}{\partial \mathbf{p}'} \cdot \dot{\mathbf{p}}'. \tag{2.49}$$

$\mathbf{q}$ and $\mathbf{p}'$ are each independent, so we have found the following equations:

$$\begin{aligned} \mathbf{p} &= \frac{\partial F}{\partial \mathbf{q}}; \\ \mathbf{q}' &= \frac{\partial F}{\partial \mathbf{p}'}; \\ \mathcal{H}'(\mathbf{q}', \mathbf{p}') &= \mathcal{H}(\mathbf{q}, \mathbf{p}). \end{aligned} \tag{2.50}$$

It is possible to use these equations to give the new coordinates in terms of the old ones. Use the first equation to derive $\mathbf{p}'$ in terms of $\mathbf{q}$ and $\mathbf{p}$. Use the second equation to derive $\mathbf{q}'$ in terms of $\mathbf{q}$ and $\mathbf{p}'$. If we substitute the formulas derived from the first equation into the formulas derived from the second equation, we get $\mathbf{q}'$ in terms of $\mathbf{q}$ and $\mathbf{p}$. Inverting the relations for $\mathbf{q}'$ and $\mathbf{p}'$ and substitution in the formula for $\mathcal{H}$ gives the new Hamiltonian.

From now on, we work in the variables $\mathbf{q}$ and $\mathbf{p}'$, so if one encounters an expression with variables $\mathbf{q}'$ or $\mathbf{p}$, it should be read as a function of $\mathbf{q}$ and $\mathbf{p}'$, i.e. $\mathbf{q}'(\mathbf{q}, \mathbf{p}')$, $\mathbf{p}(\mathbf{q}, \mathbf{p}')$. In the same way as we did in Eq. 2.41, the Hamiltonian including all terms, Eq. 2.39, can be made dependent on the small parameter $\epsilon = \frac{a_1}{a_2}$:

$$\mathcal{H}(\mathbf{q}, \mathbf{p}; \epsilon) = \sum_{k=0}^{\infty} \mathcal{H}_k(\mathbf{q}, \frac{\partial F}{\partial \mathbf{q}}) \epsilon^k. \tag{2.51}$$

We assume that we can write the new Hamiltonian $\mathcal{H}'(\mathbf{q}', \mathbf{p}'; \epsilon)$ in the same way:

$$\mathcal{H}'(\mathbf{q}', \mathbf{p}'; \epsilon) = \sum_{k=0}^{\infty} \mathcal{H}_k'(\frac{\partial F}{\partial \mathbf{p}'}, \mathbf{p}') \epsilon^k. \tag{2.52}$$

Furthermore, we assume that a Taylor expansion is valid for F, $\mathcal{H}_k$ and $\mathcal{H}_k'$ around $\epsilon = 0$, yielding:

$$\begin{aligned} F(\mathbf{q}, \mathbf{p}'; \epsilon) &= \sum_{k=0}^{\infty} \frac{1}{k!} \left(\frac{\partial^k F}{\partial \epsilon^k} \right)_{\epsilon=0} \epsilon^k = \sum_{k=0}^{\infty} F_k \epsilon^k; \\ \mathcal{H}_k(\mathbf{q}, \frac{\partial F}{\partial \mathbf{q}}) &= \sum_{m=0}^{\infty} \frac{1}{m!} \left(\frac{\partial^m \mathcal{H}_k}{\partial \epsilon^m} \right)_{\epsilon=0} \epsilon^m; \\ \mathcal{H}_k'(\frac{\partial F}{\partial \mathbf{p}'}, \mathbf{p}') &= \sum_{m=0}^{\infty} \frac{1}{m!} \left(\frac{\partial^m \mathcal{H}_k'}{\partial \epsilon^m} \right)_{\epsilon=0} \epsilon^m . \end{aligned} \tag{2.53}$$

By substitution in the third equation of Eqs. 2.50:

$$\sum_{k=0}^{\infty} \sum_{m=0}^{\infty} \frac{1}{m!} \left(\frac{\partial^m \mathcal{H}_k}{\partial \epsilon^m} \right)_{\epsilon=0} \epsilon^{m+k} = \sum_{k=0}^{\infty} \sum_{m=0}^{\infty} \frac{1}{m!} \left(\frac{\partial^m \mathcal{H}_k'}{\partial \epsilon^m} \right)_{\epsilon=0} \epsilon^{m+k}. \tag{2.54}$$

The next step is to equate the coefficients of equal powers in this equation. This gives us a series of differential equations which we can solve (if we are lucky) for F and $\mathcal{H}'$. To obtain the necessary equations we need an expression for $\left(\frac{\partial^m \mathcal{H}_k}{\partial \epsilon^m} \right)_{\epsilon=0}$. Using the chain rule, we find

$$\begin{aligned}\frac{\partial \mathcal{H}_k}{\partial \epsilon} &= \sum_{j=1}^{6} \frac{\partial \mathcal{H}_k}{\partial \mathbf{p}_j} \frac{d\mathbf{p}_j}{d\epsilon} \\ &= \sum_{j=1}^{6} \frac{\partial \mathcal{H}_k}{\partial \mathbf{p}_j} \frac{d}{d\epsilon} \left(\frac{\partial F}{\partial \mathbf{q}_j} \right) \\ &= \sum_{j=1}^{6} \frac{\partial \mathcal{H}_k}{\partial \mathbf{p}_j} \frac{d}{d\epsilon} \left(\sum_{r=0}^{\infty} \epsilon^r \frac{\partial F_r}{\partial \mathbf{q}_j} \right) \\ &= \sum_{j=1}^{6} \sum_{r=1}^{\infty} r\epsilon^{r-1} \frac{\partial \mathcal{H}_k}{\partial \mathbf{p}_j} \frac{\partial F_r}{\partial \mathbf{q}_j}. \end{aligned} \tag{2.55}$$

We use Leibniz's formula,

$$\frac{d^n}{dx^n} \left(f(x)g(x) \right) = \sum_{r=0}^{n} \binom{n}{r} \frac{d^r f}{dx^r} \frac{d^{n-r} g}{dx^{n-r}}, \tag{2.56}$$

to calculate:

$$\begin{aligned}\frac{\partial^m \mathcal{H}_k}{\partial \epsilon^m} &= \frac{\partial^{m-1}}{\partial \epsilon^{m-1}} \left(\sum_{j=1}^{6} \sum_{r=1}^{\infty} r\epsilon^{r-1} \frac{\partial \mathcal{H}_k}{\partial \mathbf{p}_j} \frac{\partial F_r}{\partial \mathbf{q}_j} \right) \\ &= \sum_{j=1}^{6} \sum_{r=1}^{\infty} r \frac{\partial F_r}{\partial \mathbf{q}_j} \sum_{q=0}^{m-1} \binom{m-1}{q} \frac{d^q \epsilon^{r-1}}{d\epsilon^q} \frac{d^{m-1-q}}{d\epsilon^{m-1-q}} \left(\frac{\partial \mathcal{H}_k}{\partial \mathbf{p}_j} \right) \\ &= \sum_{j=1}^{6} \sum_{r=1}^{\infty} r \frac{\partial F_r}{\partial \mathbf{q}_j} \sum_{q=0}^{\min(m-1,r-1)} \binom{m-1}{q} \frac{d^q \epsilon^{r-1}}{d\epsilon^q} \frac{d^{m-1-q}}{d\epsilon^{m-1-q}} \left(\frac{\partial \mathcal{H}_k}{\partial \mathbf{p}_j} \right). \end{aligned} \tag{2.57}$$

From this expression we find that

$$\left(\frac{\partial^m \mathcal{H}_k}{\partial \epsilon^m} \right)_{\epsilon=0} = \sum_{j=1}^{6} \sum_{r=1}^{m} r \frac{\partial F_r}{\partial \mathbf{q}_j} \binom{m-1}{r-1} (r-1)! \left\{ \frac{d^{m-r}}{d\epsilon^{m-r}} \left(\frac{\partial \mathcal{H}_k}{\partial \mathbf{p}_j} \right) \right\}_{\epsilon=0} \tag{2.58}$$

for $m \geq 1$. Substitution in the expression for $\mathcal{H}$ gives

$$\mathcal{H} = \sum_{k=0}^{\infty} (\mathcal{H}_k)_{\epsilon=0} \epsilon^k + \sum_{k=0}^{\infty} \sum_{m=1}^{\infty} \sum_{j=1}^{6} \sum_{r=1}^{m} \frac{1}{m!} r \frac{\partial F_r}{\partial \mathbf{q}_j} \binom{m-1}{r-1} (r-1)! \left\{ \frac{d^{m-r}}{d\epsilon^{m-r}} \left(\frac{\partial \mathcal{H}_k}{\partial \mathbf{p}_j} \right) \right\}_{\epsilon=0} \epsilon^{m+k}. \tag{2.59}$$

A similar process for $\mathcal{H}'$ finally results in the equation:

$$\begin{aligned}&\sum_{k=0}^{\infty} (\mathcal{H}_k)_{\epsilon=0} \epsilon^k + \sum_{k=0}^{\infty} \sum_{m=1}^{\infty} \sum_{j=1}^{6} \sum_{r=1}^{m} \frac{r}{m(m-r)!} \frac{\partial F_r}{\partial \mathbf{q}_j} \left\{ \frac{d^{m-r}}{d\epsilon^{m-r}} \left(\frac{\partial \mathcal{H}_k}{\partial \mathbf{p}_j} \right) \right\}_{\epsilon=0} \epsilon^{m+k} = \\ &\sum_{k=0}^{\infty} (\mathcal{H}'_k)_{\epsilon=0} \epsilon^k + \sum_{k=0}^{\infty} \sum_{m=1}^{\infty} \sum_{j=1}^{6} \sum_{r=1}^{m} \frac{r}{m(m-r)!} \frac{\partial F_r}{\partial \mathbf{p}'_j} \left\{ \frac{d^{m-r}}{d\epsilon^{m-r}} \left(\frac{\partial \mathcal{H}'_k}{\partial \mathbf{q}'_j} \right) \right\}_{\epsilon=0} \epsilon^{m+k} \quad . \end{aligned} \tag{2.60}$$

In the following sections we will consider the powers of ϵ in Eq. 2.60 one by one until the third order (this corresponds to Eq. 2.41) and solve for $\mathcal{H}'_k$. The second and third order are also known as the quadrupole and octupole order respectively, thus we will henceforth denote $\mathcal{H}'_2$ by $\mathcal{H}_{\text{quad}}$ and $\mathcal{H}'_3$ by $\mathcal{H}_{\text{oct}}$.

2.5.1 Zeroth and First Order

The zeroth power of ϵ in Eq. 2.60 gives the following equation:

$$(\mathcal{H}_0'(\mathbf{q},\mathbf{p}'))_{\epsilon=0} \;=\; (\mathcal{H}_0(\mathbf{q},\mathbf{p}'))_{\epsilon=0}. \tag{2.61}$$

From Eqs. 2.50 and 2.53 we know that

$$\begin{aligned} \mathbf{q}' &= \sum_{k=0}^{\infty} \frac{\partial F_k}{\partial \mathbf{p}'}\epsilon^k; \\ \mathbf{p} &= \sum_{k=0}^{\infty} \frac{\partial F_k}{\partial \mathbf{q}}\epsilon^k. \end{aligned} \tag{2.62}$$

Hence,

$$\mathcal{H}_0'(\frac{\partial F_0}{\partial \mathbf{p}'},\mathbf{p}') = (\mathcal{H}_0'(\mathbf{q},\mathbf{p}'))_{\epsilon=0} = (\mathcal{H}_0(\mathbf{q},\mathbf{p}'))_{\epsilon=0} = \mathcal{H}_0(\mathbf{q},\frac{\partial F_0}{\partial \mathbf{q}}). \tag{2.63}$$

Thus it follows that F_0 is the generating function of the transformation if we only consider the zeroth power of ϵ. Because in our case, the zeroth order term in the Hamiltonian is not dependent on l_1, l_2, we want F_0 to induce the identity transformation. So

$$F_0 = \mathbf{p}' \cdot \mathbf{q}, \tag{2.64}$$

and we find that

$$\mathcal{H}_0'(\mathbf{q}',\mathbf{p}') = (\mathcal{H}_0'(\mathbf{q},\mathbf{p}'))_{\epsilon=0} = (\mathcal{H}_0(\mathbf{q},\mathbf{p}'))_{\epsilon=0} = H_0(\mathbf{q},\mathbf{p}) = -\frac{G_N m_1 m_2}{2a_1} - \frac{G_N m_3 M}{2a_2}. \tag{2.65}$$

Consider the first power of ϵ in Eq. 2.60. We find that

$$(\mathcal{H}_1'(\mathbf{q},\mathbf{p}'))_{\epsilon=0} + \sum_{j=1}^{6} \frac{\partial F_1}{\partial \mathbf{p}_j'}\left(\frac{\partial \mathcal{H}_0'}{\partial \mathbf{q}_j'}\right)_{\epsilon=0} = (\mathcal{H}_1(\mathbf{q},\mathbf{p}'))_{\epsilon=0} + \sum_{j=1}^{6} \frac{\partial F_1}{\partial \mathbf{q}_j}\left(\frac{\partial \mathcal{H}_0}{\partial \mathbf{p}_j}\right)_{\epsilon=0}. \tag{2.66}$$

Hence, the generating function of the transformation is given by $F_0 + F_1\epsilon$. Because $\mathcal{H}_1 = 0$, the transformation should be the identity one. Thus $F_1 = 0$ and in the same way as above we find that

$$\mathcal{H}_1'(\mathbf{q}',\mathbf{p}') = (\mathcal{H}_1'(\mathbf{q},\mathbf{p}'))_{\epsilon=0} = (\mathcal{H}_1(\mathbf{q},\mathbf{p}'))_{\epsilon=0} = H_1(\mathbf{q},\mathbf{p}) = 0. \tag{2.67}$$

2.5.2 Quadrupole Order

Using Eq. 2.60 (we use $\mathcal{H}_{\text{quad}}$ instead of $\mathcal{H}'_2$), $F_0 + F_1\epsilon = \mathbf{p}' \cdot \mathbf{q}$ and the expressions for $\mathcal{H}_0$ and $\mathcal{H}_0'$, we find for the second power of ϵ that

$$(\mathcal{H}_{\text{quad}}(\mathbf{q},\mathbf{p}'))_{\epsilon=0} = (\mathcal{H}_2(\mathbf{q},\mathbf{p}'))_{\epsilon=0} + \sum_{j=1}^{2} \frac{\partial F_2}{\partial l_j}\left(\frac{\partial \mathcal{H}_0}{\partial L_j}\right)_{\epsilon=0}. \tag{2.68}$$

l_1, l_2 are angles, so it seems logical that F_2 and its partial derivatives with respect to l_1 and l_2 are periodic in l_1 and l_2 with period 2π. Thus we can write F_2 as a Fourier series:

$$F_2 = \sum_{k_1,k_2=-\infty}^{\infty} f_{k_1k_2} e^{-ik_1l_1 - ik_2l_2}. \tag{2.69}$$

We have also seen that $(\mathcal{H}_2(\mathbf{q},\mathbf{p}'))_{\epsilon=0}$ is periodic in l_1 and l_2 with period 2π, hence

$$(\mathcal{H}_2(\mathbf{q},\mathbf{p}'))_{\epsilon=0} = \sum_{k_1k_2=-\infty}^{\infty} h_{k_1k_2} e^{-ik_1l_1 - ik_2l_2}, \tag{2.70}$$

where

$$h_{k_1k_2} = \frac{1}{4\pi^2}\int_0^{2\pi}\int_0^{2\pi} (\mathcal{H}_2(\mathbf{q},\mathbf{p}'))_{\epsilon=0} e^{ik_1l_1 + ik_2l_2} dl_2 dl_1. \tag{2.71}$$

Combining Eqs. 2.68, 2.69 and 2.70 we find that

$$\begin{aligned}(\mathcal{H}_{\rm quad}(\mathbf{q},\mathbf{p}'))_{\epsilon=0} &= \sum_{k_1k_2=-\infty}^{\infty} h_{k_1k_2}e^{-ik_1l_1-ik_2l_2} - \left(\frac{\partial\mathcal{H}_0}{\partial L_1}\right)_{\epsilon=0}\sum_{k_1,k_2=-\infty}^{\infty} ik_1 f_{k_1k_2}e^{-ik_1l_1-ik_2l_2} \\ &\quad - \left(\frac{\partial\mathcal{H}_0}{\partial L_2}\right)_{\epsilon=0}\sum_{k_1,k_2=-\infty}^{\infty} ik_2 f_{k_1k_2}e^{-ik_1l_1-ik_2l_2}. \end{aligned} \tag{2.72}$$

Thus if we assume that $k_1\left(\frac{\partial\mathcal{H}_0}{\partial L_1}\right)_{\epsilon=0} + k_2\left(\frac{\partial\mathcal{H}_0}{\partial L_2}\right)_{\epsilon=0} \neq 0\ \forall(k_1,k_2)\in\mathbb{Z}^2\backslash\{(0,0)\}$, we can use

$$f_{k_1k_2} = -\frac{ih_{k_1k_2}}{k_1\left(\frac{\partial\mathcal{H}_0}{\partial L_1}\right)_{\epsilon=0} + k_2\left(\frac{\partial\mathcal{H}_0}{\partial L_2}\right)_{\epsilon=0}} \tag{2.73}$$

$\forall(k_1,k_2)\in\mathbb{Z}^2\backslash\{(0,0)\}$ and $f_{00}=0$. The F_2 formed this way eliminates all the terms in $(\mathcal{H}_{\rm quad}(\mathbf{q},\mathbf{p}'))_{\epsilon=0}$ depending on l_1 and l_2, leaving

$$\begin{aligned}\mathcal{H}_{\rm quad}(\mathbf{q}',\mathbf{p}')\epsilon^2 &= (\mathcal{H}_{\rm quad}(\mathbf{q},\mathbf{p}'))_{\epsilon=0}\epsilon^2 \\ &= h_{00}\epsilon^2 \\ &= \frac{\epsilon^2}{4\pi^2}\int_0^{2\pi}\int_0^{2\pi}(\mathcal{H}_2(\mathbf{q},\mathbf{p}'))_{\epsilon=0}dl_2dl_1 \\ &= \frac{\epsilon^2}{4\pi^2}\int_0^{2\pi}\int_0^{2\pi}\mathcal{H}_2(\mathbf{q},\mathbf{p})dl_2dl_1 \\ &= \frac{1}{4\pi^2}\int_0^{2\pi}\int_0^{2\pi}-\frac{1}{2}G_NM_2\frac{a_1^2}{a_2^3}\left(\frac{r_1}{a_1}\right)^2\left(\frac{a_2}{r'}\right)^3(3\cos^2(\Phi)-1)dl_2dl_1. \end{aligned} \tag{2.74}$$

Note that we substituted $\mathcal{H}_2(\mathbf{q},\mathbf{p})$ from Eq. 2.41. Since the integration is over l_j, the results from Sec. 2.4.1 can be applied to the integrand. We will first calculate

$$\mathcal{H}'_{\rm quad}(\mathbf{q}',\mathbf{p}')\epsilon^2 = \frac{1}{2\pi}\int_0^{2\pi}-\frac{1}{2}G_NM_2\frac{a_1^2}{a_2^3}\left(\frac{r_1}{a_1}\right)^2\left(\frac{a_2}{r'}\right)^3(3\cos^2(\Phi)-1)dl_2. \tag{2.75}$$

To calculate Eq. 2.75, we transform it to f_2. We already calculated the jacobian for this transformation in Eq. 2.31. To write the expression for $\cos(\Phi)$ (Eq. 2.48) in a more convenient way, we use the trigonometric identities T.8 and T.9:

$$\begin{aligned}\cos(\Phi) &= -\cos(f_1+g_1)\big[\cos(f_2)\cos(g_2)-\sin(f_2)\sin(g_2)\big] \\ &\quad -\sin(f_1+g_1)\big[\sin(f_2)\cos(g_2)+\cos(f_2)\sin(g_2)\big]\cos(i_{\rm tot}) \\ &= A_1\cos(f_2)+A_2\sin(f_2), \end{aligned} \tag{2.76}$$

where we defined:

$$\begin{aligned}A_1 &= -\cos(f_1+g_1)\cos(g_2)-\sin(f_1+g_1)\sin(g_2)\cos(i_{\rm tot}); \\ A_2 &= \cos(f_1+g_1)\sin(g_2)-\sin(f_1+g_1)\cos(g_2)\cos(i_{\rm tot}). \end{aligned} \tag{2.77}$$

Thus we have to calculate the following integral:

$$\begin{aligned}\mathcal{H}'_{\text{quad}}(\mathbf{q}',\mathbf{p}')\epsilon^2 &= \frac{1}{2\pi}\int_0^{2\pi} -\frac{1}{2}G_N M_2 \frac{a_1^2}{a_2^3}\left(\frac{r_1}{a_1}\right)^2\left(\frac{a_2}{r'}\right)^3\Big(3(A_1\cos(f_2)+A_2\sin(f_2))^2-1\Big)\frac{1}{\sqrt{1-e_2}}\left(\frac{r'}{a_2}\right)^2 df_2 \\ &= -\frac{1}{4\pi}G_N M_2 \frac{1}{(1-e_2^2)^{3/2}}\frac{a_1^2}{a_2^3}\left(\frac{r_1}{a_1}\right)^2\int_0^{2\pi}\big(1+e_2\cos(f_2)\big) \\ &\quad \times\Big[3\big(A_1^2\cos^2(f_2)+A_2^2\sin^2(f_2)+2A_1A_2\sin(f_2)\cos(f_2)\big)-1\Big]df_2,\end{aligned} \tag{2.78}$$

where we substituted Eq. 2.14 for r'. To make this expression more manageable we define:

$$C_{\text{quad}} = \frac{1}{16}G_N M_2 \frac{1}{(1-e_2^2)^{3/2}}\frac{a_1^2}{a_2^3}. \tag{2.79}$$

We know that sin is anti-symmetric about 0 and symmetric about $\frac{\pi}{2}$, and cos is anti-symmetric about $\frac{\pi}{2}$ and symmetric about 0, hence $\cos^l(\alpha)\sin^{2k+1}(\alpha)$ for $k,l\in\mathbb{N}$ is anti-symmetric in $\alpha=0$ and $\cos^{2l+1}(\alpha)\sin^k(\alpha)$ for $k,l\in\mathbb{N}$ is anti-symmetric in $\alpha=\frac{\pi}{2}$. This means that

$$\begin{aligned}\int_0^{2\pi}\cos^l(\alpha)\sin^{2k+1}(\alpha)d\alpha &= 0; \\ \int_0^{2\pi}\cos^{2l+1}(\alpha)\sin^k(\alpha)d\alpha &= 0; \\ k,l\in\mathbb{N}.\end{aligned} \tag{2.80}$$

Using the identities from section 2.2, one can also calculate that

$$\begin{aligned}\int_0^{2\pi}\cos^4(\alpha)d\alpha &= \frac{3}{4}\pi; \\ \int_0^{2\pi}\cos^2(\alpha)\sin^2(\alpha)d\alpha &= \frac{1}{4}\pi; \\ \int_0^{2\pi}\cos^2(\alpha)d\alpha &= \pi; \\ \int_0^{2\pi}\sin^2(\alpha)d\alpha &= \pi.\end{aligned} \tag{2.81}$$

With the integrals from Eqs. 2.80 and 2.81, we find:

$$\begin{aligned}\mathcal{H}'_{\text{quad}}(\mathbf{q}',\mathbf{p}')\epsilon^2 &= -\frac{4}{\pi}C_{\text{quad}}\left(\frac{r_1}{a_1}\right)^2\int_0^{2\pi}\Big[3A_1^2\cos^2(f_2)+3A_2^2\sin^2(f_2)+6A_1A_2\sin(f_2)\cos(f_2)-1+3e_2A_1^2\cos^3(f_2) \\ &\quad +3e_2A_2^2\cos(f_2)\sin^2(f_2)+6e_2A_1A_2\sin(f_2)\cos^2(f_2)-e_2\cos(f_2)\Big]df_2 \\ &= -\frac{4}{\pi}C_{\text{quad}}\left(\frac{r_1}{a_1}\right)^2(3A_1^2\pi+3A_2^2\pi-2\pi).\end{aligned} \tag{2.82}$$

We will now calculate the outer integral in Eq. 2.74:

$$\mathcal{H}_{\text{quad}}(\mathbf{q}',\mathbf{p}')\epsilon^2 = -\frac{2}{\pi}\int_0^{2\pi}\left(\frac{r_1}{a_1}\right)^2 C_{\text{quad}}(3A_1^2+3A_2^2-2)dl_1. \tag{2.83}$$

Using Eqs. 2.77, and the identities T.8 and T.9 we can write

$$
\begin{aligned}
A_1 &= -\big[\cos(f_1)\cos(g_1)-\sin(f_1)\sin(g_1)\big]\cos(g_2)-\big[\sin(f_1)\cos(g_1)+\cos(f_1)\sin(g_1)\big]\sin(g_2)\cos(i_{\rm tot})\\
&= B_1\cos(f_1)+B_2\sin(f_1);\\
A_2 &= \big[\cos(f_1)\cos(g_1)-\sin(f_1)\sin(g_1)\big]\sin(g_2)-\big[\sin(f_1)\cos(g_1)+\cos(f_1)\sin(g_1)\big]\cos(g_2)\cos(i_{\rm tot})\\
&= B_3\cos(f_1)+B_4\sin(f_1),
\end{aligned}
\tag{2.84}
$$

where we defined:

$$
\begin{aligned}
B_1 &= -\cos(g_1)\cos(g_2)-\sin(g_1)\sin(g_2)\cos(i_{\rm tot});\\
B_2 &= \sin(g_1)\cos(g_2)-\cos(g_1)\sin(g_2)\cos(i_{\rm tot});\\
B_3 &= \cos(g_1)\sin(g_2)-\sin(g_1)\cos(g_2)\cos(i_{\rm tot});\\
B_4 &= -\sin(g_1)\sin(g_2)-\cos(g_1)\cos(g_2)\cos(i_{\rm tot}).
\end{aligned}
\tag{2.85}
$$

To calculate the integral in Eq. 2.83, we transform to the eccentric anomaly. The jacobian for this transformation is given by Eq. 2.30. From Eq. 2.18 we find

$$
\frac{r_1}{a_1}=1-e_1\cos(E_1) \tag{2.86}
$$

and from Eq. 2.21:

$$
\sin(f_1)=\sqrt{1-\cos^2(f_1)}=\sqrt{1-\left(\frac{\cos(E_1)-e_1}{1-e_1\cos(E_1)}\right)^2}=\sqrt{\frac{(1-\cos^2(E_1))(1-e_1^2)}{(1-e_1\cos(E_1))^2}}=\frac{\sin(E_1)\sqrt{1-e_1^2}}{1-e_1\cos(E_1)}. \tag{2.87}
$$

Using Eqs. 2.80 and 2.81 we find that

$$
\begin{aligned}
\mathcal{H}_{\rm quad}(\mathbf{q}',\mathbf{p}')\epsilon^2 &= -\frac{2}{\pi}\int_0^{2\pi}\left(\frac{r_1}{a_1}\right)^2 C_{\rm quad}(3A_1^2+3A_2^2-2)dl_1\\
&= -\frac{2}{\pi}\int_0^{2\pi} C_{\rm quad}\left(\frac{r_1}{a_1}\right)^2\Big[3(B_1^2+B_3^2)\cos^2(f_1)+3(B_2^2+B_4^2)\sin^2(f_1)\\
&\quad +6(B_1B_2+B_3B_4)\cos(f_1)\sin(f_1)-2\Big]dl_1\\
&= -\frac{2}{\pi}\int_0^{2\pi} C_{\rm quad}\left(\frac{r_1}{a_1}\right)^2\Big[3(B_1^2+B_3^2-B_2^2-B_4^2)\cos^2(f_1)\\
&\quad +6(B_1B_2+B_3B_4)\cos(f_1)\sin(f_1)-2+3(B_2^2+B_4^2)\Big]dl_1\\
&= -\frac{2}{\pi}\int_0^{2\pi} C_{\rm quad}(1-e_1\cos(E_1))\Big[3(B_1^2+B_3^2-B_2^2-B_4^2)(\cos(E_1)-e_1)^2+6(B_1B_2+B_3B_4)\\
&\quad \times(\cos(E_1)-e_1)\sqrt{(1-\cos^2(E_1))(1-e_1^2)}+\big(3(B_2^2+B_4^2)-2\big)\big(1-e_1\cos(E_1)\big)^2\Big]dE_1\\
&= -24C_{\rm quad}(B_1^2+B_3^2-B_2^2-B_4^2)e_1^2-6C_{\rm quad}(B_1^2+B_3^2-B_2^2-B_4^2)\\
&\quad -4\big[3(B_2^2+B_4^2)-2\big]C_{\rm quad}-6\big[3(B_2^2+B_4^2)-2\big]e_1^2C_{\rm quad}\\
&= -C_{\rm quad}\Big[(B_1^2+B_3^2-B_2^2-B_4^2)(6+24e_1^2)+\big(6(B_2^2+B_4^2)-4\big)(2+3e_1^2)\Big].
\end{aligned}
\tag{2.88}
$$

With Eqs. 2.85 it follows that:

$$
\begin{aligned}
B_2^2+B_4^2 &= \sin^2(g_1)+\cos^2(g_1)\cos^2(i_{\rm tot})\\
&= 1-\cos^2(g_1)\sin^2(i_{\rm tot});\\
B_1^2+B_3^2-B_2^2-B_4^2 &= \cos^2(g_1)+\sin^2(g_1)\cos^2(i_{\rm tot})-\sin^2(g_1)-\cos^2(g_1)\cos^2(i_{\rm tot})\\
&= \cos(2g_1)-\cos(2g_1)\cos^2(i_{\rm tot})\\
&= \cos(2g_1)\sin^2(i_{\rm tot}).
\end{aligned}
\tag{2.89}
$$

Hence,

$$\begin{aligned}
\mathcal{H}_{\rm quad}(\mathbf{q}',\mathbf{p}')\epsilon^2 &= -C_{\rm quad}\Big[\cos(2g_1)\sin^2(i_{\rm tot})(6+24e_1^2)+\big(6(1-\cos^2(g_1)\sin^2(i_{\rm tot}))-4\big)(2+3e_1^2)\Big]\\
&= -C_{\rm quad}\Big[\cos(2g_1)\sin^2(i_{\rm tot})(6+24e_1^2)+\Big(3\big(2-(\cos(2g_1)+1)\sin^2(i_{\rm tot})\big)-4\Big)(2+3e_1^2)\Big]\\
&= -C_{\rm quad}\Big[\cos(2g_1)\sin^2(i_{\rm tot})(6+24e_1^2)+\Big(-1-3\cos(2g_1)\sin^2(i_{\rm tot})+3\cos^2(i_{\rm tot})\Big)(2+3e_1^2)\Big]\\
&= -C_{\rm quad}\Big[(3\cos^2(i_{\rm tot})-1)(2+3e_1^2)+15\cos(2g_1)\sin^2(i_{\rm tot})e_1^2\Big]. \qquad (2.90)
\end{aligned}$$

2.5.3 Octupole Order

The equation for the third power of ϵ in Eq. 2.60 is (we use $\mathcal{H}_{\rm oct}$ instead of $\mathcal{H'}_3$):

$$(\mathcal{H}_{oct}(\mathbf{q},\mathbf{p}'))_{\epsilon=0}=(\mathcal{H}_3(\mathbf{q},\mathbf{p}'))_{\epsilon=0}+\sum_{j=1}^{2}\frac{2}{3}\frac{\partial F_2}{\partial l_j}\left(\frac{d}{d\epsilon}\left(\frac{\partial\mathcal{H}_0}{\partial L_j}\right)\right)_{\epsilon=0}+\sum_{j=1}^{2}\frac{\partial F_3}{\partial l_j}\left(\frac{\partial\mathcal{H}_0}{\partial L_j}\right)_{\epsilon=0}. \qquad (2.91)$$

We will proceed in a way similar to what we did for the quadrupole order. We find that

$$\mathcal{H}_{\rm oct}(\mathbf{q}',\mathbf{p}')\epsilon^3=(\mathcal{H}_{\rm oct}(\mathbf{q},\mathbf{p}'))_{\epsilon=0}\epsilon^3 = \frac{-1}{8\pi^2}\int_0^{2\pi}\int_0^{2\pi}G_N M_3\frac{a_1^3}{a_2^4}\left(\frac{r_1}{a_1}\right)^3\left(\frac{a_2}{r'}\right)^4\Big(5\cos^3(\Phi)-3\cos(\Phi)\Big)dl_2dl_1. \qquad (2.92)$$

We will first calculate the inner integral,

$$\begin{aligned}
\mathcal{H}'_{\rm oct}(\mathbf{q}',\mathbf{p}')\epsilon^3 &= -\frac{1}{4\pi}\int_0^{2\pi}G_N M_3\frac{a_1^3}{a_2^4}\left(\frac{r_1}{a_1}\right)^3\left(\frac{a_2}{r'}\right)^4\Big(5\cos^3(\Phi)-3\cos(\Phi)\Big)dl_2\\
&= -\frac{1}{4\pi}G_N M_3\frac{a_1^3}{a_2^4}\left(\frac{r_1}{a_1}\right)^3\int_0^{2\pi}\Big(5\cos^3(\Phi)-3\cos(\Phi)\Big)\frac{(1+e_2\cos(f_2))^2}{(1-e_2^2)^{5/2}}df_2. \qquad (2.93)
\end{aligned}$$

Using Eqs. 2.76 and 2.80, and defining $C_{\rm oct}=-\frac{15}{64}G_N M_3\frac{a_1^3}{a_2^4}\frac{1}{(1-e_2^2)^{5/2}}$, we find

$$\begin{aligned}
\mathcal{H'}_{\rm oct}(\mathbf{q}',\mathbf{p}')\epsilon^3 &= \frac{16}{15\pi}C_{\rm oct}\left(\frac{r_1}{a_1}\right)^3\int_0^{2\pi}\Big[5\big(A_1\cos(f_2)+A_2\sin(f_2)\big)^3-3\big(A_1\cos(f_2)+A_2\sin(f_2)\big)\Big]\big(1+e_2\cos(f_2)\big)^2df_2\\
&= \frac{16}{15\pi}C_{\rm oct}\left(\frac{r_1}{a_1}\right)^3\int_0^{2\pi}\Big[5\big(A_1^3\cos^3(f_2)+3A_1^2A_2\cos^2(f_2)\sin(f_2)+3A_1A_2^2\cos(f_2)\sin^2(f_2)\\
&\quad +A_2^3\sin^3(f_2)\big)-3\big(A_1\cos(f_2)+A_2\sin(f_2)\big)\Big]\Big[1+e_2^2\cos^2(f_2)+2e_2\cos(f_2)\Big]df_2\\
&= \frac{16}{15\pi}C_{\rm oct}\left(\frac{r_1}{a_1}\right)^3\int_0^{2\pi}\Big[10A_1^3e_2\cos^4(f_2)+30A_1A_2^2e_2\cos^2(f_2)\sin^2(f_2)-6A_1e_2\cos^2(f_2)\Big]df_2. \qquad (2.94)
\end{aligned}$$

With Eqs. 2.81 this results in

$$\mathcal{H}'_{\rm oct}(\mathbf{q}',\mathbf{p}')\epsilon^3 = \frac{16}{15}C_{\rm oct}\left(\frac{r_1}{a_1}\right)^3\Big(10A_1^3-6A_1+\frac{1}{2}(15A_1A_2^2-5A_1^3)\Big)e_2. \qquad (2.95)$$

Using a similar calculation as we did to calculate the outer integral in Eq. 2.74, we find for the outer integral in Eq. 2.92:

$$\mathcal{H}_{\rm oct}(\mathbf{q}',\mathbf{p}')\epsilon^3 = e_1e_2C_{\rm oct}\Big[AB_1-10(1-e_1^2)\sin(g_1)\sin(g_2)\cos(i_{\rm tot})\sin^2(i_{\rm tot})\Big], \qquad (2.96)$$

where

$$A = -3e_1^2 - 4 + \frac{5}{2}B\sin^2(i_{\rm tot}), \tag{2.97}$$

and

$$B = 2 + 5e_1^2 - 7e_1^2\cos(2g_1). \tag{2.98}$$

Details of this derivation can be found in appendix A.

2.5.4 Secular Hamiltonian

Combining the results from Sections 2.5.1, 2.5.2 and 2.5.3, we find that the secular Hamiltonian is equal to:

$$\begin{aligned}\mathcal{H} &= -\frac{G_N m_1 m_2}{2a_1} - \frac{G_N m_3 M}{2a_2} - C_{\rm quad}\Big((3\cos^2(i_{\rm tot})-1)(2+3e_1^2) + 15\cos(2g_1)\sin^2(i_{\rm tot})e_1^2\Big) \\ &\quad + e_1 e_2 C_{\rm oct}\Big(AB_1 - 10(1-e_1^2)\sin(g_1)\sin(g_2)\cos(i_{\rm tot})\sin^2(i_{\rm tot})\Big),\end{aligned} \tag{2.99}$$

where

$$\begin{aligned}C_{\rm quad} &= \frac{1}{16}G_N\frac{m_1m_2m_3}{m_1+m_2}\frac{1}{(1-e_2^2)^{3/2}}\frac{a_1^2}{a_2^3}; \\ C_{\rm oct} &= -\frac{15}{64}G_N\frac{m_1m_2m_3(m_1-m_2)}{(m_1+m_2)^2}\frac{a_1^3}{a_2^4}\frac{1}{(1-e_2^2)^{5/2}}; \\ B_1 &= -\cos(g_1)\cos(g_2) - \sin(g_1)\sin(g_2)\cos(i_{\rm tot}); \\ A &= -3e_1^2 - 4 + \frac{5}{2}B\sin^2(i_{\rm tot}); \\ B &= 2 + 5e_1^2 - 7e_1^2\cos(2g_1).\end{aligned} \tag{2.100}$$

Note that Eq. 2.99 can differ a minus sign from the secular Hamiltonian in former research (e.g. Harrington (1968)), because they defined the Hamiltonian that way such that for bound systems $\mathcal{H} > 0$. Note also that the new variables are not exactly equal to Delaunay's elements, but only to first order in ϵ. But we assume that $\epsilon \ll 1$, such that we can treat them as Delaunay's elements.

2.6 Equations of Motion

We will now calculate the Hamiltonian equations of motion. Originally, we had 6 variables l_j, g_j and h_j and 6 conjugate momenta L_j, G_j and H_j for $j = 1, 2$. We lost the dependency on h_j when we substituted $h_1 - h_2 = \pi$. In the secularization process we lost l_j, hence L_j and thus a_j are constants. Note that H_j is not a constant, but dependent on the other variables via Eqs. 2.45 and 2.46. We are not interested in the equation of motion of l_j, because that is a variable that describes the short-term behavior, thus we are left with the variables: g_j and G_j for $j = 1, 2$. In practice, we are only interested in the evolution of g_j and e_j. Using Eqs. 2.40, we find that

$$\frac{\partial e_j}{\partial G_j} = \frac{1}{2e_j}\cdot -2\frac{G_j}{L_j^2} = \frac{e_j^2-1}{e_j G_j}. \tag{2.101}$$

The Hamiltonian equations of motion for g_j and G_j are given by

$$\begin{aligned}\dot{g}_j &= \frac{\partial \mathcal{H}}{\partial G_j}; \\ \dot{G}_j &= -\frac{\partial \mathcal{H}}{\partial g_j}.\end{aligned} \tag{2.102}$$

It follows that the equations of motion for e_j and g_j are given by

$$\begin{aligned}\dot{g}_j &= \frac{\partial \mathcal{H}}{\partial G_j} = \left(\frac{\partial \mathcal{H}_{\rm quad}}{\partial G_j} + \frac{\partial \mathcal{H}_{\rm oct}}{\partial G_j}\right) = \dot{g}_{j,\rm quad} + \dot{g}_{j,\rm oct}; \\ \dot{e}_j &= \frac{\partial e_j}{\partial G_j}\dot{G}_j = -\frac{\partial e_j}{\partial G_j}\frac{\partial \mathcal{H}}{\partial g_j} = \frac{1-e_j^2}{e_j G_j}\left(\frac{\partial \mathcal{H}_{\rm quad}}{\partial g_j} + \frac{\partial \mathcal{H}_{\rm oct}}{\partial g_j}\right) = \dot{e}_{j,\rm quad} + \dot{e}_{j,\rm oct},\end{aligned} \tag{2.103}$$

because $\mathcal{H}_1' = 0$ and $\mathcal{H}_0'$ is a constant.

Note that via Eq. 2.47 $i_{\rm tot}$ is dependent on G_1. From Eq. 2.90 we find that

$$\dot{g}_{1,\rm quad} = \frac{\partial \mathcal{H}_{\rm quad}}{\partial G_1} = \frac{\partial \mathcal{H}_{\rm quad}}{\partial e_1}\frac{\partial e_1}{\partial G_1} + \frac{\partial \mathcal{H}_{\rm quad}}{\partial i_{\rm tot}}\frac{\partial i_{\rm tot}}{\partial G_1}. \tag{2.104}$$

It follows that

$$\begin{aligned}\frac{\partial \mathcal{H}_{\rm quad}}{\partial e_1}\frac{\partial e_1}{\partial G_1} &= -C_{\rm quad}\Big(30\cos(2g_1)\sin^2(i_{\rm tot})e_1 + 6(3\cos^2(i_{\rm tot})-1)e_1\Big)\cdot\frac{e_1^2-1}{e_1 G_1}\\ &= 6\frac{1-e_1^2}{G_1}C_{\rm quad}\Big(5\cos(2g_1)\sin^2(i_{\rm tot}) + 3\cos^2(i_{\rm tot}) - 1\Big),\end{aligned} \tag{2.105}$$

where we used Eq. 2.101. From Eq. 2.47 one finds that

$$\begin{aligned}\frac{\partial i_{\rm tot}}{\partial G_1} &= \frac{-1}{\sqrt{1-\cos^2(i_{\rm tot})}}\frac{2G_1G_2\cdot -2G_1 - (G^2-G_1^2-G_2^2)\cdot 2G_2}{4G_1^2G_2^2}\\ &= \frac{1}{\sin(i_{\rm tot})}\left(\frac{1}{G_2} + \frac{\cos(i_{\rm tot})}{G_1}\right).\end{aligned} \tag{2.106}$$

Hence,

$$\begin{aligned}\frac{\partial \mathcal{H}_{\rm quad}}{\partial i_{\rm tot}}\frac{\partial i_{\rm tot}}{\partial G_1} &= -C_{\rm quad}\Big(30\cos(2g_1)\sin(i_{\rm tot})\cos(i_{\rm tot})e_1^2 - 6\cos(i_{\rm tot})\sin(i_{\rm tot})(2+3e_1^2)\Big)\cdot\frac{1}{\sin(i_{\rm tot})}\left(\frac{1}{G_2}+\frac{\cos(i_{\rm tot})}{G_1}\right)\\ &= -6C_{\rm quad}\Big(5\cos(2g_1)\cos(i_{\rm tot})e_1^2 - \cos(i_{\rm tot})(2+3e_1^2)\Big)\cdot\left(\frac{1}{G_2}+\frac{\cos(i_{\rm tot})}{G_1}\right).\end{aligned} \tag{2.107}$$

Combining all of these, results in

$$\begin{aligned}\dot{g}_{1,\rm quad} &= 6\frac{1-e_1^2}{G_1}C_{\rm quad}\Big(5\cos(2g_1)\sin^2(i_{\rm tot}) + 3\cos^2(i_{\rm tot}) - 1\Big) - 6C_{\rm quad}\Big(5\cos(2g_1)\cos(i_{\rm tot})e_1^2\\ &\quad - \cos(i_{\rm tot})(2+3e_1^2)\Big)\cdot\left(\frac{1}{G_2}+\frac{\cos(i_{\rm tot})}{G_1}\right)\\ &= 6C_{\rm quad}\Big\{\frac{1}{G_1}\Big[(1-e_1^2)\Big(5\cos(2g_1)\sin^2(i_{\rm tot}) + 3\cos^2(i_{\rm tot}) - 1\Big) - 5\cos(2g_1)\cos^2(i_{\rm tot})e_1^2\\ &\quad + \cos^2(i_{\rm tot})(2+3e_1^2)\Big] - \frac{\cos(i_{\rm tot})}{G_2}\left[5\cos(2g_1)e_1^2 - (2+3e_1^2)\right]\Big\}\\ &= 6C_{\rm quad}\Big\{\frac{1}{G_1}\left[4\cos^2(i_{\rm tot}) + \big(5\cos(2g_1)-1\big)\big(1-e_1^2-\cos^2(i_{\rm tot})\big)\right]\\ &\quad + \frac{\cos(i_{\rm tot})}{G_2}\left[2 + e_1^2\big(3-5\cos(2g_1)\big)\right]\Big\}.\end{aligned} \tag{2.108}$$

In the same way, we find that

$$\dot{g}_{2,\rm quad} = \frac{\partial \mathcal{H}_{\rm quad}}{\partial G_2} = \frac{\partial \mathcal{H}_{\rm quad}}{\partial e_2}\frac{\partial e_2}{\partial G_2} + \frac{\partial \mathcal{H}_{\rm quad}}{\partial i_{\rm tot}}\frac{\partial i_{\rm tot}}{\partial G_2}. \tag{2.109}$$

Note that $C_{\rm quad}$ is dependent on e_2 such that with Eq. 2.79:

$$\frac{\partial C_{\rm quad}}{\partial e_2} = 3\frac{e_2 C_{\rm quad}}{1-e_2^2}, \tag{2.110}$$

hence,

$$\begin{aligned}\frac{\partial \mathcal{H}_{\rm quad}}{\partial e_2}\frac{\partial e_2}{\partial G_2} &= -3\frac{e_2 C_{\rm quad}}{1-e_2^2}\Big(15\cos(2g_1)\sin^2(i_{\rm tot})e_1^2 + \big(3\cos^2(i_{\rm tot})-1\big)\big(2+3e_1^2\big)\Big)\cdot\frac{e_2^2-1}{e_2 G_2}\\ &= 3\frac{C_{\rm quad}}{G_2}\Big(15\cos(2g_1)\sin^2(i_{\rm tot})e_1^2 + \big(3\cos^2(i_{\rm tot})-1\big)\big(2+3e_1^2\big)\Big).\end{aligned} \tag{2.111}$$

Because of symmetry, it follows from Eqs. 2.47 and 2.106 that

$$\frac{\partial i_{\rm tot}}{\partial G_2} = \frac{1}{\sin(i_{\rm tot})}\left(\frac{1}{G_1} + \frac{\cos(i_{\rm tot})}{G_2}\right). \tag{2.112}$$

Hence, using Eq. 2.107:

$$\frac{\partial \mathcal{H}_{\rm quad}}{\partial i_{\rm tot}}\frac{\partial i_{\rm tot}}{\partial G_2} = -6C_{\rm quad}\Big(5\cos(2g_1)\cos(i_{\rm tot})e_1^2 - \cos(i_{\rm tot})(2+3e_1^2)\Big)\cdot\left(\frac{1}{G_1} + \frac{\cos(i_{\rm tot})}{G_2}\right). \tag{2.113}$$

And finally, we find from substitution of Eqs. 2.111 and 2.113 in Eq. 2.109:

$$\begin{aligned}
\dot{g}_{2,\rm quad} &= 3\frac{C_{\rm quad}}{G_2}\Big(15\cos(2g_1)\sin^2(i_{\rm tot})e_1^2 + \big(3\cos^2(i_{\rm tot})-1\big)\big(2+3e_1^2\big)\Big) \\
&\quad -6C_{\rm quad}\Big(5\cos(2g_1)\cos(i_{\rm tot})e_1^2 - \cos(i_{\rm tot})(2+3e_1^2)\Big)\cdot\left(\frac{1}{G_1} + \frac{\cos(i_{\rm tot})}{G_2}\right) \\
&= 3C_{\rm quad}\Bigg\{\frac{1}{G_2}\Big[15\cos(2g_1)\sin^2(i_{\rm tot})e_1^2 + \big(3\cos^2(i_{\rm tot})-1\big)\big(2+3e_1^2\big) - 10\cos(2g_1)\cos^2(i_{\rm tot})e_1^2 \\
&\quad +2\cos^2(i_{\rm tot})(2+3e_1^2)\Big] + \frac{2\cos(i_{\rm tot})}{G_1}\left[-5\cos(2g_1)e_1^2 + 2 + 3e_1^2\right]\Bigg\} \\
&= 3C_{\rm quad}\Bigg\{\frac{2\cos(i_{\rm tot})}{G_1}\left[2 + e_1^2(3-5\cos(2g_1))\right] \\
&\quad +\frac{1}{G_2}\Big[4 + 6e_1^2 + \big(5\cos^2(i_{\rm tot})-3\big)\Big(2 + e_1^2\big(3-5\cos(2g_1)\big)\Big)\Big]\Bigg\}.
\end{aligned} \tag{2.114}$$

For $\dot{e}_{1,\rm quad}$ one finds the following equation:

$$\begin{aligned}
\dot{e}_{1,\rm quad} &= \frac{1-e_1^2}{e_1 G_1}\frac{\partial \mathcal{H}_{\rm quad}}{\partial g_1} \\
&= \frac{1-e_1^2}{e_1 G_1}\cdot 30C_{\rm quad}\sin(2g_1)\sin^2(i_{\rm tot})e_1^2 \\
&= 30e_1 C_{\rm quad}\frac{1-e_1^2}{G_1}\sin^2(i_{\rm tot})\sin(2g_1).
\end{aligned} \tag{2.115}$$

Since $\mathcal{H}_{\rm quad}$ is not dependent on g_2:

$$\dot{e}_{2,\rm quad} = \frac{1-e_2^2}{e_2 G_2}\frac{\partial \mathcal{H}_{\rm quad}}{\partial g_2} = 0. \tag{2.116}$$

We can do the same process for the octupole part of the Hamiltonian. We will only give the results, the details are in appendix B. The full equations of motion are:

$$
\begin{cases}
\dot{g}_{1,\mathrm{N}} = & 6C_{\mathrm{quad}}\Big\{ \frac{1}{G_1}\left[4\cos^2(i_{\mathrm{tot}}) + \big(5\cos(2g_1)-1\big)\big(1-e_1^2-\cos^2(i_{\mathrm{tot}})\big)\right] + \frac{\cos(i_{\mathrm{tot}})}{G_2}\left[2+e_1^2\big(3-5\cos(2g_1)\big)\right] \Big\} \\
& -C_{\mathrm{oct}}e_2\Big\{ e_1\left(\frac{1}{G_2}+\frac{\cos(i_{\mathrm{tot}})}{G_1}\right)\Big[\sin(g_1)\sin(g_2)\Big(-A+10(3\cos^2(i_{\mathrm{tot}})-1)(1-e_1^2)\Big)-5BB_1\cos(i_{\mathrm{tot}})\Big] \\
& +\frac{1-e_1^2}{e_1G_1}\left[B_1\big(3A+10\cos^2(i_{\mathrm{tot}})-2\big)-10(1-3e_1^2)\sin(g_1)\sin(g_2)\cos(i_{\mathrm{tot}})\sin^2(i_{\mathrm{tot}})\right] \Big\} \\
\dot{g}_{2,\mathrm{N}} = & 3C_{\mathrm{quad}}\Big\{ \frac{2\cos(i_{\mathrm{tot}})}{G_1}\left[2+e_1^2\big(3-5\cos(2g_1)\big)\right] + \frac{1}{G_2}\left[4+6e_1^2+\Big(5\cos^2(i_{\mathrm{tot}})-3\Big)\Big(2+e_1^2\big(3-5\cos(2g_1)\big)\Big)\right] \Big\} \\
& +C_{\mathrm{oct}}e_1\Big\{ e_2\left\{\sin(g_1)\sin(g_2)\left[A+10(1-e_1^2)(1-3\cos^2(i_{\mathrm{tot}}))\right]+5BB_1\cos(i_{\mathrm{tot}})\right\}\left(\frac{1}{G_1}+\frac{\cos(i_{\mathrm{tot}})}{G_2}\right) \\
& +\left(-\frac{1+4e_2^2}{e_2G_2}\right)\Big[AB_1-10(1-e_1^2)\sin(g_1)\sin(g_2)\cos(i_{\mathrm{tot}})\sin^2(i_{\mathrm{tot}})\Big]\Big\}. \\
\dot{e}_{1,\mathrm{N}} = & 30C_{\mathrm{quad}}e_1\frac{1-e_1^2}{G_1}\sin^2(i_{\mathrm{tot}})\sin(2g_1) + C_{\mathrm{oct}}e_2\frac{1-e_1^2}{G_1}\Big\{A\Big(\sin(g_1)\cos(g_2)-\cos(g_1)\sin(g_2)\cos(i_{\mathrm{tot}})\Big) \\
& +35B_1e_1^2\sin(2g_1)\sin^2(i_{\mathrm{tot}})-10(1-e_1^2)\cos(g_1)\sin(g_2)\cos(i_{\mathrm{tot}})\sin^2(i_{\mathrm{tot}})\Big\} \\
\dot{e}_{2,\mathrm{N}} = & C_{\mathrm{oct}}e_1\frac{1-e_2^2}{G_2}\Big\{A\Big(\cos(g_1)\sin(g_2)-\sin(g_1)\cos(g_2)\cos(i_{\mathrm{tot}})\Big)-10\left(1-e_1^2\right)\sin(g_1)\cos(g_2)\cos(i_{\mathrm{tot}})\sin^2(i_{\mathrm{tot}})\Big\}
\end{cases}
\tag{2.117}
$$

where the N stands for Newtonian. These equations can also be found in e.g. Ford et al. (2000)[1].

Thus we started with the 3-body Hamiltonian and expressed it in the Hamiltonians of two isolated binary systems and perturbations to the Keplerian orbits of both binaries. We neglected all perturbation terms with a factor $\left(\frac{a_1}{a_2}\right)^n$ where $n \geq 4$, transformed to Delaunay's elements and performed a transformation to a Hamiltonian which is not dependent on the mean anomalies l_1 and l_2. From this secular Hamiltonian (Eq. 2.99) the equations of motion (Eqs. 2.117) were derived.

Numerical N-body calculations have shown that for hierarchical triple systems, i.e. for triples such that

$$
\frac{a_2}{a_1} > \frac{2.8}{1-e_2}\left(\left(1+\frac{m_3}{m_1+m_2}\right)\frac{1+e_2}{\sqrt{1-e_2}}\right)^{2/5}\left(1-\frac{0.3}{\pi}i_{\mathrm{tot}}\right) \tag{2.118}
$$

(Aarseth and Mardling, 2001), the description with the equations of motion, Eqs. 2.117, is really good (e.g. Naoz et al. (2011)).

2.7 Post-Newtonian Terms

In deriving the equations of motion (Eqs. 2.117) we only took terms of the Newtonian Hamiltonian into account. Although these equations of motion form an approximation to the mechanics that would follow from Einstein's general relativity theory, it is shown that adding relativity effects qualitatively changes the behavior of systems (Naoz et al., 2012). In the so called Post-Newtonian (PN) approximation, corrections to the Newtonian mechanics are made in powers of $(v/c)^n$ where c is the velocity of light, v is the orbital velocity and n is an integer. In this work, we will include the 1PN and 2.5PN correction terms. The 1PN term is the first correction term and the 2.5PN term represents gravitational radiation loss of the system, further details of both terms can be found in Sections 2.7.1 and 2.7.2.

2.7.1 1PN Correction Term

The 1PN part of the Hamiltonian is (e.g. Schäfer (1987); Naoz et al. (2012)):

$$
\mathcal{H}_{1\mathrm{PN}} = -\frac{1}{8c^2}\sum_{i=1}^{3} m_i\left(\frac{p_i^2}{m_i^2}\right)^2 - \frac{G_N}{4c^2}\sum_{i,i\neq j}\frac{m_im_j}{r_{ij}}\left[6\frac{p_i^2}{m_i^2}-7\frac{\mathbf{p}_i\cdot\mathbf{p}_j}{m_im_j}-\frac{(\mathbf{n}_{ij}\cdot\mathbf{p}_i)(\mathbf{n}_{ij}\cdot\mathbf{p}_j)}{m_im_j}\right]+\frac{G_N^2}{2c^2}\sum_{i,j\neq i,k'\neq i}\frac{m_im_jm_{k'}}{r_{ij}r_{ik'}}, \tag{2.119}
$$

[1] There is a sign error in the equations of Ford et al. (2000) which has been corrected by Blaes et al. (2002). All terms with C_3 in Eqs. (22) and (29)-(32) of their paper should have the opposite sign.

where $\mathbf{r}_{ij}$ is the relative position vector pointing from mass m_i toward m_j and r_{ij} is the magnitude of this vector. Furthermore, $\mathbf{p}_i$ is the momentum vector of mass m_i in an arbitrary plane and p_i is the magnitude of this vector, i, j and k' are indices running from 1 to 3 (corresponding to the masses) and $\mathbf{n}_{ij} = \mathbf{r}_{ij}/r_{ij}$.

A similar process as we did for the Newtonian Hamiltonian can be done for Eq. 2.119 (Naoz et al., 2012): a transformation to the center of mass frame after which the Hamiltonian is expressed in terms of $\frac{a_1}{a_2}$. After that, the short-term effects are eliminated by an application of the Von Zeipel method and this results in the following secular Hamiltonian terms (with order up to $\mathcal{O}\left(\left(\frac{a_1}{a_2}\right)^3\right)$) (Naoz et al., 2012):

$$\mathcal{H}_{\rm 1PN} = \mathcal{H}^{\rm 1PN}_{a_1^{-2}} + \mathcal{H}^{\rm 1PN}_{a_1 a_2} + \mathcal{H}^{\rm 1PN}_{a_2^{-2}} + \mathcal{H}^{\rm 1PN}_{\rm int}, \tag{2.120}$$

where

$$\mathcal{H}^{\rm 1PN}_{a_1^{-2}} = \frac{G_N^2 \mu_{\rm in}(15m_1^2 + 29m_1m_2 + 15m_2^2)}{8a_1^2c^2} + \frac{C_4}{\sqrt{1-e_1^2}}; \tag{2.121}$$

$$\mathcal{H}^{\rm 1PN}_{a_1 a_2} = \frac{G_N^2 m_1m_2m_3\big(2(m_1+m_2)+3m_3\big)}{4a_1a_2c^2(m_1+m_2+m_3)}; \tag{2.122}$$

$$\mathcal{H}^{\rm 1PN}_{a_2^{-2}} = \frac{G_N^2 \mu_{\rm out}\Big(15(m_1+m_2)^2 + 29(m_1+m_2)m_3 + 15m_3^2\Big)}{8a_2^2c^2(m_1+m_2+m_3)} - \frac{3G_N^2(m_1+m_2)m_3(m_1+m_2+m_3)}{a_2^2c^2\sqrt{1-e_2^2}}; \tag{2.123}$$

$$\begin{aligned}\mathcal{H}^{\rm 1PN}_{\rm int} &= C_5\Big\{C_6\sqrt{1-e_1^2}\cos(i_{\rm tot}) + C_7\Big[\Big(1-3\cos^2(i_{\rm tot})\Big)\Big((2-5e_1^2)(m_1^2+m_2^2) - 3(2-e_1^2)m_1m_2\Big) \\ &+ C_8e_1^2\cos(2g_1)\sin^2(i_{\rm tot})\Big]\Big\},\end{aligned} \tag{2.124}$$

and where

$$\begin{aligned} C_4 &= -\frac{3G_N^2m_1m_2(m_1+m_2)}{a_1^2c^2}; \\ C_5 &= \frac{G_N}{4a_2^3c^2(1-e_2^2)^{3/2}(m_1+m_2)}; \\ C_6 &= L_1G_2[8(m_1+m_2)+6m_3]; \\ C_7 &= \frac{a_1G_Nm_1m_2m_3}{8(m_1+m_2)}; \\ C_8 &= 9(m_1^2+m_1m_2+m_2^2); \\ \mu_{\rm in} &= \frac{m_1m_2}{m_1+m_2}; \\ \mu_{\rm out} &= \frac{m_3(m_1+m_2)}{m_1+m_2+m_3}. \end{aligned} \tag{2.125}$$

Not all of these terms influence the evolution of the system. $\mathcal{H}^{\rm 1PN}_{a_1a_2}$ and the first term in $\mathcal{H}^{\rm 1PN}_{a_1^{-2}}$ and $\mathcal{H}^{\rm 1PN}_{a_2^{-2}}$ are only dependent on the masses and semi-major axes, thus there is no dependence on one of the coordinates g_j or e_j for $j = 1, 2$ and that means that these terms do not influence the equations of motion. The second terms in $\mathcal{H}^{\rm 1PN}_{a_1^{-2}}$ and in $\mathcal{H}^{\rm 1PN}_{a_2^{-2}}$ influence the time derivative of g_1 and g_2 via the dependence on e_1 and e_2 respectively. The time derivatives of g_j for $j = 1, 2$ that follow from Eqs. 2.121 and 2.123 are (Naoz et al., 2012)[2]:

$$\begin{aligned}\dot{g}_{1,a_1^{-2}} &= \frac{3G_N^{3/2}(m_1+m_2)^{3/2}}{a_1^{5/2}c^2(1-e_1^2)}; \\ \dot{g}_{2,a_2^{-2}} &= \frac{3G_N^{3/2}(m_1+m_2+m_3)^{3/2}}{a_2^{5/2}c^2(1-e_2^2)}.\end{aligned} \tag{2.126}$$

Note that both expressions in Eq. 2.126 are strictly positive, this is an 1PN effect which is called GR precession. The 1PN term causes that oscillation around a certain value of g_j is less possible. The interaction term, $\mathcal{H}^{\rm 1PN}_{\rm int}$ is

[2] Both Eqs. (35) and (36) in Naoz et al. (2012) should have the opposite sign.

for most systems we will consider negligible. In Naoz et al. (2012) the parameter space is given where this term is important, but the systems we simulated are outside of this parameter space. The time derivative of the eccentricity that follows from $\mathcal{H}_{\rm 1PN}$ is equal to:

$$\dot{e}_{1,\rm 1PN} = -\frac{9a_1e_1\sqrt{1-e_1^2}G_N^2m_1m_2m_3(m_1^2+m_1m_2+m_2^2)\sin^2(i_{\rm tot})\sin(2g_1)}{16a_2^3c^2(1-e_2^2)^{3/2}L_1(m_1+m_2)^2} \tag{2.127}$$

(Naoz et al., 2012); we will need this expression in section 4.2.

The Hamiltonian, including the 1PN term, is conserved during the evolution of the system.

2.7.2 2.5PN Correction Term

We will follow Blaes et al. (2002) and add the 2.5PN correction terms for a two-body system to the equations of motion of the inner binary in Eqs. 2.117. These terms are:

$$\begin{aligned}
\dot{a}_{1,\rm 2.5PN} &= -\frac{64G_N^3m_1m_2(m_1+m_2)}{5c^5a_1^3(1-e_1^2)^{7/2}}\left(1+\frac{73}{24}e_1^2+\frac{37}{96}e_1^4\right); \\
\dot{e}_{1,\rm 2.5PN} &= -\frac{304G_N^3m_1m_2(m_1+m_2)e_1}{15c^5a_1^4(1-e_1^2)^{5/2}}\left(1+\frac{121}{304}e_1^2\right);
\end{aligned} \tag{2.128}$$

(Peters, 1964). Similar correction terms can be given for the outer binary:

$$\begin{aligned}
\dot{a}_{2,\rm 2.5PN} &= -\frac{64G_N^3m_3(m_1+m_2)(m_1+m_2+m_3)}{5c^5a_2^3(1-e_2^2)^{7/2}}\left(1+\frac{73}{24}e_2^2+\frac{37}{96}e_2^4\right); \\
\dot{e}_{2,\rm 2.5PN} &= -\frac{304G_N^3m_3(m_1+m_2)(m_1+m_2+m_3)e_2}{15c^5a_2^4(1-e_2^2)^{5/2}}\left(1+\frac{121}{304}e_2^2\right).
\end{aligned} \tag{2.129}$$

Most hierarchical triples are so wide that these terms are negligible, but for completeness we incorporate them.

The terms, Eqs. 2.128, represent gravitational radiation carried away from the system. Since a_1 decreases during the evolution, it follows from Eq. 2.16 that the energy of the inner orbit decreases. Note that $\dot{a}_{1,\rm 2.5PN}$ depends strongly on the eccentricity: $-\dot{a}_{1,\rm 2.5PN}$ becomes very large when e_1 approaches 1. Thus, the Hamiltonian including these terms is not conserved during the evolution.

Chapter 3

Simulation Equations of Motion

The equations of motion, Eqs. 2.117, can only be solved analytically if we only take into account the quadrupole terms and consider them in the limit $\frac{L_1}{L_2} \to 0$. In general, these equations and including the 1PN and 2.5PN terms have to be calculated numerically. We used the following system of differential equations:

$$\begin{cases} \dot{g}_1 & = \dot{g}_{1,\mathrm{N}} + \dot{g}_{1,1\mathrm{PN}} \\ \dot{g}_2 & = \dot{g}_{2,\mathrm{N}} + \dot{g}_{2,1\mathrm{PN}} \\ \dot{e}_1 & = \dot{e}_{1,\mathrm{N}} + \dot{e}_{1,2.5\mathrm{PN}} \\ \dot{e}_2 & = \dot{e}_{2,\mathrm{N}} + \dot{e}_{2,2.5\mathrm{PN}} \\ \dot{a}_1 & = \dot{a}_{1,2.5\mathrm{PN}} \\ \dot{a}_2 & = \dot{a}_{2,2.5\mathrm{PN}} \\ \cos(\dot{i}_{\mathrm{tot}}) & = \frac{-1}{G_1 G_2}\left[\dot{G}_{1,\mathrm{N}}\left(G_1 + G_2\cos(i_{\mathrm{tot}})\right) + \dot{G}_{2,\mathrm{N}}\left(G_2 + G_1\cos(i_{\mathrm{tot}})\right)\right] \end{cases} \tag{3.1}$$

where $\dot{g}_{1,\mathrm{N}}$, $\dot{g}_{2,\mathrm{N}}$, $\dot{e}_{1,\mathrm{N}}$ and $\dot{e}_{2,\mathrm{N}}$ are given by Eqs. 2.117, $\dot{e}_{1,2.5\mathrm{PN}}$ and $\dot{a}_{1,2.5\mathrm{PN}}$ by Eqs. 2.128, $\dot{e}_{2,2.5\mathrm{PN}}$ and $\dot{a}_{2,2.5\mathrm{PN}}$ by Eqs. 2.129 and $\dot{g}_{1,1\mathrm{PN}}$ and $\dot{g}_{2,1\mathrm{PN}}$ by Eqs. 2.126. We did not include the time derivatives that follow from $\mathcal{H}_{\mathrm{int}}^{1\mathrm{PN}}$, but for the systems we simulated this term is not important.

The expression for $\cos(\dot{i}_{\mathrm{tot}})$ in Eqs. 3.1 can be found as follows. We know from Eq. 2.47 that

$$\cos(i_{\mathrm{tot}}) = \frac{G^2 - G_1^2 - G_2^2}{2G_1G_2}, \tag{3.2}$$

thus

$$\dot{G}_1 G_2\cos(i_{\mathrm{tot}}) + G_1\dot{G}_2\cos(i_{\mathrm{tot}}) + G_1G_2\cos(\dot{i}_{\mathrm{tot}}) = G\dot{G} - G_1\dot{G}_1 - G_2\dot{G}_2. \tag{3.3}$$

If we neglect the 2.5PN terms for the outer orbit (they are negligible), only G and G_1 are affected by gravitational radiation. G_1 also changes because of the Newtonian terms in the equations of motion, while G does not. Thus, we can write $\dot{G}_1 = \dot{G}_{1,2.5\mathrm{PN}} + \dot{G}_{1,\mathrm{N}}$ and $G\dot{G} = G\dot{G}_{2.5\mathrm{PN}} = \dot{G}_{1,2.5\mathrm{PN}}G_2\cos(i_{\mathrm{tot}}) + G_1\dot{G}_{1,2.5\mathrm{PN}}$ where the subscript 2.5PN refers to the time derivative as result of gravitational radiation and N to the Newtonian terms. Inserting these relations in Eq. 3.3 yields

$$\begin{aligned} \left(\dot{G}_{1,2.5\mathrm{PN}} + \dot{G}_{1,\mathrm{N}}\right)G_2\cos(i_{\mathrm{tot}}) + G_1\dot{G}_2\cos(i_{\mathrm{tot}}) + G_1G_2\cos(\dot{i}_{\mathrm{tot}}) &= \dot{G}_{1,2.5\mathrm{PN}}G_2\cos(i_{\mathrm{tot}}) + G_1\dot{G}_{1,2.5\mathrm{PN}} \\ &\quad -G_1\left(\dot{G}_{1,2.5\mathrm{PN}} + \dot{G}_{1,\mathrm{N}}\right) - G_2\dot{G}_2, \end{aligned} \tag{3.4}$$

or

$$\dot{G}_{1,\mathrm{N}}G_2\cos(i_{\mathrm{tot}}) + G_1\dot{G}_2\cos(i_{\mathrm{tot}}) + G_1G_2\cos(\dot{i}_{\mathrm{tot}}) = -G_1\dot{G}_{1,\mathrm{N}} - G_2\dot{G}_2, \tag{3.5}$$

from which we can conclude:

$$\begin{aligned} \cos(\dot{i}_{\mathrm{tot}}) &= \frac{-G_1\dot{G}_{1,\mathrm{N}} - G_2\dot{G}_2 - \dot{G}_{1,\mathrm{N}}G_2\cos(i_{\mathrm{tot}}) - G_1\dot{G}_2\cos(i_{\mathrm{tot}})}{G_1G_2} \\ &= \frac{-1}{G_1G_2}\left[\dot{G}_{1,\mathrm{N}}\left(G_1 + G_2\cos(i_{\mathrm{tot}})\right) + \dot{G}_2\left(G_2 + G_1\cos(i_{\mathrm{tot}})\right)\right]. \end{aligned} \tag{3.6}$$

This is the last derivative in Eqs. 3.1.

We have done the integration of the system 3.1 using the Boost odeint libraries implemented in AMUSE (Hamers, 2012). AMUSE (Portegies Zwart et al., 2009, 2013), the Astrophysical Multi-purpose Software Environment, combines codes that are written for different purposes into one framework[1]. The integration parameters, we could adapt are the relative and absolute tolerance, the snapshot time step: the time after which the library reported to the script, the initial integration time step, the time from which the integration started and the end time of the integration. The integrator adapted the integration time step internally using the snapshot time step as the maximum possible value.

After each snapshot we checked for a merger of the inner binary by comparing $a_1(1-e_1)$, the distance at periastron, with R_1+R_2 where $R_1=\frac{2G_N m_1}{c^2}$ and $R_2=\frac{2G_N m_2}{c^2}$ are the Schwarzschild radii of mass 1 and mass 2 respectively. When $R_1+R_2>a_1(1-e_1)$, the inner binary is merged. As we will see in Sec. 3.1, short before the merger a_1 decreases very fast. To be sure that the merger time we found was precise enough, we adapted the snapshot time during the evolution. For most systems, we started with as snapshot time step dt the Kozai timescale (the timescale of the oscillations in the eccentricity that we mentioned in the Introduction):

$$T_{\rm K}=1.3\times10^5{\rm yr}\left(\frac{m_1+m_2}{2\times10^6{\rm M_{Sun}}}\right)^{-1/2}\left(\frac{a_1}{10^{-2}{\rm pc}}\right)^{3/2}\left(\frac{m_1+m_2}{2m_3}\right)\left(\frac{a_2}{10a_1}\right)^3(1-e_2^2)^{3/2} \tag{3.7}$$

(e.g. Holman et al. (1997); Blaes et al. (2002)). For some systems we used a smaller initial time step to make sure that the plots we produced had a resolution that was high enough. Denote a certain snapshot by the natural number n. For the snapshot time step we used $dt_{n+1}=dt_n\left(1-\frac{a_{1,n}-a_{1,n-1}}{5a_{1,n-1}}\right)$. As merger time we used $t_{\rm end}+dt_{\rm end}/2$, where 'end' refers to the last snapshot before the merger.

[1] www.amusecode.org

3.1 Examples

We will treat two examples of hierarchical triples to get a better understanding of the physics. For the first example we use a system with $m_1 = m_2 = 10^4$ M_{Sun}, $m_3 = 10^6$ M_{Sun}, $a_1 = 10^{-3}$ pc, $a_2 = 80a_1$, $e_1 = 0.1$, $e_2 = 0.5$, $i_{tot} = 88$ deg, $g_1 = 0$ and $g_2 = \pi$. Note that for this system the octupole term disappears (i.e. $m_1 = m_2$). In Fig. 3.1 we show the evolution of a_1, e_1, e_2, g_1, g_2 and i_{tot} of this system during the first 0.3 Myr. For this system, we find oscillations in the eccentricity of the inner orbit; although we started with $e_1 = 0.1$, the eccentricity reaches values $e_1 > 1 - 10^{-2}$. This mechanism is called the Kozai mechanism, e.g. Kozai (1962). Since eccentricities close to 1 are reached, a_1 changes significantly (see Eq. 2.128) and that can be seen in Fig. 3.1 upper left. The eccentricity of the outer orbit e_2 is not affected by the 1PN terms and is affected by the Newtonian terms only to octupole order (Eqs. 2.117). This explains why e_2 does not change: for this system the octupole term is zero. We find circular motion in g_1 and g_2: $\frac{dg_1}{dt}, \frac{dg_2}{dt} > 0$ at all times. We find oscillations in the evolution of i_{tot} with the same period as for e_1. This follows from Eq. 2.47: $\cos(i_{tot})$ is equal to an expression in which the only significantly changing variable on small timescales is e_1.

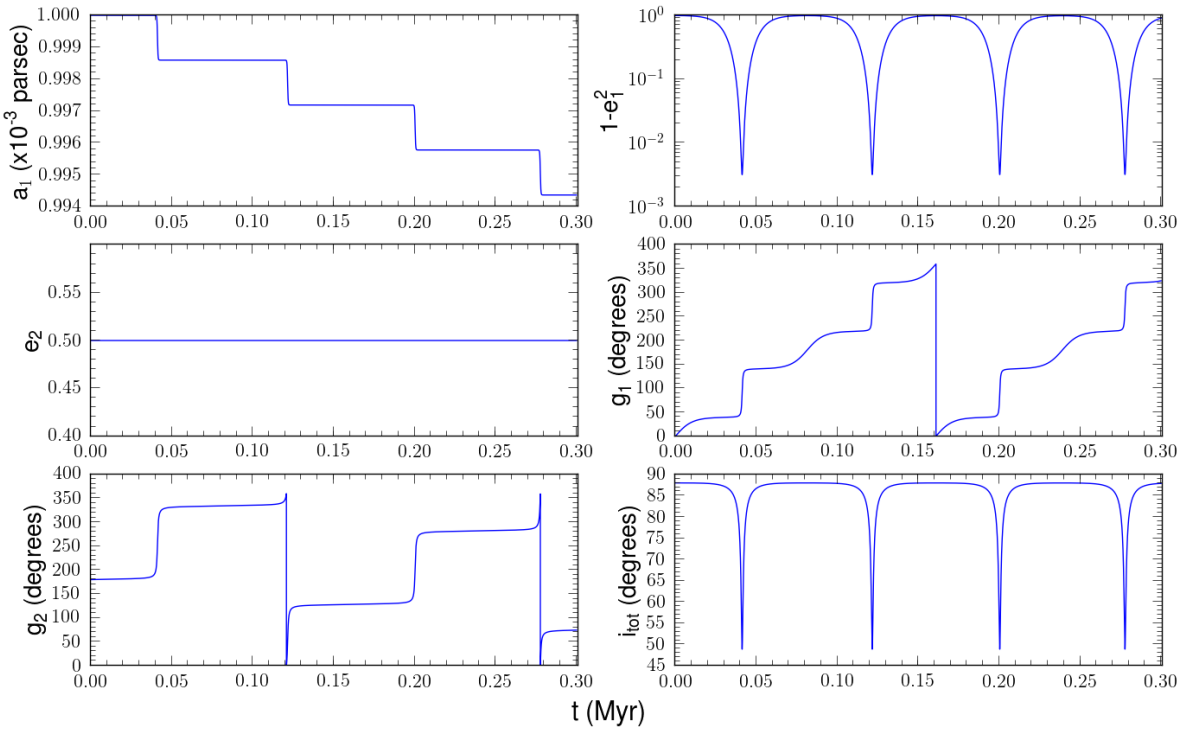

Figure 3.1: Evolution of a_1, e_1, e_2, g_1, g_2 and i_{tot} during the first 0.3 Myr of a system with $m_1 = m_2 = 10^4$ M_{Sun}, $m_3 = 10^6$ M_{Sun}, $a_1 = 10^{-3}$ pc, $a_2 = 80a_1$, $e_1 = 0.1$, $e_2 = 0.5$, $i_{tot} = 88$ deg, $g_1 = 0$ and $g_2 = \pi$.

In Fig. 3.2 the evolution of a_1, e_1, g_1 and i_{tot} is plotted until the inner binary merges. We conclude that the maximum eccentricity of the Kozai cycles remains nearly constant during the evolution. This does not happen for all systems, although for most pure quadrupole systems ($m_1 = m_2$) the evolution is non-chaotic, just like we find for this system. We can see the influence of the general relativistic periastron precession in the the evolution of g_1 because the plot becomes denser near the time the inner binary merges. As can be seen from Eqs. 2.126, $\dot{g}_1$ increases when a_1 decreases and that is what we see in Fig. 3.2 (bottom left). From the plot of the evolution of i_{tot} we conclude that just before the merger, the inclination becomes fixed. This is explained by noticing that just before the merger the gravitational radiation is dominant with respect to the Newtonian and 1PN terms. The total inclination is the angle between the angular momentum vectors of both orbits. Due to the radiation, only the length of the angular momentum of the inner orbit changes, but not its direction. Thus just before the merger, the total inclination does not change anymore.

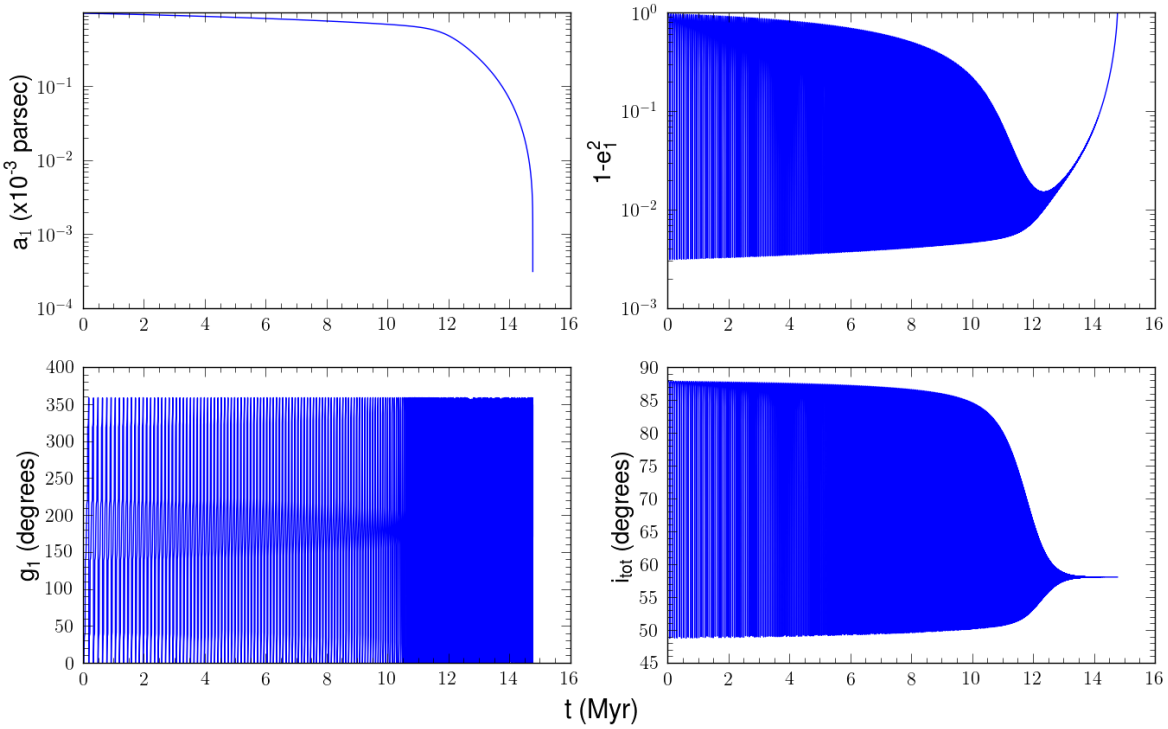

Figure 3.2: Evolution of a_1, e_1, g_1 and $i_{\rm tot}$ of the same system as in Fig. 3.1, but now for the whole evolution until the inner binary merges.

For systems where $m_1 \neq m_2$, the octupole term in the Hamiltonian is not equal to zero. That the evolution of the orbital parameters can change by this octupole term is shown in Fig. 3.3. In that figure the evolution is shown of a_1, e_1, e_2, g_1, g_2 and $i_{\rm tot}$ during the first 2 Myr of a system with $m_1 = 10^4$ $\rm M_{Sun}$, $m_2 = 5 \cdot 10^4$ $\rm M_{Sun}$, $m_3 = 10^6$ $\rm M_{Sun}$, $a_1 = 10^{-3}$ pc, $a_2 = 60a_2$, $e_1 = 0.1$, $e_2 = 0.6$, $i_{\rm tot} = 88$ deg, $g_1 = 0$ and $g_2 = \pi$. If we compare the evolution of e_1 of both examples, we find a difference. For the pure quadrupole system, the maximum eccentricity of the cycles remained equal during the evolution, but for this system we find a common envelope. In general, for systems with $m_1 \neq m_2$, the evolution of e_1 and $i_{\rm tot}$ is more chaotic than for systems with $m_1 = m_2$. Other examples of octupole systems are shown below, in Figs. 4.4a and 4.4b, which will be discussed in Sec. 4.2.7.2.

The evolution of a_1, e_1, g_1 and $i_{\rm tot}$ of this system during the whole time before the merger of the inner binary is shown in Fig. 3.4. We find that the common envelope in the eccentricity evolution disappears; this does not happen for all systems where $m_1 \neq m_2$.

We want to emphasize that we do not find oscillations in the eccentricity of the inner orbit for all triple systems. Obviously, when a_2/a_1 becomes very large, a triple can be treated as two independent binaries in which we do not have this oscillation.

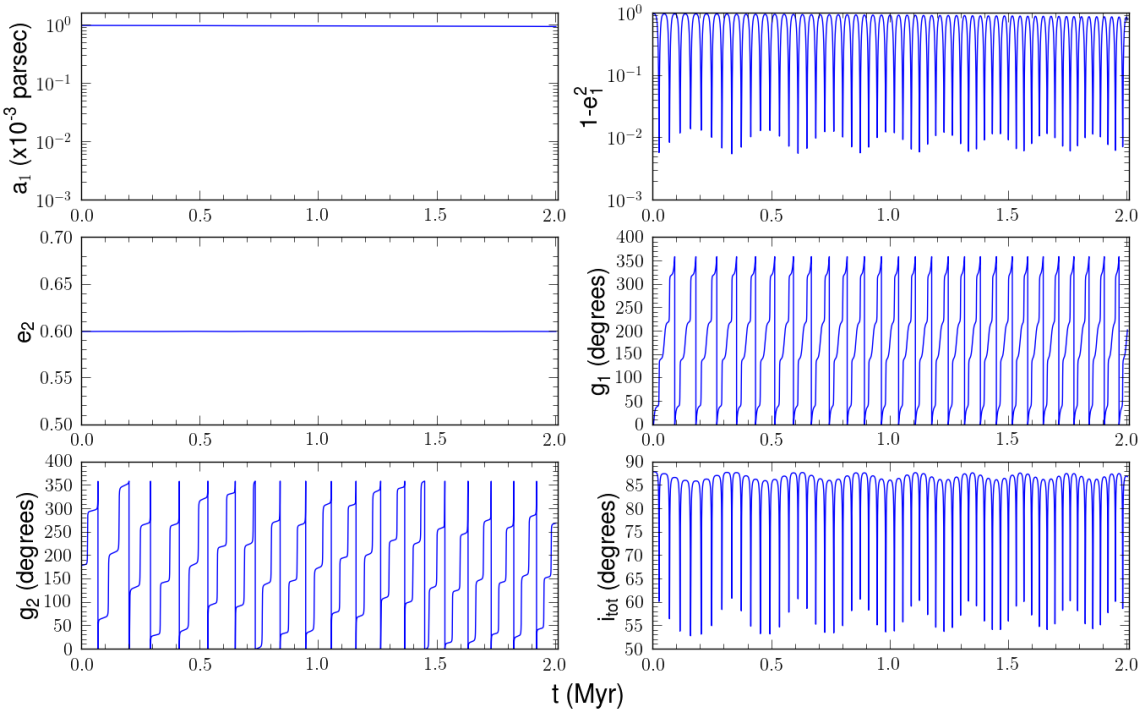

Figure 3.3: Evolution of a_1, e_1, e_2, g_1, g_2 and $i_{\rm tot}$ during the first 2 Myr of a system with $m_1 = 10^4$ $\mathrm{M_{Sun}}$, $m_2 = 5 \cdot 10^4$ $\mathrm{M_{Sun}}$, $m_3 = 10^6$ $\mathrm{M_{Sun}}$, $a_1 = 10^{-3}$ pc, $a_2 = 60a_2$, $e_1 = 0.1$, $e_2 = 0.6$, $i_{\rm tot} = 88$ deg, $g_1 = 0$ and $g_2 = \pi$.

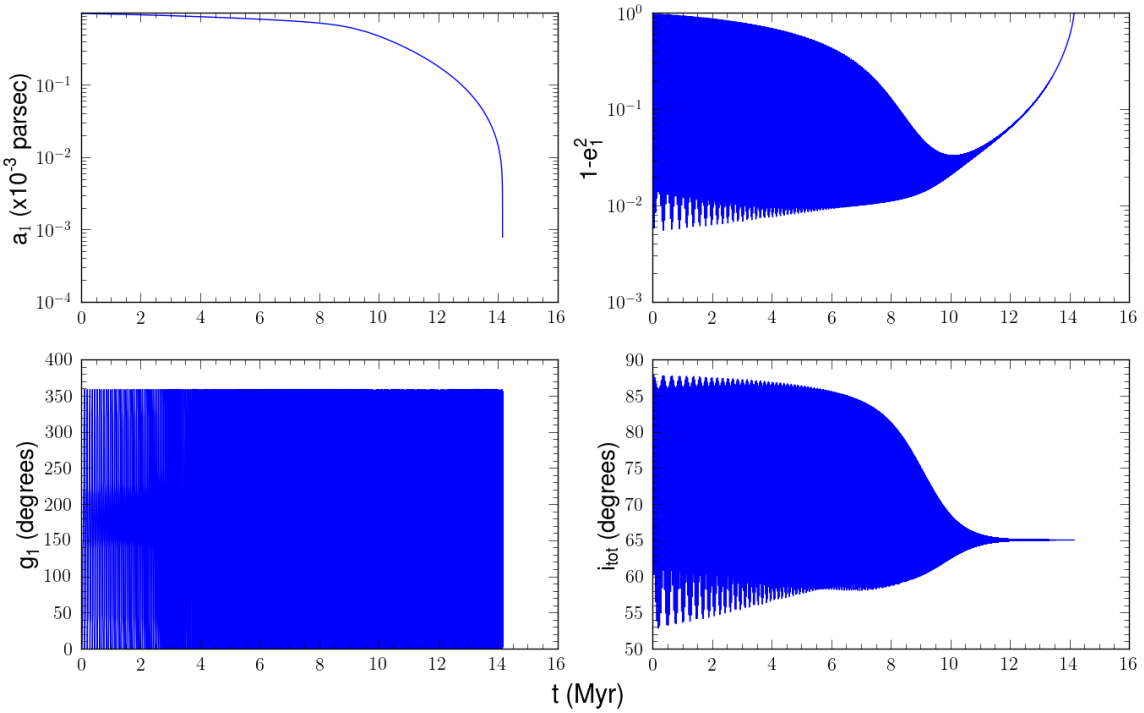

Figure 3.4: Evolution of a_1, e_1, g_1 and $i_{\rm tot}$ of the same system as in Fig. 3.3, but now for the whole evolution until the inner binary merges.

Chapter 4

Merger Time Inner Binary

4.1 Merger Time Isolated Binary

Because of gravitational radiation an isolated binary, consisting of point masses, moving in an elliptical orbit will loose energy. For such a system $a = -G_N m_1 m_2/(2E)$ (Eq. 2.16), hence eventually, the masses will merge. A formula for the merger time has been derived by Peters (1964):

$$t_{\rm merge,p}(e_1, a_1) = \frac{12}{19}\frac{1}{\beta}\left(\frac{a_1(1-e_1^2)}{e_1^{12/19}[1+\frac{121}{304}e_1^2]^{870/2299}}\right)^4 \int_0^{e_1}(1+\frac{121}{304}x^2)^{1181/2299}\frac{x^{29/19}}{(1-x^2)^{3/2}}dx, \tag{4.1}$$

where

$$\beta = \frac{64}{5}\frac{G_N^3 m_1 m_2(m_1+m_2)}{c^5}. \tag{4.2}$$

Peters found this formula by expanding the field equations of general relativity in powers of the gravitational coupling constant, yielding conservation laws for energy and angular momentum. From these laws, he found the loss of energy and angular momentum of a system due to gravitational radiation. This was applied to a bound system of two point masses moving in elliptical orbits. He derived expressions for the secular time derivatives of the semi-major axis and the eccentricity. By integrating these formulas, Eq. 4.1 is found.

For small e_1 we can ignore the factors e_1^2 and the formula reduces to

$$\begin{aligned} t_{\rm merge,p}(e_1, a_1) &\approx \frac{12}{19}\frac{1}{\beta}\left(\frac{a_1(1-e_1^2)}{e_1^{12/19}}\right)^4 \int_0^{e_1} x^{29/19}dx \\ &\approx \frac{1}{4}\frac{1}{\beta}\left(\frac{a_1(1-e_1^2)}{e_1^{12/19}}\right)^4 e_1^{48/19} \\ &\approx \frac{1}{4}\frac{1}{\beta}a_1^4(1-e_1^2)^4. \end{aligned} \tag{4.3}$$

For e_1 near 1 Eq. 4.1 becomes

$$t_{\rm merge,p}(e_1, a_1) \approx \frac{12}{19}\cdot\frac{304}{425}\frac{a_1^4}{\beta}(1-e_1^2)^4\int_0^{e_1}\frac{1}{(1-x^2)^{3/2}}dx \approx \frac{192}{425}\frac{a_1^4}{\beta}(1-e_1^2)^{7/2}. \tag{4.4}$$

Note the strong dependence of $t_{\rm merge,p}$ on e_1: if e_1 approaches 1, the merger time strongly decreases. We could have concluded that already from the first equation in Eqs. 2.128 which is the time derivative of a_1.

4.2 Merger Time Inner Binary in Hierarchical Triples

In Sec. 3.1 we have seen that for triple systems we can have oscillations in the time evolution of the eccentricity of the inner orbit: the Kozai effect. Due to this effect, eccentricities much larger than the initial eccentricity can be reached. From Eq. 2.128 we find that a_1 decreases much faster than would be the case if e_1 was constant. In

the limit of $a_2 \gg a_1$ the Kozai effect will be destroyed by general relativistic periastron precession and the inner binary will merge in the same time as would be the case without the tertiary. In this limit we can use the formula of Peters to calculate the merger time. We will also use this formula to approximate the merger time for triples where the Kozai mechanism is important. Because Eq. 4.1 is strongly dependent on the initial eccentricity, we will use the maximum eccentricity reached during the first Kozai cycles as initial value for e_1. Since Eq. 4.1 is meant for binaries which have a constant eccentricity, the merger time found this way is only correct if the eccentricity of this system does not deviate from the maximum eccentricity. When the system is at smaller eccentricity the rate gravitational radiation is radiated is smaller such that the real merger time is larger than the value found when we use the maximum eccentricity as initial value. To correct for this effect we will add a correction factor. The formula we will use for the merger time of the inner binary in a triple is of the following form:

$$t_{\rm estimate} = f\left(e_{1,\rm min}, e_{1,\rm max}\right) \cdot t_{\rm merge,p}(e_{1,\rm max}, a_1), \tag{4.5}$$

where f is the correction factor depending on the maximum eccentricity $e_{1,\rm max}$ and minimum eccentricity $e_{1,\rm min}$ reached during the first Kozai cycles. The dependence of f on $e_{1,\rm max}$ and $e_{1,\rm min}$ will be explained below. This way of calculating the merger time will henceforth be denoted by the fast method, because it is much faster than integration of the equations of motion. We will fit two different forms of f to merger times obtained by numerical integration of the equations of motions of triples; details of these fits can be found in Sec. 4.2.7. The two different forms we will use, will be denoted by fit 1 and fit 2. For fit 1 the form of f is:

$$f\left(e_{1,\rm min}, e_{1,\rm max}\right) = \left(\frac{1-e_{1,\rm max}^2}{1-e_{1,\rm min}^2}\right)^b, \tag{4.6}$$

where b is a constant. The factor $\frac{1-e_{1,\rm max}^2}{1-e_{1,\rm min}^2} < 1$ and $t_{\rm merge,p}(e_{1,\rm max}, a_1)$ is too small, hence, we expect b to be negative. Peter's formula is divided by $(1-e_{1,\rm max}^2)^{-b}$ to reduce the importance of the eccentricity part. It is multiplied by $(1-e_{1,\rm min}^2)^{-b}$ for two reasons. First, because of the strong dependence of Eq. 4.1 on the eccentricity, the merger time increases with decreasing minimum eccentricity. Second, when the Kozai effect is negligible, $e_{1,\rm max} = e_{1,\rm min}$ and the correction factor should be 1 to give the correct merger time.

Although the correction factor we use for fit 1 seems very natural, there is no evidence that this factor has the correct form. That is the reason that for fit 2, we add an extra fitting parameter to get a little bit more freedom. We will use

$$f\left(e_{1,\rm min}, e_{1,\rm max}\right) = 1 - a + a\left(\frac{1-e_{1,\rm max}^2}{1-e_{1,\rm min}^2}\right)^b. \tag{4.7}$$

Note that still $f(x,x) = 1$ as should be the case.

The correction formula mentioned in former research (e.g. Blaes et al. (2002) and Thompson (2011)), is the formula of Peters divided by $\sqrt{1-e_{1,\rm max}^2}$, thus we are using slightly different correction factors.

We are faced with two problems now: first, we need to find expressions for the minimum and maximum eccentricity and second, we have to find the correct values of the fitting parameters.

To calculate the maximum and minimum eccentricity reached during the first Kozai cycles, we will follow Wen (2003). We take the Hamiltonian up to quadrupole order and including the 1PN terms. For completeness, we also include the 1PN coupling term, although in most cases its influence is negligible. Note that at quadrupole order e_2, g_2, a_1 and a_2 are constant, so the only parameters left are g_1 and e_1. We are free to subtract a constant from the Hamiltonian. Thus using the non-constant terms in Eqs. 2.99 and 2.120, and $\epsilon = 1 - e_1^2$, we can write:

$$\begin{aligned}
\mathcal{H} \;=\; & -C_{\rm quad}\Big\{\left(2+3e_1^2\right)\left(3\cos^2(i_{\rm tot})-1\right)+15e_1^2\sin^2(i_{\rm tot})\cos(2g_1)\Big\}+\frac{C_4}{\sqrt{1-e_1^2}}+C_5\Big\{C_6\sqrt{\epsilon}\cos(i_{\rm tot}) \\
& +C_7\Big[\Big(1-3\cos^2(i_{\rm tot})\Big)\Big((2-5e_1^2)(m_1^2+m_2^2)-3(2-e_1^2)m_1m_2\Big)+C_8e_1^2\cos(2g_1)\sin^2(i_{\rm tot})\Big]\Big\} \\
=\; & -C_{\rm quad}\Big\{(5-3\epsilon)(3\cos^2(i_{\rm tot})-1)+15(1-\epsilon)\sin^2(i_{\rm tot})\cos(2g_1)\Big\}+\frac{C_4}{\sqrt{\epsilon}}+C_5\Big\{C_6\sqrt{\epsilon}\cos(i_{\rm tot}) \\
& +C_7\Big[\Big(1-3\cos^2(i_{\rm tot})\Big)\Big((5\epsilon-3)(m_1^2+m_2^2)-3(1+\epsilon)m_1m_2\Big)+C_8(1-\epsilon)\cos(2g_1)\sin^2(i_{\rm tot})\Big]\Big\},
\end{aligned} \tag{4.8}$$

where $C_{\rm quad}$, C_4, C_5, C_6, C_7 and C_8 are the same constants defined in Eqs. 2.100 and 2.125.

Using the sum of Eq. 2.127 and the quadrupole part of $\dot{e}_{1,\rm N}$ in Eqs. 2.117 (we neglect the 2.5PN term), we see that an extremum of e_1 occurs in one of the following cases: $e_1 = 0$, $e_1 = 1$, $\cos^2(i_{\rm tot}) = 1$ or $\sin(2g_1) = 0$.

$e_1 = 0$ and $e_1 = 1$ are fixed points of this differential equation, so this situation will only occur if you start with exactly these values and that is physical impossible. Using Eq. 2.47 we see that $\cos^2(i_{\rm tot}) = 1$ also gives fixed points for e_1 and thus physically impossible situations. The only possibility left is $\sin(2g_1) = 0$ and that corresponds to $2g_1 = k\pi$ for $k \in \mathbb{Z}$. Because we are neglecting the gravitational wave part of the Hamiltonian, it is a constant of motion, thus we can equate its value at arbitrary times with the initial value $\mathcal{H}_0$. To find the minimum and maximum eccentricity, we substitute the values $2g_1 = k\pi$ in the Hamiltonian and equate this with $\mathcal{H}_0$. Solving this equation for e_1 results in possible extrema of the eccentricity. The smallest solution above e_1 is the maximum eccentricity and the largest below e_1 is the minimum eccentricity. If we include gravitational radiation, these minimum and maximum eccentricity are only the extrema of e_1 during the first Kozai cycles, because for most systems, on small timescales we can neglect the loss of energy by this radiation and consider the energy to be constant. On larger timescales the energy loss becomes significant and the extrema of the eccentricity change. For some systems gravitational radiation is already important during the first Kozai cycles such that the minimum and maximum eccentricity, found in the way described above, are not correct. In Sec. 4.2.5, we will describe a method to find the extrema of the eccentricity for such systems.

We will now substitute the values $2g_1 = k\pi$ in the Hamiltonian, Eq. 4.8. We see that the Hamiltonian is only dependent on $\cos(2g_1)$, hence we will treat the cases $2g_1 = 2k\pi$ and $2g_1 = \pi + 2k\pi$ separately. It will appear that for most systems with circular motion in the $g_1 - e_1$ space (the time derivative of g_1 does not change sign), the former case corresponds to the minimum and the latter case to the maximum eccentricity.

4.2.1 Maximum Eccentricity

In this case $2g_1 = \pi + 2k\pi$. Substituting this value in Eq. 4.8, we find

$$\begin{aligned}\mathcal{H}_{\rm max} &= -C_{\rm quad}\Big\{(5-3\epsilon)(3\cos^2(i_{\rm tot})-1) - 15(1-\epsilon)\sin^2(i_{\rm tot})\Big\} + \frac{C_4}{\sqrt{\epsilon}} + C_5\Big\{C_6\sqrt{\epsilon}\cos(i_{\rm tot}) \\ &\quad + C_7\Big[\Big(1-3\cos^2(i_{\rm tot})\Big)\Big((5\epsilon-3)(m_1^2+m_2^2) - 3(1+\epsilon)m_1m_2\Big) - C_8(1-\epsilon)\sin^2(i_{\rm tot})\Big]\Big\} \\ &= Z_1^\pi\cos^2(i_{\rm tot}) + Z_2^\pi\epsilon\cos^2(i_{\rm tot}) + Z_3^\pi\epsilon + C_4\epsilon^{-1/2} + C_5C_6\sqrt{\epsilon}\cos(i_{\rm tot}) + Z_4^\pi, \end{aligned} \tag{4.9}$$

where we defined:

$$\begin{aligned} Z_1^\pi &= -30C_{\rm quad} + 18C_5C_7(m_1^2+m_1m_2+m_2^2); \\ Z_2^\pi &= 24C_{\rm quad} - 24C_5C_7(m_1^2+m_2^2); \\ Z_3^\pi &= -18C_{\rm quad} + 14C_5C_7(m_1^2+m_2^2) + 6C_5C_7m_1m_2; \\ Z_4^\pi &= 20C_{\rm quad} - 12C_5C_7(m_1^2+m_1m_2+m_2^2). \end{aligned} \tag{4.10}$$

The superscript π refers to the value of $2g_1$ that we find for $k = 0$. Using the equation for the cosine of the total inclination, Eq. 2.47, we find that

$$\begin{aligned}\mathcal{H}_{\rm max} &= Z_1^\pi\left(\frac{G^4}{4L_1^2G_2^2\epsilon} + \frac{L_1^2\epsilon}{4G_2^2} + \frac{G_2^2}{4L_1^2\epsilon} - \frac{G^2}{2G_2^2} - \frac{G^2}{2L_1^2\epsilon} + \frac{1}{2}\right) + Z_2^\pi\epsilon\Big(\frac{G^4}{4L_1^2G_2^2\epsilon} + \frac{L_1^2\epsilon}{4G_2^2} + \frac{G_2^2}{4L_1^2\epsilon} - \frac{G^2}{2G_2^2} \\ &\quad - \frac{G^2}{2L_1^2\epsilon} + \frac{1}{2}\Big) + Z_3^\pi\epsilon + C_4\epsilon^{-1/2} + C_5C_6\sqrt{\epsilon}\left(\frac{G^2}{2L_1G_2\sqrt{\epsilon}} - \frac{L_1\sqrt{\epsilon}}{2G_2} - \frac{G_2}{2L_1\sqrt{\epsilon}}\right) + Z_4^\pi \\ &= Z_5^\pi\epsilon^2 + Z_6^\pi\epsilon + Z_7^\pi\epsilon^{-1} + C_4\epsilon^{-1/2} + Z_8^\pi, \end{aligned} \tag{4.11}$$

where we defined:

$$\begin{aligned} Z_5^\pi &= \frac{Z_2^\pi L_1^2}{4G_2^2}; \\ Z_6^\pi &= \frac{Z_1^\pi L_1^2}{4G_2^2} - \frac{Z_2^\pi G^2}{2G_2^2} + \frac{Z_2^\pi}{2} + Z_3^\pi - \frac{C_5C_6L_1}{2G_2}; \\ Z_7^\pi &= \left(\frac{G^2-G_2^2}{2L_1G_2}\right)^2 Z_1^\pi; \\ Z_8^\pi &= -\frac{Z_1^\pi G^2}{2G_2^2} + \frac{Z_1^\pi}{2} + \left(\frac{G^2-G_2^2}{2L_1G_2}\right)^2 Z_2^\pi + \frac{C_5C_6G^2}{2L_1G_2} - \frac{C_5C_6G_2}{2L_1} + Z_4^\pi. \end{aligned} \tag{4.12}$$

4.2.2 Minimum Eccentricity

For the case $2g_1 = 2k\pi$ we do exactly the same. First we substitute this value in Eq. 4.8, hence

$$\begin{aligned}\mathcal{H}_{\rm min} &= -C_{\rm quad}\Big\{(5-3\epsilon)\big(3\cos^2(i_{\rm tot})-1\big)+15(1-\epsilon)\sin^2(i_{\rm tot})\Big\}+\frac{C_4}{\sqrt{\epsilon}}+C_5\Big\{C_6\sqrt{\epsilon}\cos(i_{\rm tot})\\ &\quad +C_7\Big[\Big(1-3\cos^2(i_{\rm tot})\Big)\Big((5\epsilon-3)(m_1^2+m_2^2)-3(1+\epsilon)m_1m_2\Big)+C_8(1-\epsilon)\sin^2(i_{\rm tot})\Big]\Big\}\\ &= Z_2^0\epsilon\cos^2(i_{\rm tot})+Z_3^0\epsilon+C_4\epsilon^{-1/2}+C_5C_6\sqrt{\epsilon}\cos(i_{\rm tot})+Z_4^0, \end{aligned} \tag{4.13}$$

where

$$\begin{aligned} Z_2^0 &= -6C_{\rm quad}-6C_5C_7(m_1^2+m_2^2)+18C_5C_7m_1m_2;\\ Z_3^0 &= 12C_{\rm quad}-4C_5C_7(m_1^2+m_2^2)-12C_5C_7m_1m_2;\\ Z_4^0 &= -10C_{\rm quad}+6C_5C_7(m_1^2+m_1m_2+m_2^2). \end{aligned} \tag{4.14}$$

Note that we are now using the superscript 0 to refer to the value of $2g_1$ we find for $k = 0$. Substituting Eq. 2.47, we obtain

$$\begin{aligned}\mathcal{H}_{\rm min} &= Z_2^0\epsilon\left(\frac{G^4}{4L_1^2G_2^2\epsilon}+\frac{L_1^2\epsilon}{4G_2^2}+\frac{G_2^2}{4L_1^2\epsilon}-\frac{G^2}{2G_2^2}-\frac{G^2}{2L_1^2\epsilon}+\frac{1}{2}\right)+Z_3^0\epsilon\\ &\quad +C_4\epsilon^{-1/2}+C_5C_6\sqrt{\epsilon}\left(\frac{G^2}{2L_1G_2\sqrt{\epsilon}}-\frac{L_1\sqrt{\epsilon}}{2G_2}-\frac{G_2}{2L_1\sqrt{\epsilon}}\right)+Z_4^0\\ &= Z_5^0\epsilon^2+Z_6^0\epsilon+C_4\epsilon^{-1/2}+Z_8^0, \end{aligned} \tag{4.15}$$

where

$$\begin{aligned} Z_5^0 &= \frac{Z_2^0L_1^2}{4G_2^2};\\ Z_6^0 &= -\frac{Z_2^0G^2}{2G_2^2}+\frac{Z_2^0}{2}+Z_3^0-\frac{C_5C_6L_1}{2G_2};\\ Z_8^0 &= \left(\frac{G^2-G_2^2}{2L_1G_2}\right)^2Z_2^0+\frac{C_5C_6G^2}{2L_1G_2}-\frac{C_5C_6G_2}{2L_1}+Z_4^0. \end{aligned} \tag{4.16}$$

4.2.3 Approximations

The 1PN coupling term is not very important for most systems. If we neglect this term, the formulas for $\mathcal{H}_{\rm min}$ and $\mathcal{H}_{\rm max}$ from the previous two sections reduce quite a bit. Eqs. 4.9 and 4.11 for the maximum eccentricity reduce to

$$\mathcal{H}_{\rm max,r}(\epsilon) = -30C_{\rm quad}\cos^2(i_{\rm tot})+24C_{\rm quad}\epsilon\cos^2(i_{\rm tot})-18C_{\rm quad}\epsilon+C_4\epsilon^{-1/2}+20C_{\rm quad} \tag{4.17}$$

and

$$\mathcal{H}_{\rm max,r}(\epsilon) = Z_{5,\rm r}^{\pi}\epsilon^2+Z_{6,\rm r}^{\pi}\epsilon+Z_{7,\rm r}^{\pi}\epsilon^{-1}+C_4\epsilon^{-1/2}+Z_{8,\rm r}^{\pi}, \tag{4.18}$$

where the r stands for reduced and

$$\begin{aligned} Z_{5,\rm r}^{\pi} &= \frac{6C_{\rm quad}L_1^2}{G_2^2};\\ Z_{6,\rm r}^{\pi} &= -\frac{15C_{\rm quad}L_1^2}{2G_2^2}-\frac{12C_{\rm quad}G^2}{G_2^2}-6C_{\rm quad};\\ Z_{7,\rm r}^{\pi} &= -30\left(\frac{G^2-G_2^2}{2L_1G_2}\right)^2C_{\rm quad};\\ Z_{8,\rm r}^{\pi} &= \frac{15C_{\rm quad}G^2}{G_2^2}+6\left(\frac{G^2-G_2^2}{L_1G_2}\right)^2C_{\rm quad}+5C_{\rm quad}. \end{aligned} \tag{4.19}$$

Eqs. 4.13 and 4.15 for the minimum eccentricity reduce to

$$\mathcal{H}_{\rm min,r}(\epsilon) = -6C_{\rm quad}\epsilon\cos^2(i_{\rm tot})+12C_{\rm quad}\epsilon+C_4\epsilon^{-1/2}-10C_{\rm quad} \tag{4.20}$$

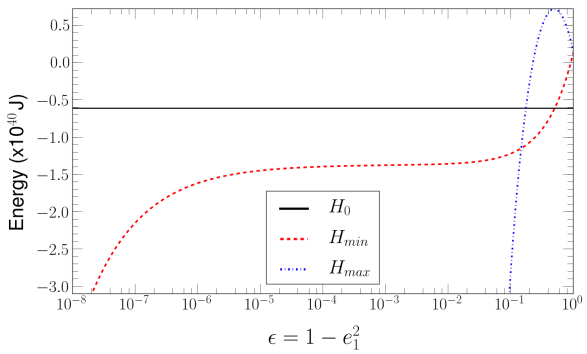

(a) The different Hamiltonian functions as function of $\epsilon = 1 - e_1^2$ for a system with $m_1 = m_2 = 10^3$ M_{Sun}, $m_3 = 10^6$ M_{Sun}, $a_1 = 10^{-3}$ pc, $a_2 = 60a_1$, $e_2 = 0.1$, $\epsilon_0 = 1 - e_{1,0}^2 = 0.5$, $g_1 = 0$ and $i_{tot} = 1.0$. The red dashed line is the Hamiltonian for the minimum eccentricity $\mathcal{H}_{min}$, the blue dashed-dotted line is the Hamiltonian for the maximum eccentricity $\mathcal{H}_{max}$, and the black line is the initial Hamiltonian of the system $\mathcal{H}_0$. Both $\mathcal{H}_{min}$ and $\mathcal{H}_{max}$ go to minus infinity for $\epsilon \to 0$ as we found analytically.

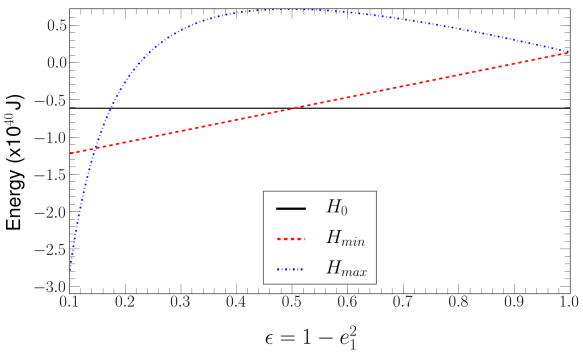

(b) We have zoomed in on the part with the intersections between the different Hamiltonian functions (in Fig. 4.1a). The intersections of $\mathcal{H}_0$ with $\mathcal{H}_{min}$ and $\mathcal{H}_{max}$ are the minimum and maximum eccentricity respectively, which means that for this system we find circular motion in g_1. The minimum eccentricity is equal to the initial e_1 because $g_1 = 0$, the value that was also used for $\mathcal{H}_{min}$. $\mathcal{H}_{max}$ and $\mathcal{H}_{min}$ intersect twice, once for $\epsilon = 1$ and once for an $\epsilon < \epsilon_0$.

Figure 4.1: Plot of the different functions that we use to find the minimum and maximum eccentricity.

and

$$\mathcal{H}_{\mathrm{min,r}}(\epsilon) = Z^0_{5,\mathrm{r}}\epsilon^2 + Z^0_{6,\mathrm{r}}\epsilon + C_4\epsilon^{-1/2} + Z^0_{8,\mathrm{r}}\,, \tag{4.21}$$

where

$$\begin{aligned} Z^0_{5,\mathrm{r}} &= -\frac{6C_{\mathrm{quad}}L_1^2}{4G_2^2}; \\ Z^0_{6,\mathrm{r}} &= \frac{3C_{\mathrm{quad}}G^2}{G_2^2} + 9C_{\mathrm{quad}}; \\ Z^0_{8,\mathrm{r}} &= -6\left(\frac{G^2 - G_2^2}{2L_1G_2}\right)^2 C_{\mathrm{quad}} - 10C_{\mathrm{quad}}. \end{aligned} \tag{4.22}$$

We have shown that to find the maximum and minimum eccentricity the equations $\mathcal{H}_{\mathrm{max,r}}(\epsilon) = \mathcal{H}_0$ and $\mathcal{H}_{\mathrm{min,r}}(\epsilon) = \mathcal{H}_0$ must be solved. This can be pictured by plotting the functions $\mathcal{H}_{\mathrm{max,r}}$ and $\mathcal{H}_{\mathrm{min,r}}$ as functions of ϵ. $\mathcal{H}_0$ is a constant, thus a line parallel to the x-axis in this plot. We show this in Fig. 4.1 for a system with $m_1 = m_2 = 10^3$ M_{Sun}, $m_3 = 10^6$ M_{Sun}, $a_1 = 10^{-3}$ pc, $a_2 = 60a_1$, $e_2 = 0.1$, $\epsilon_0 = 1 - e_{1,0}^2 = 0.5$, $g_1 = 0$ and $i_{tot} = 1.0$. Instead of $\mathcal{H}_{\mathrm{min,r}}$ and $\mathcal{H}_{\mathrm{max,r}}$, $\mathcal{H}_{\mathrm{min}}$ and $\mathcal{H}_{\mathrm{max}}$ are plotted. Since the difference between these functions, the 1PN coupling term, is negligible for this system, this does not make a difference.

In the following, we will derive some general features of $\mathcal{H}_{\mathrm{min,r}}$, $\mathcal{H}_{\mathrm{max,r}}$ and the solutions of $\mathcal{H}_{\mathrm{max,r}}(\epsilon) = \mathcal{H}_0$ and $\mathcal{H}_{\mathrm{min,r}}(\epsilon) = \mathcal{H}_0$, the possible values for the minimum and maximum eccentricity. These features will also be valid if we consider the non-reduced Hamiltonians $\mathcal{H}_{\mathrm{min}}$ and $\mathcal{H}_{\mathrm{max}}$, because for most systems the coupling term is negligible.

Because $C_4 < 0$ and $Z^{\pi}_{7,\mathrm{r}} < 0$ it follows that $\lim_{\epsilon\to 0}\mathcal{H}_{\mathrm{min,r}}(\epsilon) = \lim_{\epsilon\to 0}\mathcal{H}_{\mathrm{max,r}}(\epsilon) = -\infty$ and $\lim_{\epsilon\to 0}(\mathcal{H}_{\mathrm{min,r}}(\epsilon) - \mathcal{H}_{\mathrm{max,r}}(\epsilon)) = \infty$. $\mathcal{H}_{\mathrm{max,r}}$ and $\mathcal{H}_{\mathrm{min,r}}$ are both a superposition of a monotonically increasing function and a parabola. Because $Z^0_{5,\mathrm{r}} < 0$, $\mathcal{H}_{\mathrm{min,r}}$ has at most one maximum and no minima. $Z^{\pi}_{5,\mathrm{r}} > 0$, hence $\mathcal{H}_{\mathrm{max,r}}$ can have both a minimum and a maximum. From Eq. 4.8 follows that $\mathcal{H}_{\mathrm{min,r}}(\epsilon_0) \leq \mathcal{H}_0 \leq \mathcal{H}_{\mathrm{max,r}}(\epsilon_0)$: we find $\mathcal{H}_{\mathrm{max,r}}(\epsilon_0)$ from $\mathcal{H}_0$ by using $2g_1 = \pi$ instead of the initial value of g_1 and we find $\mathcal{H}_{\mathrm{min,r}}(\epsilon_0)$ by using $g_1 = 0$, and these values give the minimum and maximum value of $\cos(2g_1)$ respectively. Thus $\mathcal{H}_0$ is a line parallel to the x-axis such that for $\epsilon = \epsilon_0$ it is in between the other two functions. Therefore, solving $\mathcal{H}_{\mathrm{min,r}}(\epsilon) = \mathcal{H}_0$ delivers a maximum of two solutions and solving $\mathcal{H}_{\mathrm{max,r}} = \mathcal{H}_0$ gives at least one solution and a maximum of three solutions. So in principle there are a lot of different behaviors possible with respect to g_1: we can have circular motion, or oscillation around $g_1 = 0$ or $g_1 = \pi$. For oscillation around $g_1 = 0$ there should be at least two solutions of $\mathcal{H}_{\mathrm{min,r}} = \mathcal{H}_0$ and for two solutions a minimum or a maximum in $\mathcal{H}_{\mathrm{min,r}}$ is needed. $\mathcal{H}_{\mathrm{min,r}}$ has at most one maximum and no minima, thus assume it has

a maximum. If the maximum and minimum eccentricity are given by $\mathcal{H}_{\min,\mathrm{r}}$, one of the solutions of $\mathcal{H}_{\min,\mathrm{r}} = \mathcal{H}_0$ should be larger than ϵ_0 and one smaller than ϵ_0, thus we need $\mathcal{H}_0 < \mathcal{H}_{\min,\mathrm{r}}(\epsilon_0)$ and that is impossible. It follows that oscillation around $g_1 = 0$ is impossible.

If we consider the difference of Eq. 4.20 and Eq. 4.17 we find that $\mathcal{H}_{\min,\mathrm{r}}$ and $\mathcal{H}_{\max,\mathrm{r}}$ intersect when $\epsilon = 1$ or $\cos^2(i_{\mathrm{tot}}) = 1$. Of course this also follows from the fact that these points are the fixed points of the differential equation for the eccentricity. From Eq. 2.47 follows that $\cos^2(i_{\mathrm{tot}}) = 1$ corresponds with the points where

$$G^2 - L_1^2\epsilon - G_2^2 = \pm 2L_1G_2\sqrt{\epsilon}, \tag{4.23}$$

hence, using the quadratic formula:

$$\sqrt{\epsilon} = \frac{\pm 2L_1G_2 \pm \sqrt{4L_1^2G_2^2 + 4L_1^2(G^2 - G_2^2)}}{-2L_1^2} = \frac{\pm G_2 \pm G}{-L_1}. \tag{4.24}$$

We thus have two possible solutions for ϵ. By definition of ϵ, $0 < \sqrt{\epsilon} \leq 1$, hence $\epsilon = \left(\frac{G+G_2}{L_1}\right)^2$ is for most systems not a solution, because it is often larger than one. The other solution is given by $\epsilon = \left(\frac{G-G_2}{L_1}\right)^2$. From Eq. 2.47 follows that $G^2 \geq (G_1 - G_2)^2$, hence for $G_1 \geq G_2$: $\left(\frac{G+G_2}{L_1}\right)^2 \geq \left(\frac{G_1}{L_1}\right)^2 = \epsilon_0$ and for $G_2 > G_1$: $\left(\frac{G+G_2}{L_1}\right)^2 \geq \left(\frac{2G_2-G_1}{L_1}\right)^2 > \left(\frac{G_1}{L_1}\right)^2 = \epsilon_0$. In the same way we find that $G \leq G_1 + G_2$, thus $\left(\frac{G-G_2}{L_1}\right)^2 \leq \left(\frac{G_1}{L_1}\right)^2 = \epsilon_0$. Because of this intersection point, one expects that for most systems with circular motion in the $g_1 - e_1$ space, the minimum eccentricity is given by $\mathcal{H}_{\min,\mathrm{r}}$ and the maximum eccentricity by $\mathcal{H}_{\max,\mathrm{r}}$. If the minimum eccentricity is given by $\mathcal{H}_{\max,\mathrm{r}}$ and the maximum eccentricity by $\mathcal{H}_{\min,\mathrm{r}}$, there must be a maximum in $\mathcal{H}_{\min,\mathrm{r}}$ and ϵ_0 must be to the right of this maximum. We have never found this behavior in the systems we used, thus it seems that the names $\mathcal{H}_{\min}$ and $\mathcal{H}_{\max}$ are appropriate.

We now derive approximations for the minimum and maximum eccentricity. Eq. 4.18 can be approximated by

$$\mathcal{H}_{\max,\mathrm{r}}(\epsilon) \approx Z^{\pi}_{7,\mathrm{r}}\epsilon^{-1} + C_4\epsilon^{-1/2} + Z^{\pi}_{8,\mathrm{r}}. \tag{4.25}$$

Setting this equal to $\mathcal{H}_0$ gives us the solution:

$$1 - e^2_{1,\max} = \epsilon_{\min} \approx \left(\frac{-C_4 + \sqrt{C_4^2 - 4Z^{\pi}_{7,\mathrm{r}}(Z^{\pi}_{8,\mathrm{r}} - \mathcal{H}_0)}}{2(Z^{\pi}_{8,\mathrm{r}} - \mathcal{H}_0)}\right)^2. \tag{4.26}$$

We take the positive solution because $\mathcal{H}_0 \leq \mathcal{H}_{\max,\mathrm{r}}(\epsilon_0) < Z^{\pi}_{8,\mathrm{r}}$ and $\sqrt{\epsilon_{\min}}$ should be positive.

If we apply a Taylor approximation around $\epsilon = \epsilon_0$ to Eq. 4.21, we find

$$\begin{aligned}
\mathcal{H}_{\min,\mathrm{r}}(\epsilon) &\approx Z^0_{5,\mathrm{r}}\epsilon^2 + Z^0_{6,\mathrm{r}}\epsilon + C_4\epsilon_0^{-1/2} - \frac{1}{2\epsilon_0^{3/2}}C_4(\epsilon - \epsilon_0) + \frac{3}{8\epsilon_0^{5/2}}C_4(\epsilon - \epsilon_0)^2 + Z^0_{8,\mathrm{r}} \\
&= \left(Z^0_{5,\mathrm{r}} + \frac{3}{8\epsilon_0^{5/2}}C_4\right)\epsilon^2 + \left(Z^0_{6,\mathrm{r}} - \frac{5}{4\epsilon_0^{3/2}}C_4\right)\epsilon + \frac{15}{8\epsilon_0^{1/2}}C_4 + Z^0_{8,\mathrm{r}} \\
&= D_1\epsilon^2 + D_2\epsilon + D_3,
\end{aligned} \tag{4.27}$$

where we defined

$$\begin{aligned}
D_1 &= Z^0_{5,\mathrm{r}} + \frac{3}{8\epsilon_0^{5/2}}C_4; \\
D_2 &= Z^0_{6,\mathrm{r}} - \frac{5}{4\epsilon_0^{3/2}}C_4; \\
D_3 &= \frac{15}{8\epsilon_0^{1/2}}C_4 + Z^0_{8,\mathrm{r}}.
\end{aligned} \tag{4.28}$$

This gives an approximation for $\epsilon_{\max} = 1 - e^2_{1,\min}$, the solution of $\mathcal{H}_{\min,\mathrm{r}}(\epsilon) = \mathcal{H}_0$, namely:

$$\epsilon_{\max} \approx \frac{-D_2 + \sqrt{D_2^2 - 4D_1(D_3 - \mathcal{H}_0)}}{2D_1}. \tag{4.29}$$

For most systems $G_2 > 2G_1$ such that $G \geq G_2 - G_1 > G_1 \geq L_1$ and using this inequality, and Eqs. 4.22 and 4.28 we find that

$$\begin{aligned} -D_2 &= -Z^0_{6,\mathrm{r}} + \frac{5}{4\epsilon_0^{3/2}} C_4 \\ &= -\frac{3C_{\mathrm{quad}}G^2}{G_2^2} - 9C_{\mathrm{quad}} + \frac{5}{4\epsilon_0^{3/2}} C_4 \\ &< -\frac{3C_{\mathrm{quad}}L_1^2}{G_2^2} - 9C_{\mathrm{quad}} + \frac{3}{4\epsilon_0^{3/2}} C_4 \\ &= 2Z^0_{5,\mathrm{r}} - 9C_{\mathrm{quad}} + 2\frac{3}{8\epsilon_0^{3/2}} C_4. \end{aligned} \tag{4.30}$$

This is smaller than $2D_1$ for most systems. Since $2D_1$, $-D_2 < 0$, we use the positive solution in Eq. 4.29, otherwise we do not have $\epsilon_{\mathrm{max}} \leq 1$.

4.2.4 Newtonian Kozai Mechanism

If we only consider the quadrupole term in the Hamiltonian (Newtonian term), we find for Eq. 4.9:

$$\mathcal{H} = -30C_{\mathrm{quad}} \cos^2(i_{\mathrm{tot}}) + 24C_{\mathrm{quad}}\epsilon \cos^2(i_{\mathrm{tot}}) - 18C_{\mathrm{quad}}\epsilon + 20C_{\mathrm{quad}}. \tag{4.31}$$

From Eq. 2.47 we find that

$$\begin{aligned} \cos(i_{\mathrm{tot}}) &= \frac{G^2 - G_1^2 - G_2^2}{2G_1G_2} \\ &= \frac{2L_1\sqrt{\epsilon_0}G_2\cos(i_{\mathrm{tot},0}) + L_1^2\epsilon_0 + G_2^2 - G_1^2 - G_2^2}{2G_1G_2} \\ &= \frac{\cos(i_{\mathrm{tot},0})\sqrt{\epsilon_0}}{\sqrt{\epsilon}} + \frac{L_1}{2L_2\sqrt{\epsilon}\sqrt{1-e_2^2}}(\epsilon_0 - \epsilon). \end{aligned} \tag{4.32}$$

To find the maximum eccentricity, $1 - e^2_{1,\mathrm{max}} = \epsilon_{\mathrm{min}} < \epsilon_0$, one has to solve $\mathcal{H} = \mathcal{H}_0$, thus

$$C_{\mathrm{quad}} \cos^2(i_{\mathrm{tot,min}})\,(30 - 24\epsilon_{\mathrm{min}}) + 18C_{\mathrm{quad}}\epsilon_{\mathrm{min}} = -\mathcal{H}_0, \tag{4.33}$$

where $i_{\mathrm{tot,min}}$ is the inclination at a maximum in the eccentricity (i_{tot} is at a minimum when e_1 is at a maximum). Because $\epsilon_0 - \epsilon_{\mathrm{min}} > 0$ we find from Eq. 4.32 that $\cos(i_{\mathrm{tot,min}})$ increases when a_2 decreases and ϵ_{min} remains constant. The left-hand side of Eq. 4.33 should decrease such that this equality still holds. Because $0 < \epsilon_{\mathrm{min}} \leq 1$ and there is a factor $\sqrt{\epsilon_{\mathrm{min}}}$ in the denominator in the expression of $\cos(i_{\mathrm{tot,min}})$, in general this left-hand side decreases only when ϵ_{min} increases. Thus when a_2 decreases, ϵ_{min} increases and $e_{1,\mathrm{max}}$ decreases. This behavior is shown in Fig. 2.4 of Hamers (2012).

In the limit that $\frac{L_1}{L_2} \ll 1$, Eq. 4.32 reduces to

$$\cos(i_{\mathrm{tot}}) \approx \cos(i_{\mathrm{tot},0})\sqrt{\frac{\epsilon_0}{\epsilon}}. \tag{4.34}$$

Using this expression, Eq. 4.31 and the quadrupole part of Eq. 4.8, we can solve for the maximum eccentricity: $\mathcal{H} = \mathcal{H}_0$ or

$$\begin{aligned} 30\cos^2(i_{\mathrm{tot},0})\frac{\epsilon_0}{\epsilon} - 24\cos^2(i_{\mathrm{tot},0})\epsilon_0 + 18\epsilon - 20 = \\ (5 - 3\epsilon_0)(3\cos^2(i_{\mathrm{tot},0}) - 1) + 15(1 - \epsilon_0)\sin^2(i_{\mathrm{tot},0})\cos(2g_{1,0}). \end{aligned} \tag{4.35}$$

This expression is not dependent on a_2, hence the maximum eccentricity has no dependence on a_2 when a_2 becomes large (the expression above is only valid in the limit $\frac{L_1}{L_2} \ll 1$, this is the limit for large a_2). This may seem a bit surprising, because one may expect the Kozai effect to become less effective when the tertiary is further away. The physical explanation for this effect is that the period of the Kozai cycles also increases when a_2 becomes larger. If

a_2 becomes large enough, the period will be so large that the inner binary is already merged before the eccentricity changes significantly. Thus, the Kozai effect does not influence the merger time of the inner binary and we could as well say that the Kozai effect is not effective for large a_2.

If we take the limit of $e_{1,0}$ to 0 in Eq. 4.35 we get:

$$5\cos^2(i_{\rm tot,0}) - 5\cos^2(i_{\rm tot,0})\epsilon + 3\epsilon^2 - 3\epsilon = 0, \tag{4.36}$$

which has the solution:

$$\begin{aligned}\epsilon &= \frac{5\cos^2(i_{\rm tot,0}) + 3 + \sqrt{(5\cos^2(i_{\rm tot,0})+3)^2 - 60\cos^2(i_{\rm tot,0})}}{6} \\ &= \frac{5\cos^2(i_{\rm tot,0}) + 3 + (5\cos^2(i_{\rm tot,0}) - 3)}{6} = \frac{5}{3}\cos^2(i_{\rm tot,0}).\end{aligned} \tag{4.37}$$

This is the value which is often mentioned in previous research, (e.g. Blaes et al. (2002)). Note that this value is not the maximum eccentricity for $e_{1,0} = 0$. From Eqs. 2.117 and 2.127 it follows that $e_{1,0} = 0$ does not correspond to oscillations, hence $e_1(t) = 0$ for all t.

4.2.5 Gravitational Wave Term

Wen (2003) and Thompson (2011) also included the gravitational wave term in the derivative for e_1 in their calculation of the maximum eccentricity and neglected the coupling term. In that case the condition $\frac{\partial e_1}{\partial t} = 0$ gives:

$$\sin(2g_{1,\rm m}) = \frac{304 G_N^3 m_1 m_2 (m_1+m_2) e_{1,\rm m}}{15 c^5 a_1^4 (1-e_{1,\rm m}^2)^{5/2}} \left(1 + \frac{121}{304} e_{1,\rm m}^2\right) \frac{G_{1,\rm m}}{30 C_{\rm quad} e_{1,\rm m} (1-e_{1,\rm m}^2)\sin^2(i_{\rm tot,m})}, \tag{4.38}$$

where the subscript m refers to the values of g_1, $i_{\rm tot}$ and e_1 at the extremum of e_1. Using this relation and assuming a_1 is constant, solving $\mathcal{H}(e_{1,\rm m}, g_{1,\rm m}) = \mathcal{H}_0$ gives the minimum and maximum value of e_1. This equation must be solved numerically. We did not use this method because in most cases the difference between this method and the method we use ($\sin(2g_{1,\rm m}) = 0$) is negligible.

Blaes et al. (2002) derived that the Kozai effect is important for systems where

$$\frac{a_2}{a_1} < 34 \left(\frac{a_1}{10^{-2}\rm pc}\right)^{1/3} \left(\frac{m_1+m_2}{2\cdot 10^6 \rm M_{Sun}}\right)^{-1/3} \left(\frac{2m_3}{m_1+m_2}\right)^{1/3} \left(\frac{1-e_1^2}{1-e_2^2}\right)^{1/2}. \tag{4.39}$$

Applying this inequality to the right-hand side of Eq. 4.38 and using Eq. 2.79 yields:

$$\begin{aligned}\sin(2g_{1,\rm m}) &< \frac{G_N^{5/2} m_1 m_2 (m_1+m_2)^{3/2}}{c^5 a_1^{5/2}(1-e_{1,\rm m}^2)^3} \frac{425}{30} \frac{16(1-e_2^2)^{3/2}}{15 m_3 \sin^2(i_{\rm tot,m})} \left(\frac{a_2}{a_1}\right)^3 \\ &< \frac{G_N^{5/2} m_1 m_2 (m_1+m_2)^{3/2}}{c^5 a_1^{5/2}(1-e_{1,\rm m}^2)^3} \frac{425}{30} \frac{16(1-e_2^2)^{3/2}}{15 m_3 \sin^2(i_{\rm tot,m})} \frac{34^3 a_1}{10^{-2}\rm pc} \frac{2\cdot 10^6 \rm M_{Sun}}{m_1+m_2} \frac{2m_3}{m_1+m_2} \left(\frac{1-e_{1,\rm m}^2}{1-e_2^2}\right)^{3/2} \\ &\approx \frac{1}{10^{40}} \frac{1}{a_1^{3/2}(1-e_{1,\rm m}^2)^{3/2}} \frac{1}{\sin^2(i_{\rm tot,m})} \frac{m_1 m_2}{\sqrt{m_1+m_2}} \left(\frac{\rm metre}{\rm kg}\right)^{3/2}.\end{aligned} \tag{4.40}$$

For most systems we will use, this quantity is very small. Only when the eccentricity becomes very close to 1, the value of $\sin(2g_{1,\rm m})$ can become significant. In that case the extrema of the eccentricity that we find with $\sin(2g_1) = 0$ are wrong. In the systems we simulated, we have only seen a few examples where the calculated maximum eccentricity was not the correct value.

4.2.6 Criterion Importance Kozai Mechanism

Using the expressions for the minimum and maximum eccentricity, Eqs. 4.26 and 4.29, one may give a criterion for the Kozai effect to be effective, namely:

$$\epsilon_{\rm min} - \epsilon_{\rm max} > 0.05, \tag{4.41}$$

where the value 0.05 was found by trial and error. From Eqs. 4.26 and 4.29 we conclude that expression 4.41 is very complicated, but it has proved to be better than the condition given in Blaes et al. (2002): Eq. 4.39 (see Figs.

4.5 and 4.12 in Sec. 4.3). That expression gives a criterion for the general relativistic periastron precession to stop the Kozai resonance. It actually gives a criterion for this precession to be so effective to change the evolution of g_1 from oscillation around $g_1 = \pi/2$ to circular motion in g_1, thus $\dot{g}_1 > 0$ or $\dot{g}_1 < 0$ at all times. This change also causes a decreasement of the maximum eccentricity of the oscillations in the evolution of e_1. This explains why Eq. 4.41 is better: it uses the maximum and minimum eccentricity directly while Eq. 4.39 makes use of the argument of periastron g_1. Instead of the Eqs. 4.26 and 4.29 for the maximum and minimum eccentricity respectively, one could also derive other expressions: for instance a Taylor approximation applied to Eq. 4.18 around $\epsilon = \epsilon_0$ or different orders of the Taylor approximation.

4.2.7 Correction Factor

To determine the value of the fitting parameters of the different forms of f,

$$\begin{aligned} \text{fit 1}: \quad f\left(e_{1,\min}, e_{1,\max}\right) &= \left(\frac{1-e_{1,\max}^2}{1-e_{1,\min}^2}\right)^b \\ \text{fit 2}: \quad f\left(e_{1,\min}, e_{1,\max}\right) &= 1-a+a\left(\frac{1-e_{1,\max}^2}{1-e_{1,\min}^2}\right)^b, \end{aligned} \tag{4.42}$$

in the correction factor in Eq. 4.5, we calculated the merger time of systems with integration of the equations of motion and we evaluated $t_{\text{merge,p}}(e_{1,\max}, a_1)$. We used systems with $m_1 = 10^{x_1}$ M_{Sun}, $m_2 = 10^{x_2}$ M_{Sun}, $m_3 = 10^{x_3}$ M_{Sun} and $a_1 = 10^{x_4}$ pc where x_1 and x_2 were drawn from a flat distribution ranging between 1 and 7, x_3 from a flat distribution between 4 and 7 and x_4 from a flat distribution between -4 and -2. Furthermore, e_1, $e_2 \in (0,1)$, $i_{\text{tot}} \in (1, 2.1)$, g_1, $g_2 \in (0, 2\pi)$ and $\frac{a_2}{a_1} \in (10, 100)$ where flat distributions were used for all of these. We used these specific ranges of initial values to increase the chance to find systems where the Kozai effect is important. We used the fast method with correction factor $f(e_{1,\min}, e_{1,\max}) = \sqrt{\frac{1-e_{1,\min}^2}{1-e_{1,\max}^2}}$ for an estimate of the merger time t_{estimate}. Initially, we only simulated systems where the merger time without a tertiary t_{without} was larger than 1.1 T_{Hubble} and $t_{\text{estimate}} < \text{T}_{\text{Hubble}}$, because we were interested in systems in which the tertiary was the cause that the inner binary merged within a Hubble time. Later on, we allowed systems where $t_{\text{estimate}} < 1.1 t_{\text{without}}$ (and $t_{\text{estimate}} < \text{T}_{\text{Hubble}}$) since in these systems the Kozai effect is also important. We only used systems where $t_{\text{estimate}} < \text{T}_{\text{Hubble}}$ to ensure that we only simulated systems with a 'realistic' merger time. Of course, t_{estimate} is not the real merger time such that the merger time was sometimes larger than T_{Hubble}. After the integration we inspected each system to determine if there was indeed a merger by looking at the time-evolution of a_1 and e_1. We divided these simulations into two classes: systems where $m_1 = m_2$ such that the octupole term disappears and systems where the inner masses were chosen independently. These cases are named quadrupole and octupole case respectively.

4.2.7.1 Quadrupole Case

Fig. 4.2a is a plot of $t_{\text{merge}}/t_{\text{merge,p}}(a_1, e_{1,\max})$, where t_{merge} is the merger time of a system, as function of $x := \left(\frac{1-e_{1,\max}^2}{1-e_{1,\min}^2}\right)$ where we fitted the correction factors of Eq. 4.42. The maximum and minimum eccentricity that are used in x were calculated as explained in the previous sections. We left one simulated system out of the fitting, because in that system the gravitational radiation was so important during the first Kozai cycle that the calculated maximum eccentricity was not correct. We used 274 systems for this fit but we left 3 systems out of the plot in Fig. 4.2a to clearly show the fitted formulas with respect to the data. Note that as x approaches 1, the fraction $t_{\text{merge}}/t_{\text{merge,p}}(e_{1,\max}, a_1)$ of the systems, shown with the red dots, goes to 1 as we predicted in the beginning of Sec. 4.2. Fit 1 resulted in a best fit when b takes the value -0.53, the resulting function is the solid, black curve in Fig. 4.2a. The best-fitting parameters of the function that we used for fit 2 are $a = 2.17$ and $b = -0.45$, this function is the dashed, blue curve in Fig. 4.2a. Using the correction factors resulting from fit 1 and fit 2, we show in Fig. 4.2b, a cumulative histogram of the factor by which t_{estimate}, Eq. 4.5, differs from t_{merge}. We divided the plotted regime in 20 bins. Again, the solid, black line is used for the distribution resulting from fit 1 and the dashed, blue line for the distribution resulting from fit 2. In this plot we included all the systems we used for the fit, thus also the three systems that were left out of Fig. 4.2a. We find that fit 2 resulted in a better correction factor than fit 1, as we expected before. With the correction factor resulting from fit 1, around 75% of the systems merge within a factor of 2 of t_{estimate} and with the correction factor resulting from fit 2 around 95% of the systems merges within

a factor of 2 of the estimated merger time. Around 97% of the systems merges within a factor 3 of t_{estimate} for the correction factors resulting from both fits.

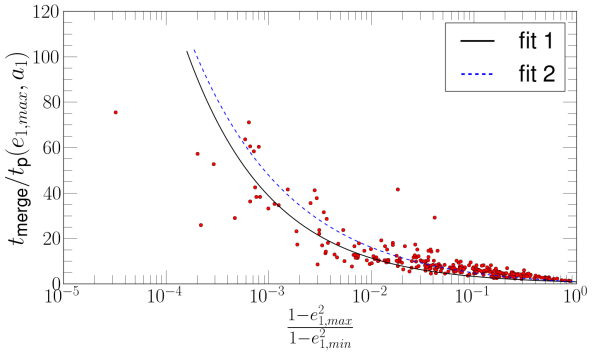

(a) The red dots are the fractions $t_{\text{merge}}/t_{\text{merge,p}}(e_{1,\text{max}}, a_1)$ of 271 pure quadrupole systems ($m_1 = m_2$) plotted as function of $x := (1 - e^2_{1,\text{max}})/(1 - e^2_{1,\text{min}})$. Also shown are the functions resulting from fits with the functions from Eq. 4.42. The dashed, blue curve is the function resulting from fit 2 and the solid, black curve is the function resulting from fit 1.

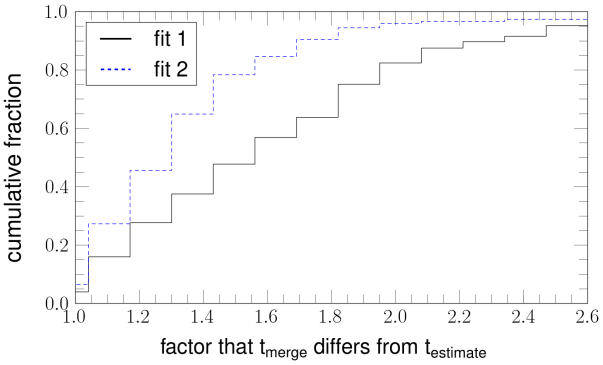

(b) A cumulative plot of the factor that t_{merge} differs from t_{estimate} when we use the correction factors resulting from fit 1 and fit 2. 274 systems are used for this distribution and the plotted regime is divided in 20 bins. The solid, black line is the distribution resulting from t_{estimate} with the correction factor of fit 1 and the dashed, blue line is the distribution resulting from the correction factor of fit 2.

Figure 4.2: Fits to the quadrupole case

4.2.7.2 Octupole Case

We found that in the octupole case ($m_1 \neq m_2$) the data was not suitable to fit the functions from Eq. 4.42. For 15% of the systems $t_{\text{merge}} < t_{\text{merge,p}}(e_{1,\text{max}}, a_1)$ a behavior that we did not find for systems in the quadrupole case. This behavior is caused by different mechanisms which we will discuss below. Because we have fractions $t_{\text{merge}}/t_{\text{merge,p}}(e_{1,\text{max}}, a_1)$ that are below one for all values of $x \equiv \left(\frac{1-e^2_{1,\text{max}}}{1-e^2_{1,\text{min}}}\right)$, we lose the characteristic behavior that we found in the quadrupole case: the fraction $t_{\text{merge}}/t_{\text{merge,p}}(e_{1,\text{max}}, a_1)$ increases for decreasing x. We assumed this behavior when we suggested the correction factors, Eq. 4.42. Of course, t_{estimate} that resulted from fit 1 and fit 2 in the quadrupole case is still an approximation for the merger time. We have shown the fractions $t_{\text{merge}}/t_{\text{merge,p}}(e_{1,\text{max}}, a_1)$ of the systems of the octupole case in Fig. 4.3a (the red dots) and we have also shown the corrections factors the we found in the quadrupole case from fit 1 (solid, black curve) and fit 2 (dashed, blue curve). Thus we have not done a fit again, but we only show how good the correction factors from the quadrupole case are for the octupole case. We have simulated 382 systems for the octupole case and we used 363 systems to make Fig. 4.3a. The excluded systems had a $t_{\text{merge}}/t_{\text{merge,p}}(e_{1,\text{max}}, a_1) > 300$. In Fig. 4.3b we show the cumulative distribution of the factor by which t_{merge} differs from t_{estimate} resulting from fit 1 (solid, black line) and fit 2 (dashed, blue line). All 382 systems are used and the plotted regime is divided in 20 bins. It is found that for factors smaller than 2, t_{estimate} resulting from fit 2 is slightly better. For larger factors, t_{estimate} resulting from fit 1 and fit 2 are nearly the same. For around 55% of the systems t_{estimate} is within a factor of 2 from t_{merge} for both formulas.

The difference between the octupole case and quadrupole case is caused by a few mechanisms. First, since we neglect the octupole Hamiltonian in the calculation of the initial minimum and maximum eccentricity, this calculation is meant for the quadrupole case. This means that we sometimes use totally wrong values for the extrema of the eccentricity. A second mechanism is the chaotic behavior in the eccentricity evolution that we find in the octupole case. Although the initial maximum eccentricity can be the calculated one, $1 - e^2_{1,\text{max}}$ can change orders of magnitude during the evolution. An increasement of the maximum eccentricity during the evolution, causes the merger time to decrease compared to the value that we would find if the maximum eccentricity was approximately constant. In the same way, if the maximum eccentricity decreases, the merger time increases compared to the merger time that we would find if the maximum eccentricity was approximately constant. In Fig. 4.4a one can find the evolution of $\epsilon = 1 - e_1^2$ of a system that has an envelope in the eccentricity evolution. The system starts with an eccentricity that is slightly smaller than the calculated value $\epsilon_{\text{min},0} = 2.9 \cdot 10^{-3}$, (because $m_1 \neq m_2$) and the minimum of ϵ increases nearly 2 orders of magnitude and decreases more than one order of magnitude during the evolution compared to the initial minimum value. Because the rate of radiation of gravitational waves is highly dependent on this eccentricity, and the fraction of time the system has $\epsilon_{\text{min}} > \epsilon_{\text{min},0}$ is much larger than the fraction of time the system has $\epsilon_{\text{min}} < \epsilon_{\text{min},0}$, the merger time is much smaller than t_{estimate}. In Fig. 4.4b the evolution

of ϵ is shown for a system that merges during the first Kozai cycle. The maximum eccentricity reached is smaller than the value, $1-e^2_{1,\max} = 1.2 \cdot 10^{-4}$ that is calculated. Because the calculated maximum eccentricity is very close to 1, the gravitational radiation becomes dominant before this value is reached. The merger time of this system is approximately $166 t_{\text{estimate}}$. This large difference is explained by the fact that the Kozai period is relatively large (3.7 kyr) such that the maximum eccentricity is never reached.

If the maximum eccentricity increases a few orders of magnitude during the evolution, the fraction $t_{\text{merge}}/t_{\text{merge,p}}(e_{1,\max}, a_1)$ becomes smaller than 1, this is the behavior we found for some systems in the octupole case.

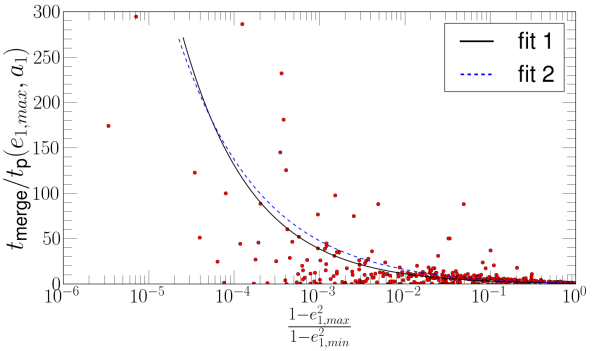

(a) $t_{\text{merge}}/t_{\text{merge,p}}(e_{1,\max}, a_1)$ for 363 systems as function of $x := (1-e^2_{1,\max})/(1-e^2_{1,\min})$. Also shown are the functions resulting from fits with the functions from Eq. 4.42 that we did for the quadrupole case. The dashed, blue curve is the function resulting from fit 2 and the solid, black curve is the function resulting from fit 1.

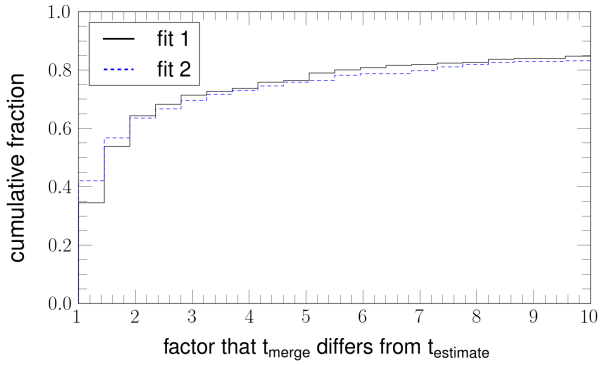

(b) A cumulative plot of the factor that t_{merge} differs from t_{estimate} for the two correction factors that resulted from fit 1 and fit 2 that we did in the quadrupole case. 382 systems are used for this distribution and the plotted regime is divided in 20 bins. The solid, black line is the distribution resulting from t_{estimate} with the correction factor of fit 1 and the dashed, blue line is the distribution resulting from the correction factor of fit 2.

Figure 4.3: Octupole case

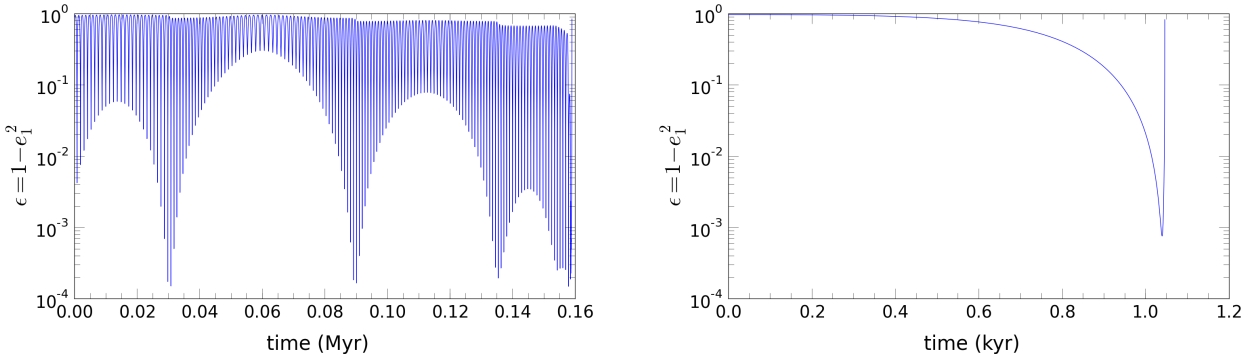

Figure 4.4: Eccentricity evolution of systems with $m_1 \neq m_2$ that have a merger time that is totally different from the estimated merger time t_{estimate}.

4.2.7.3 Snapshot Time Step Integrator

As described in Chapter 3, we used the timescale of the Kozai cycles as the snapshot time step. During the integration of the systems used for the quadrupole and octupole case, we ran into some systems for which this time step was too large such that the found evolution of the system was not correct and for which integration with a smaller maximum time step was computationally too expensive. We have left all the systems for which we found this behavior out of the fits and plots. We have checked all the systems for which t_{merge} differed a factor greater than 2.5 from t_{estimate} in the quadrupole case and the systems for which t_{merge} differed more than a factor 10 from t_{estimate} in the octupole case for this behavior.

4.3 Dependence Merger Time Inner Binary on the Initial Conditions

Because integration of the equations of motion of systems is computationally expensive for systems which have many eccentricity oscillations before the inner binary merges, it is difficult to map out the influence of the initial conditions on the merger time using integration. Although the fast method only provides an estimate, it enables one to show the general behavior. Using the fast method we have examined the space of initial parameters by making plots like Fig. 4.5. We used the correction factor resulting from fit 1 in Eq. 4.5, because it is the most natural one. In Fig. 4.5 we made a contour plot in the $a_1 - a_2$ space of the merger time of the inner binary in a triple (dotted-dashed lines) with $m_1 = 10^3$ $M_{\rm Sun}$, $m_2 = 10^4$ $M_{\rm Sun}$, $m_3 = 10^6$ $M_{\rm Sun}$, $g_1 = g_2 = 0$, $e_1 = e_2 = 0.4$ and $i_{\rm tot} = 70$ deg. We also added the contours of the merger time in case we do not have a tertiary (dashed lines). Of course, they are not dependent on a_2. Only contours are drawn for systems that are, at least initially, dynamically stable. A triple is dynamically stable when it satisfies Eq. 2.118; the curve for which there is equality in Eq. 2.118 is the solid black line. In this plot we also show Eq. 4.39 (black, dashed line), the criterion for general relativistic periastron precession, and Eq. 4.41 (black, dashed-dotted line), the criterion that we derived in Sec. 4.2.6. As can be seen from this figure, the latter condition is a much better criterion for the Kozai effect. We show in Fig. 4.5 also the contours of the merger time that follow from integration of the equations of motion (the solid lines). For the systems where the Kozai effect is most important, the merger time that follows from the fast method is slightly too large; in the region where the Kozai effect disappears, the merger time given by the fast method is slightly too small. Note that this plot is made for a system in which $m_1 \neq m_2$ such that it belongs to the octupole case. The larger a_2 is, the smaller the Kozai effect should be, because the influence of the tertiary on the binary decreases; indeed, we can see that in the plot. If a_2 is large enough, the same merger time is found as would be the case if the binary would not reside near a third black hole.

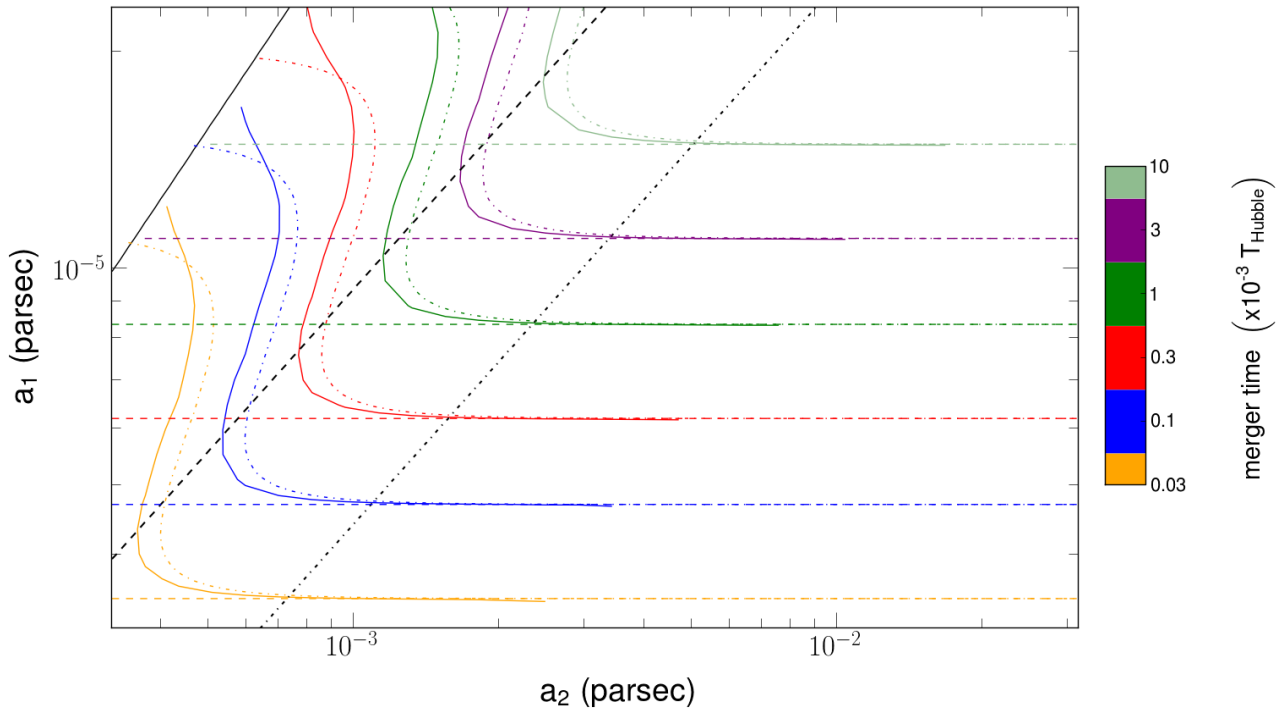

Figure 4.5: Contours of the merger time of the inner binary of triples with $m_1 = 10^3$ $M_{\rm Sun}$, $m_2 = 10^4$ $M_{\rm Sun}$, $m_3 = 10^6$ $M_{\rm Sun}$, $g_1 = g_2 = 0$, $e_1 = e_2 = 0.4$ and $i_{\rm tot} = 70$ deg. We show contours that follow from integration of the equations of motion (solid lines) and from the fast method (dashed-dotted lines). Also shown are contours of the merger time for an isolated binary (dashed lines). The black solid line is Eq. 2.118, the criterion for stability, the black dashed line is Eq. 4.39, the criterion for general relativistic periastron precession and the black dashed-dotted line is Eq. 4.41, the criterion for the Kozai effect that we derived in Sec. 4.2.6.

For the contour plots we made to examine the parameter space, we took a_1 between $10^{-4.5}$ and $10^{-1.9}$ pc, and a_2 between $10^{-2.5}$ and $10^{-0.5}$ pc. We used the following values for the other parameters:
$i_{\rm tot} \in \{0.01, 0.8, 1.3, 1.4, 1.5, 1.6, 1.7, 2.3, 3.1\}$, $m_1 = m_2 \in \{1, 10^2, 10^4, 10^6\}$ $\rm M_{Sun}$, $m_3 \in \{10^2, 10^4, 10^6, 10^8\}$ $\rm M_{Sun}$, $e_1, e_2 \in \{0.01, 0.1, 0.4, 0.8\}$ and $g_1 \in \{0.1, 0.9, 1.8, 2.8\}$. We do not show the plots that followed from that search, but in the coming sections we will show the characteristic behavior we found, by means of a system where $m_1 = m_2 = 10^4$ $\rm M_{Sun}$, $m_3 = 10^6$ $\rm M_{Sun}$, $e_1 = e_2 = 0.6$, $g_1 = 0$, $i_{\rm tot} = 75$ deg, a_1 between 10^{-5} and $10^{-2.5}$ pc, and a_2 between $10^{-2.1}$ and $10^{-0.5}$ pc. In each section we vary one of the initial parameters to show the influence of that particular parameter on the merger time of the inner binary in a triple.

4.3.1 Initial Inclination

In Fig. 4.6 we show the contour plots for the system described above, for different values of the initial inclination. We used nine different values for $i_{\rm tot}$: 0, 45, 75, 85, 90, 95, 105, 135 and 180 degrees. As in Fig. 4.5 we did this only for systems that are at least initially stable. The solid lines are the contours of the merger time of the binary that follow with the fast method. The contours in the case we do not have a tertiary are the dashed lines. The strong dependence of the Kozai effect on the initial inclination is very clear in these plots. We see that the Kozai effect is very effective for inclinations near 90 degrees whereas it is not effective for inclinations near 0 and 180 degrees. What is striking in these plots is that for relative small a_2, the merger time is independent of a_2. This can be explained if we consider the different mechanisms at work.

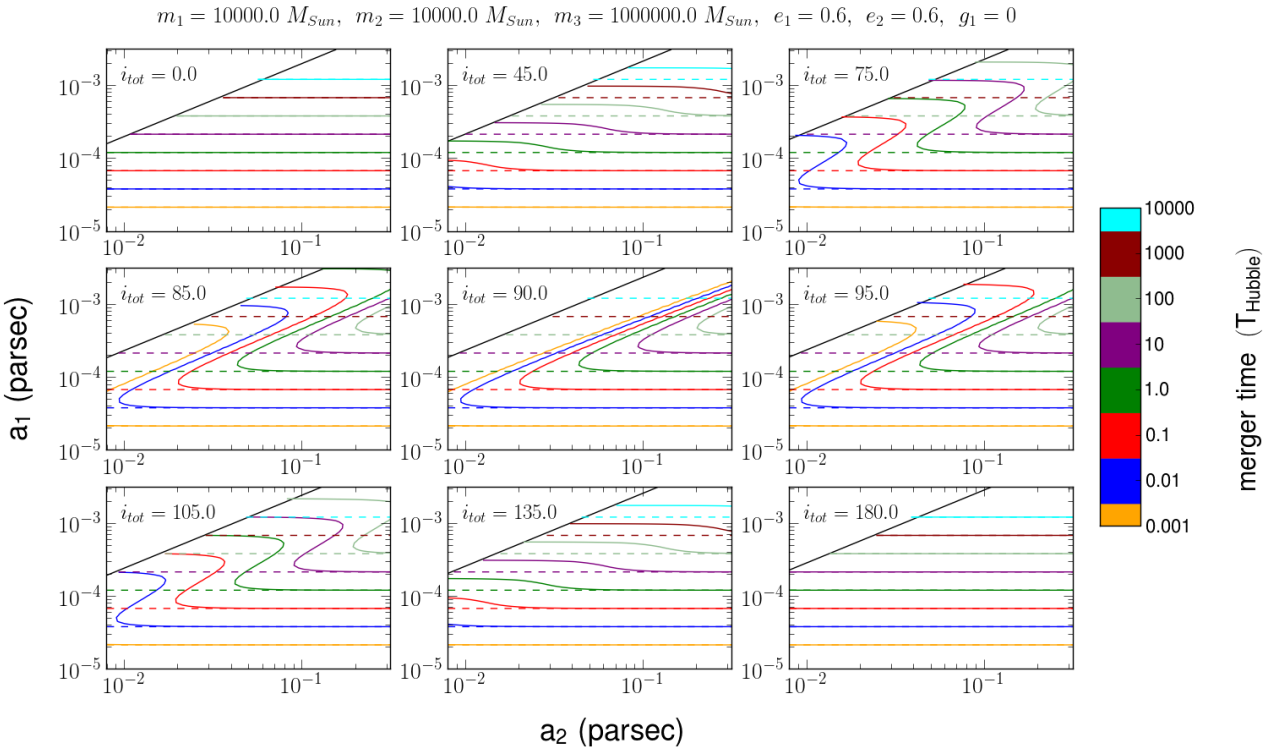

Figure 4.6: Contour plots of the merger time of the inner binary of triples with $m_1 = m_2 = 10^4$ $\rm M_{Sun}$, $m_3 = 10^6$ $\rm M_{Sun}$, $e_1 = e_2 = 0.6$ and $g_1 = 0$. We varied the initial inclination (in degrees) and show contours for the inner binary in a triple (solid lines) and for the case of no tertiary (dashed lines).

There are two competing mechanisms: the (Newtonian) Kozai mechanism which causes oscillations in the eccentricity, and the general relativistic periastron precession which tends to destroy these oscillations. In Sec. 4.2.4 we found that the maximum eccentricity of the oscillations increases as a_2 increases and we have also seen that it goes to the constant value $\sqrt{1 - \frac{5}{3}\cos^2(i_{\rm tot,0})}$ for large a_2. The GR precession becomes effective for a certain value of a_2, given by Eq. 4.39, and kills the Kozai mechanism as discussed before. What is happening for the systems with relative small a_2 and merger time independent of a_2, is that a_2 is already large enough such that

the maximum eccentricity of the oscillations is constant. Thus for small a_2 where the GR precession is not yet effective, the merger time becomes independent of a_2. What is also happening is that in that region the maximum eccentricity does not depend on a_1. A quick look at Eq. 4.1 teaches us that in a case when the semi-major axis of two systems differ by a factor k, their merger times differ by a factor k^4. This explains the equally spaced contour lines in the plots.

4.3.2 Inner Masses

In Fig. 4.7 contour plots are made for various values of the inner masses $m_1 = m_2$ between 10 M_{Sun} and 10^7 M_{Sun}. We see in these plots that the merger time decreases as the inner masses grow. We also see that the region in the $a_1 - a_2$ plane where the Kozai effect is effective is strongly determined by the inner masses. This is because the condition for stability, Eq. 2.118, and the condition for the importance of the GR precession, Eq. 4.39, are strongly dependent on the inner masses.

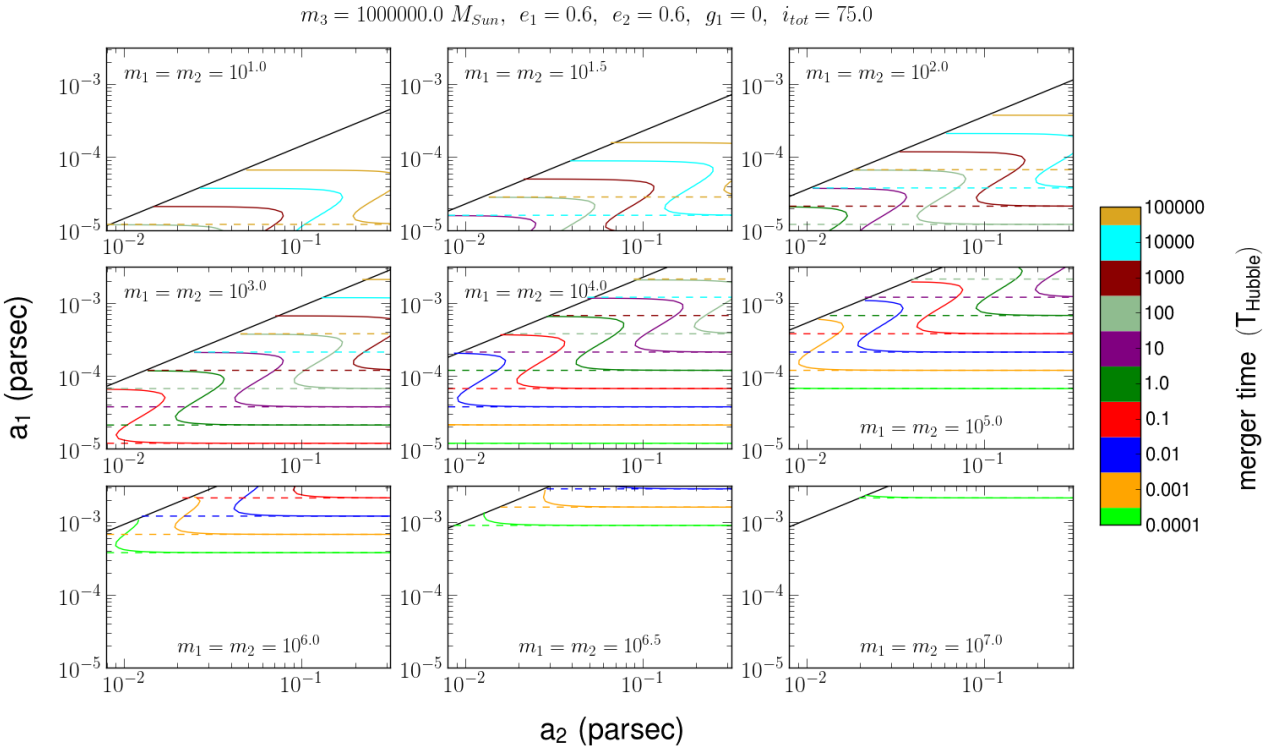

Figure 4.7: Contour plots of the merger time of the inner binary of triples with different values for the inner masses $m_1 = m_2$. The masses $m_1 = m_2 = 10^x$ M_{Sun} for $x = 1, 1.5, 2, 3, 4, 5, 6, 6.5, 7$ are used.

4.3.3 Initial Argument of Periastron Inner Binary

In Fig. 4.8 one finds contour plots for the merger time of the inner binary of triples for which we vary the initial value of the argument of periastron ($g_1 = 0, \pi/2, \pi$). The plots for $g_1 = 0$ and $g_1 = \pi$ are the same, because the equations of motion for a hierarchical triple only depend on $2g_1$. Note that in Sec. 4.2.3 we found that for a system that has circular motion in g_1 and has initial value $g_1 = 0$, e_1 is the minimum eccentricity and for a system that has initial value $g_1 = \pi/2$, e_1 is the maximum eccentricity. This explains that in the plot for $g_1 = \pi/2$ the contour lines of the triple are below the contour lines of the isolated binary for a small region in the a_2 space, behavior which we do not find in the other plots. That region corresponds to circular motion in g_1 such that for the plots of $g_1 = 0$ and $g_1 = \pi$ the maximum eccentricity is larger than the initial value. For the plot of $g_1 = \pi/2$ the maximum eccentricity is equal to the initial value such that also eccentricities smaller than the initial value are reached.

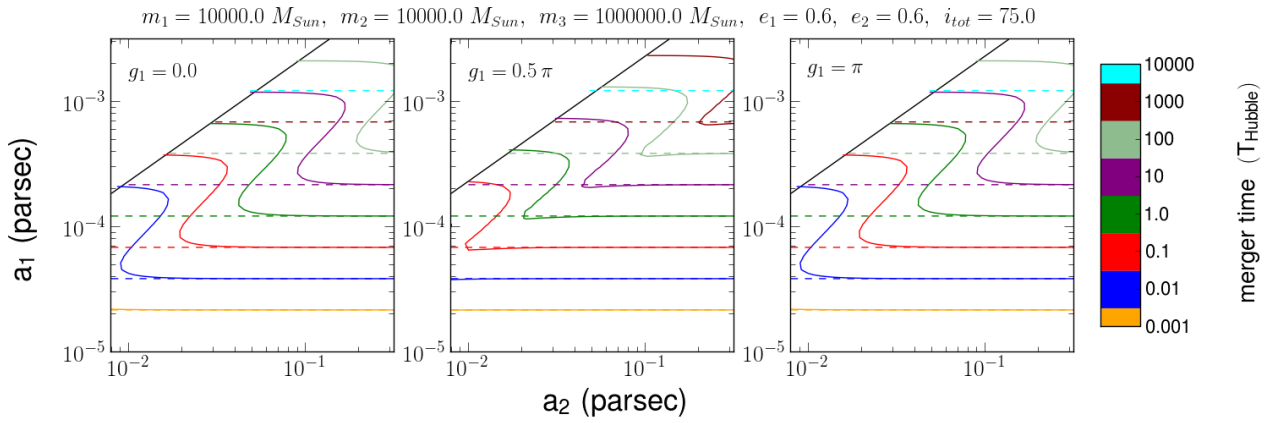

Figure 4.8: Contour plots of the merger time for different values of g_1 (0, $\pi/2$ and π), the initial value of the argument of periastron.

4.3.4 Mass Tertiary Component

In Fig. 4.9 contour plots of the merger time are shown for different values of the mass of the tertiary component m_3 between 10 M_{Sun} and 10^9 M_{Sun}. One can see in these plots that for $m_3 > 10^5$ M_{Sun}, the contours keep the same shape, but shift to the right. This shifting occurs because the general relativistic periastron precession, Eq. 4.39, and the stability of the triples, Eq. 2.118, depend strongly on m_3. For smaller m_3 : $m_3 = 10^3$ M_{Sun} and $m_3 = 10^4$ M_{Sun} we see that the contour lines band down for decreasing a_2, this is the effect we mentioned in Sec. 4.2.4: the maximum eccentricity increases for increasing a_2 such that the merger time decreases.

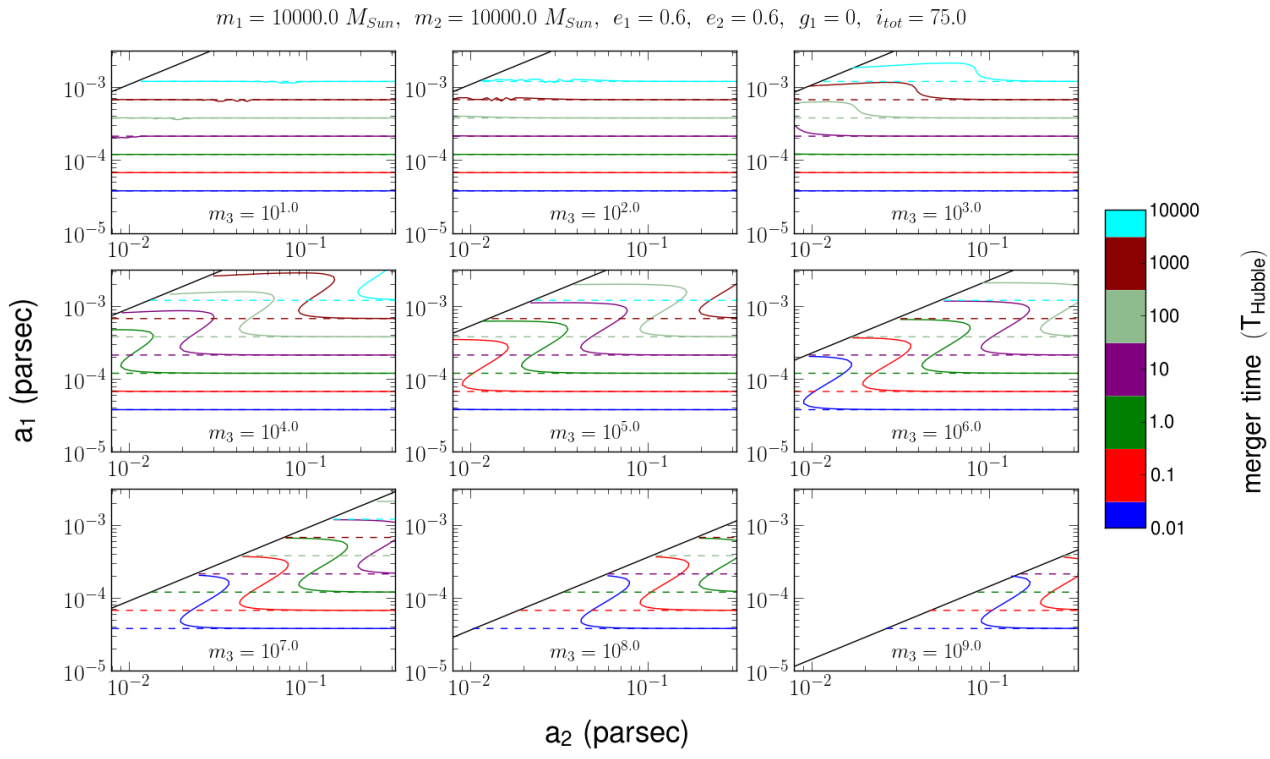

Figure 4.9: Contour plots of the merger time of the inner binary of triples with different values for the mass of the tertiary component. We use $m_3 = 10^x$ M_{Sun} for $x = 1, 2, 3, 4, 5, 6, 7, 8, 9$.

4.3.5 Initial Eccentricity Inner Orbit

In Fig. 4.10 contour plots are shown for different values of the initial eccentricity of the inner orbit e_1, namely, $e_1 = 0.01$, 0.6 and 0.9. We conclude from these contour plots that the factor the merger time of an inner binary increases with respect to the merger time of an isolated binary, increases slightly for larger e_1. One also finds that the contours of the system with a tertiary deviate from the contours without a tertiary more abruptly for smaller e_1.

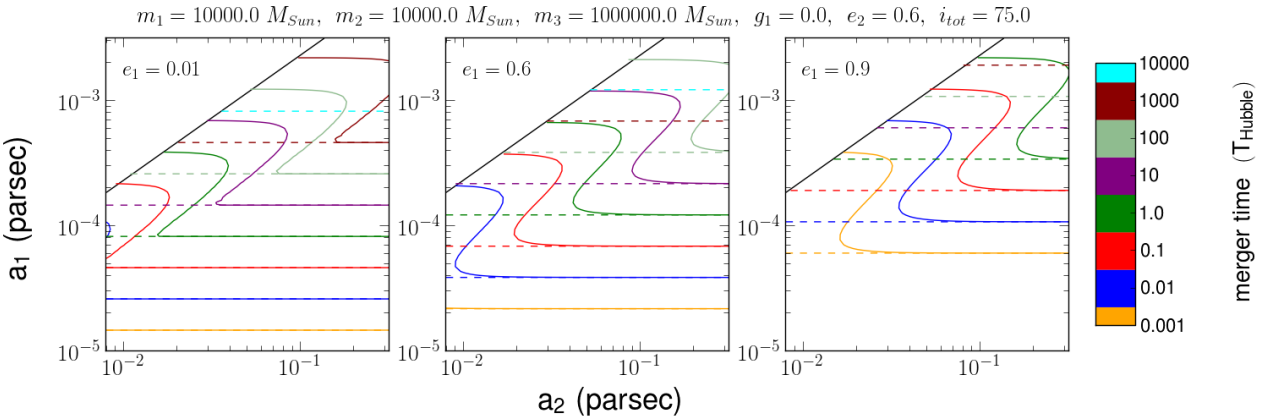

Figure 4.10: Contour plots of the merger time of the inner binary of triples with different values for the initial eccentricity of the inner orbit.

4.3.6 Initial Eccentricity Outer Orbit

Fig. 4.11 shows contour plots of the merger time of the inner binary of triples with different values for e_2, the initial eccentricity of the outer orbit. The values $e_2 = 0.01$, 0.6, 0.9 are used. We conclude from these plots that the contours keep the same shape, but shift to the right as e_2 increases. This has to do with the dependence of the criteria for stability, Eq. 2.118, and periastron precession, Eq. 4.39, on e_2.

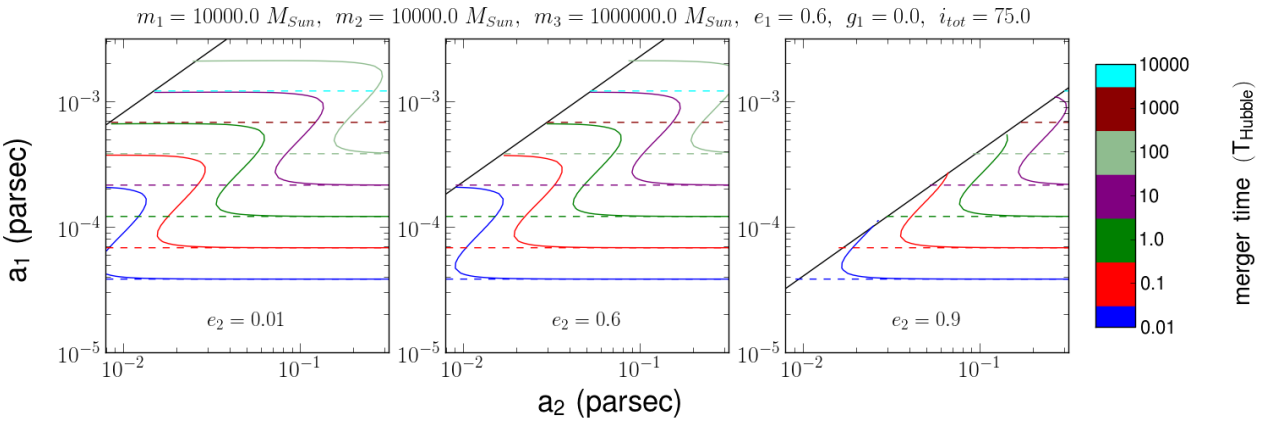

Figure 4.11: Contour plots for different values of the initial eccentricity of the outer orbit.

4.3.7 Mass Space

Instead of contour plots of the merger time in the $a_1 - a_2$ space, we can also show them in the $m_1 - m_2$ space. A problem is that we then consider systems in which the octupole term is important, such that the fast method is not very effective. This is the reason that we only show a plot made in the $m_1 - m_2$ space in which we also add the contour lines that follow from integration of the equations of motion (like Fig. 4.5). This plot can be found in Fig. 4.12 for a system with $a_1 = 10^{-5}$ pc, $a_2 = 0.0008$ pc, $m_3 = 10^6$ $M_{\rm Sun}$, $g_1 = 0.1$, $g_2 = 0$, $e_1 = e_2 = 0.4$ and $i_{\rm tot} = 85.9$ deg. Again the contours of the merger time of the inner binary that follow from integration of the equations of motion are the solid lines, the contours that follow from the fast method are the dashed-dotted lines

and the contours of an isolated triple are the dashed lines. The black solid line is the criterion for stability, Eq. 2.118, the black dashed line is the criterion for periastron precession, Eq. 4.39, and the black dashed-dotted line is the criterion for the Kozai effect, Eq. 4.41. From Fig. 4.12 we find that the fast method is a good approximation for the systems in this plot. Only for m_2 small and m_1 near the stability limit it seems to go wrong. This effect is caused by an anti-symmetry in the equations of motion: there is a factor $m_1 - m_2$ in the octupole term. Because the fast method is derived from the quadrupole Hamiltonian, we do not find this behavior with the fast method. This anti-symmetry is very strange, because in deriving the equations of motion, we average over the mean anomaly. Thus, you expect that the equations of motion should be symmetric under interchanging m_1 and m_2.

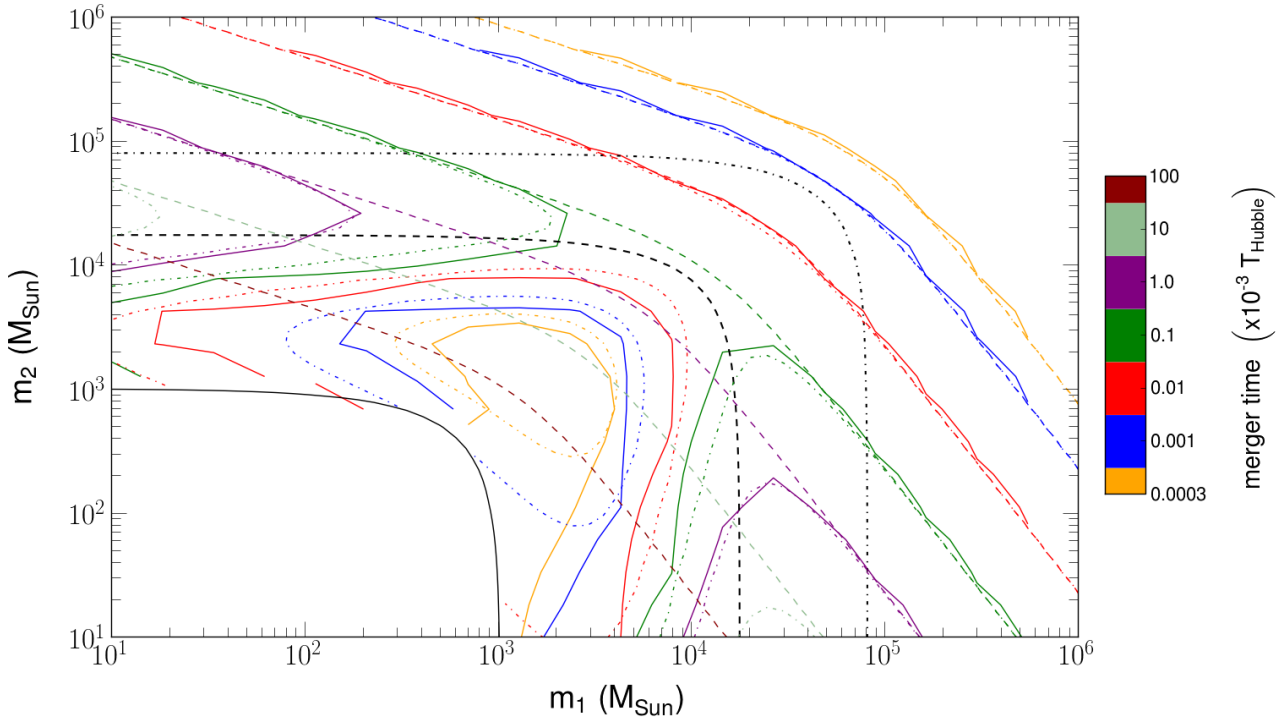

Figure 4.12: Contours of the merger time of the inner binary of triples with $a_1 = 10^{-5}$ pc, $a_2 = 0.0008$ pc, $m_3 = 10^6$ M_{Sun}, $g_1 = 0.1$, $g_2 = 0$, $e_1 = e_2 = 0.4$ and $i_{tot} = 85.9$ deg. We show contours that follow from integration of the equations of motion (solid lines) and from the fast method (dashed-dotted lines). Also shown are contours of the merger time for an isolated binary (dashed lines). The black solid line is Eq. 2.118, the criterion for stability, the black dashed line is Eq. 4.39, the criterion for general relativistic periastron precession and the black dashed-dotted line is Eq. 4.41, the criterion for the Kozai effect that we derived in Sec. 4.2.6.

The behavior we find in this plot is caused by two mechanisms. One, the Kozai mechanism which is stronger for smaller masses and second, the merger time of an isolated binary which is smaller for larger masses. One expects from these two mechanisms, that there is a combination of m_1 and m_2 for which we find a local minimum in the merger time in $m_1 - m_2$ space. We find that behavior with the fast method, but not when we integrate the equations of motion because of the anti-symmetry in m_1 and m_2.

Chapter 5

Merger Time Outer Binary

Consider a hierarchical triple in which the inner binary merges. As we have seen before, this triple can be treated as a system of two binaries: the inner binary consisting of masses m_1 and m_2, and the outer binary consisting of the tertiary component with mass m_3 and the center of mass of the inner binary with mass $m_1 + m_2$. This outer orbit has semi-major axis a_2 and eccentricity e_2. When we derived the Newtonian secularized equations of motion for a hierarchical triple, we have seen that e_2 only changes in octupole order. e_2 and a_2 also change because of gravitational radiation, but for most hierarchical triples the tertiary is on such a wide orbit, that the gravitational radiation is not effective before the merger of the inner binary. We can thus consider e_2 and a_2 to be constant.

When the merger occurs, the triple system reduces to a binary consisting of the tertiary component and the merger product of the inner binary; we will still refer to this binary as the outer binary. Gravitational radiation carries away linear momentum. Because of conservation of this momentum, the mass of the merger product is not simply the sum of the inner masses, but slightly less; it also gets a velocity kick and a spin. We will assume this kick to be instantaneous. Lousto et al. (2010) found empirical formulas for these quantities using theoretical expressions and nonlinear numerical simulations. Assuming that the masses before the merger have a zero spin, these quantities are:

$$\begin{aligned} v_{\rm kick} &= 1.2 \cdot 10^4 \frac{\eta^2(1-q)}{1+q} \left[1 - 0.93\eta\right] \text{ km/s}; \\ m &= \left(1 - \eta\tilde{E}_{\rm ISCO} - E_2\eta^2 - E_3\eta^3\right)(m_1+m_2); \\ \alpha_{\rm final} &= \left(\frac{m}{m_1+m_2}\right)^{-2} \left\{\eta\tilde{\mathbf{J}}_{\rm ISCO} + (J_2\eta^2 + J_3\eta^3)\hat{n}_{\rm par}\right\}, \end{aligned} \tag{5.1}$$

where $v_{\rm kick}$ is the speed of the velocity kick (the recoil velocity), m is the new mass, $\alpha_{\rm final}$ is the spin of the merger product, $q = m_1/m_2 \leq 1$, $\eta = \frac{q}{(1+q)^2}$, $\tilde{E}_{\rm ISCO} \approx (1-\sqrt{8}/3) + 0.103803\eta$, $E_2 = 0.341 \pm 0.014$, $E_3 = 0.522 \pm 0.062$, $\tilde{\mathbf{J}}_{\rm ISCO} = \left(2\sqrt{3} - 1.5255862\eta\right)\hat{n}_{\rm par}$, $J_2 = -2.81 \pm 0.11$, $J_3 = 1.69 \pm 0.51$ and $\hat{n}_{\rm par}$ is the unit vector parallel to the orbital angular momentum of the inner binary. Assuming that the black holes of the inner binary have a zero spin before the merger, the velocity kick is in the orbital plane of the inner binary. If we consider $v_{\rm kick}$ as a function of q, we find a maximum of $v_{\rm kick} = 153$ km/s for $q = m_1/m_2 = 0.24$. We will neglect the final spin and only consider the velocity kick and mass loss. By these two effects the orbital elements of the outer orbit change and this effects the merger time of the outer binary: depending on the speed of the velocity kick, the direction with respect to the remaining mass and the position of the merger product in the outer orbit, the merger time increases or decreases. We will now calculate how the merger time of the outer binary changes as result of the merger of the inner binary. Because we neglect the spin that the merger product receives by the merger, we can use Eq. 4.1 to calculate the merger time. If the black holes have a spin, more gravitational energy is radiated by the masses such that the merger time will become smaller than if they do not have a spin. Eq. 4.1 for the merger time depends on the resulting mass of the inner binary m, the mass of the tertiary component m_3, the new eccentricity e_2', and new semi-major axis a_2'.

5.1 Expressions Changed Semi-Major Axis and Eccentricity

In this section, expressions will be derived for the new eccentricity e_2' and new semi-major axis a_2' of the outer orbit after the inner binary receives a kick. The orbital elements of the outer orbit before the merger of the inner binary

are the eccentricity e_2, the semi-major axis a_2, the argument of periastron g_2, and the position of the masses in the orbit f_2; Fig. 5.1b illustrates both f_2 and g_2.

In Sec. 2.3 we stated that the length of the vector pointing from the tertiary component to the (center of mass of the) inner binary can be written as:

$$r = \frac{c}{1 + e_2 \cos(f_2)}, \tag{5.2}$$

where

$$c = a_2(1 - e_2^2). \tag{5.3}$$

Also, the length of the vector pointing from the center of mass of the triple to the inner binary is:

$$r_1 = \frac{m_3}{m_1 + m_2 + m_3} r = \frac{m_3}{M_\mathrm{t}} r, \tag{5.4}$$

where $M_\mathrm{t} = m_1 + m_2 + m_3$. The angular momentum of the orbit is:

$$G_2 = \frac{m_3(m_1 + m_2)}{\sqrt{m_1 + m_2 + m_3}} \sqrt{G_N a_2 (1 - e_2^2)} = \sqrt{c\gamma\mu}, \tag{5.5}$$

where

$$\begin{aligned} \gamma &= G_N m_3 (m_1 + m_2); \\ \mu &= \frac{m_3(m_1 + m_2)}{m_1 + m_2 + m_3}. \end{aligned} \tag{5.6}$$

We also know that

$$G_2 = \mu r^2 \dot{f}_2. \tag{5.7}$$

$\dot{f}_2$ is also the angular velocity of the inner binary, thus from Eq. 5.7 we are able to find an expression for the tangential velocity component v_f of the inner binary:

$$v_f = r_1 \dot{f}_2 = r_1 \frac{G_2}{\mu r^2}. \tag{5.8}$$

The radial velocity component of the inner binary follows with Eqs. 5.2, 5.4, 5.5 and 5.8 as

$$\begin{aligned} v_r &= \frac{m_3}{M_\mathrm{t}} \frac{c}{(1 + e_2 \cos(f_2))^2} e_2 \sin(f_2) \dot{f}_2 \\ &= \frac{m_3}{M_\mathrm{t}} \frac{e_2 \sin(f_2)}{c} r^2 \dot{f}_2 \\ &= \frac{m_3}{M_\mathrm{t}} \frac{G_2 e_2 \sin(f_2)}{c\mu} \\ &= \frac{m_3}{M_\mathrm{t}} \frac{\gamma e_2 \sin(f_2)}{G_2}. \end{aligned} \tag{5.9}$$

Finally, using Eq. 2.16, the energy of the orbit is equal to:

$$E_2 = \frac{m_1 + m_2}{2} \frac{M_\mathrm{t}}{m_3} v_r^2 - \frac{\gamma}{r} + \frac{G_2^2}{2\mu r^2} = \frac{\gamma^2 \mu (e_2^2 - 1)}{2 G_2^2}. \tag{5.10}$$

Note that Eqs. 5.2 - 5.10 are also valid for the outer binary after the kick if we substitute $e_2 \to e_2'$, $a_2 \to a_2'$, $c \to c'$, $f_2 \to f_2'$, $r_1 \to r_1'$, $m_1 + m_2 \to m$, $\mu \to \mu'$, $\gamma \to \gamma'$, $G_2 \to G_2'$ and $E_2 \to E_2'$ where the apostrophe indicates the new value. Since we assume that the kick is instantaneous, the distance between the tertiary component and inner binary r does not change by the merger of the inner binary.

Define in the orbital plane of the outer binary the y-axis in the direction of periastron and the x-axis perpendicular to this direction (Fig. 5.1b) and let the z-axis be perpendicular to this plane such that we have a right-handed coordinate system. The kick velocity can be expanded in components in x, y and z direction, which will be denoted by $v_{\mathrm{k}x}$, $v_{\mathrm{k}y}$, $v_{\mathrm{k}z}$ respectively. This can also be done for the initial velocity $\mathbf{v}_\mathrm{i}$. From Fig. 5.1b we find that the components of $\mathbf{v}_\mathrm{i}$ in this coordinate system are equal to:

$$\begin{aligned} v_{\mathrm{i}x} &= -v_f \cos(f_2) - v_r \sin(f_2); \\ v_{\mathrm{i}y} &= -v_f \sin(f_2) + v_r \cos(f_2); \\ v_{\mathrm{i}z} &= 0. \end{aligned} \tag{5.11}$$

The new velocity of the inner binary $\mathbf{v}_{\rm n}$ has components:

$$\begin{aligned} v_{{\rm n}x} &= v_{{\rm i}x} + v_{{\rm k}x}; \\ v_{{\rm n}y} &= v_{{\rm i}y} + v_{{\rm k}y}; \\ v_{{\rm n}z} &= v_{{\rm k}z}. \end{aligned} \tag{5.12}$$

The position vector of the inner binary $\mathbf{r}_1$ has coordinates $\mathbf{r}_1 = (-r_1 \sin(f_2), r_1 \cos(f_2), 0)$ in this coordinate system. The new orbital plane is the plane spanned by $\mathbf{r}_1$ and $\mathbf{v}_{\rm n}$. To calculate the components $v_{{\rm n}f}$ and $v_{{\rm n}r}$ of $\mathbf{v}_{\rm n}$ in the new orbital plane, we need the angle θ between $\mathbf{r}_1$ and $\mathbf{v}_{\rm n}$, which follows from the inner product:

$$\theta = \arccos\left(\frac{\mathbf{r}_1 \cdot \mathbf{v}_{\rm n}}{r_1 v_{\rm n}}\right), \tag{5.13}$$

where $v_{\rm n}$ is the magnitude of $\mathbf{v}_{\rm n}$. We then find that

$$\begin{aligned} v_{{\rm n}f} &= v_{\rm n} \sin(\theta); \\ v_{{\rm n}r} &= v_{\rm n} \cos(\theta). \end{aligned} \tag{5.14}$$

Using the new mass m of the remainder of the inner binary, the constants μ and γ change into:

$$\begin{aligned} \mu' &= \frac{m m_3}{m + m_3}; \\ \gamma' &= G_N m m_3. \end{aligned} \tag{5.15}$$

r is conserved during the merger, but the center of mass is not. Hence, the value for r_1 changes to:

$$r_1' = \frac{m_3}{m + m_3} r. \tag{5.16}$$

The angular velocity of the remainder of the inner binary is:

$$\dot{f}_2' = \frac{v_{{\rm n}f}}{r_1'}, \tag{5.17}$$

hence, using Eq. 5.7, we find that the new angular momentum is equal to:

$$G_2' = \mu' r^2 \dot{f}_2'. \tag{5.18}$$

With Eq. 5.5 this results in

$$c' = \frac{G_2'^2}{\gamma' \mu'}. \tag{5.19}$$

From Eq. 5.10 we can calculate the new energy:

$$E_2' = \frac{m}{2} \frac{m + m_3}{m_3} v_{\rm nr}^2 - \frac{\gamma'}{r} + \frac{G_2'^2}{2\mu' r^2} \tag{5.20}$$

and by Eq. 5.10 we find the new eccentricity to be:

$$e_2' = \sqrt{\frac{2 G_2'^2 E_2'}{\gamma'^2 \mu'} + 1}\,. \tag{5.21}$$

From Eq. 5.3 the new semi-major axis follows as:

$$a_2' = \frac{c'}{1 - e_2'^2}. \tag{5.22}$$

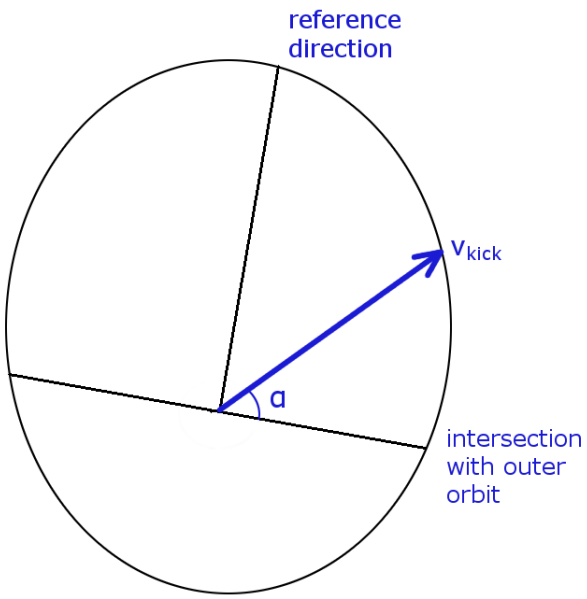

(a) Orbital plane of the inner binary. There is an angle $i_{\rm tot}$ between this plane and the orbital plane of the outer binary. The intersection with the outer orbit is drawn, also the reference direction, which is perpendicular to this intersection. Between the velocity kick and intersection is an angle α.

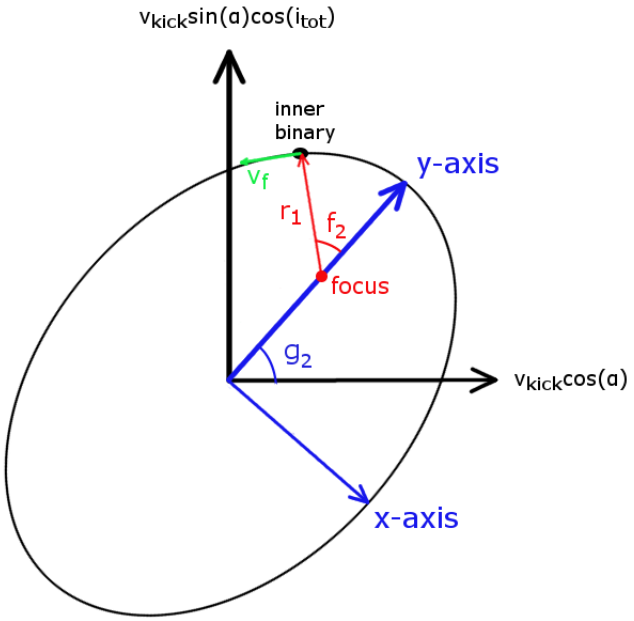

(b) The orbit of the inner binary in the outer orbital plane. The component of the kick velocity $v_{\rm kick}\sin(\alpha)\cos(i_{\rm tot})$ makes an angle $i_{\rm tot}$ with the reference direction in the orbital plane of the inner binary. The component $v_{\rm kick}\cos(\alpha)$ is in the direction of the intersection of the inner and outer orbital plane. The y-axis is in the direction of periastron and makes an angle g_2 with the intersection with the inner orbital plane. The x-axis is perpendicular to the y-axis. The position of the inner binary is shown by means of the true anomaly f_2. The distance between the focus and the inner binary is r_1 and the velocity of the inner binary in tangential direction with respect to the focus is v_f.

Figure 5.1

We have verified the equations for the changed eccentricity and semi-major axis against the Kepler solver implemented in AMUSE.

We still have to find expressions for $v_{{\rm k}x}$, $v_{{\rm k}y}$ and $v_{{\rm k}z}$. In the following we denote the orbit of the inner binary in the outer orbital plane by the outer orbit. Note that this definition is slightly different from the one we used before, because there we denoted the orbit of the vector between the tertiary and inner binary by the outer orbit.

Define the reference direction in the orbital plane of the inner binary perpendicular to the intersection of the orbital planes of inner and outer binary. Denote the angle between the velocity kick and the intersection with the outer orbital plane by α. In Fig. 5.1a one can find an illustration of the orbital plane of the inner binary. The velocity component in the orbital plane of the inner binary in the reference direction is $v_{\rm kick}\sin(\alpha)$, the angle between the inner and outer orbital plane is $i_{\rm tot}$, so the component of $v_{\rm kick}\sin(\alpha)$ in the orbital plane of the outer binary is $v_{\rm kick}\sin(\alpha)\cos(i_{\rm tot})$. And the velocity component perpendicular to the orbital plane of the outer binary is $v_{{\rm k}z} = -v_{\rm kick}\sin(\alpha)\sin(i_{\rm tot})$. The velocity component in the orbital plane of the inner binary in the direction perpendicular to the reference direction is $v_{\rm kick}\cos(\alpha)$. From these components and using Fig. 5.1b, we find that the components of the kick velocity in x, y and z-direction are:

$$\begin{aligned} v_{{\rm k}x} &= -v_{\rm kick}\sin(\alpha)\cos(i_{\rm tot})\cos(g_2) + v_{\rm kick}\cos(\alpha)\sin(g_2); \\ v_{{\rm k}y} &= v_{\rm kick}\sin(\alpha)\cos(i_{\rm tot})\sin(g_2) + v_{\rm kick}\cos(\alpha)\cos(g_2); \\ v_{{\rm k}z} &= -v_{\rm kick}\sin(\alpha)\sin(i_{\rm tot}). \end{aligned} \tag{5.23}$$

5.2 New Merger Time

The kick can cause the system to become unbound, this is equivalent to $e_2' \geq 1$. If this does not happen, the outer binary will eventually merge. If we use the new mass m, m_3 and Eqs. 5.21 and 5.22 as input for Eq. 4.1 we have

a formula for the merger time of the binary, but this formula is rather complicated. It is possible to derive an expression that is more manageable. If we use Eq. 4.3 as approximation for the merger time, we find

$$t_{\rm merge} \approx \frac{1}{4}\frac{1}{\beta}a_2'^4(1-e_2'^2)^4 = \frac{5c^5}{256G_N^3}\frac{a_2'^4(1-e_2'^2)^4}{mm_3(m+m_3)}, \tag{5.24}$$

where we also used Eq. 4.2. Define $C = \frac{5c^5}{256G_N^3}$ and recall that $c' = a_2'(1-e_2'^2)$, so that we can approximate

$$t_{\rm merge} \approx C\frac{c'^4}{mm_3(m+m_3)}. \tag{5.25}$$

Furthermore, if one assumes that $m < m_1 + m_2 \ll m_3$ we find that $\frac{\mu'}{\gamma'} = \frac{1}{G_N(m+m3)} \approx \frac{\mu}{\gamma}$ and $r_1 \approx r$, hence from Eqs. 5.18 and 5.19 it follows that

$$c' = \frac{\mu' r^2 v_{{\rm n}f}^2}{\gamma'} \approx \lambda^2 c, \tag{5.26}$$

where

$$\lambda = \frac{v_{{\rm n}f}}{v_f}. \tag{5.27}$$

Applying Eqs. 5.2, 5.5 and 5.8 we find that

$$\begin{aligned}
\frac{1}{v_f} &\approx \frac{\mu r}{G_2} \\
&= \frac{\mu c}{\sqrt{c\gamma\mu}(1+e_2\cos(f_2))} \\
&= \sqrt{\frac{a_2(1-e_2^2)}{G_N(m_1+m_2+m_3)}}\frac{1}{(1+e_2\cos(f_2))} \\
&\approx \sqrt{\frac{a_2(1-e_2^2)}{G_N m_3}}\frac{1}{(1+e_2\cos(f_2))}.
\end{aligned} \tag{5.28}$$

where we, in the final step, once again used that $m_1 + m_2 \ll m_3$.

Inverting Eqs. 5.11 yields

$$v_f = -v_{{\rm i}x}\cos(f_2) - v_{{\rm i}y}\sin(f_2) \tag{5.29}$$

and similar we find that

$$v_{{\rm k}f} = -v_{{\rm k}x}\cos(f_2) - v_{{\rm k}y}\sin(f_2) \tag{5.30}$$

where $v_{{\rm k}f}$ is the tangential component of the kick velocity in the orbital plane of the outer binary before the merger. Using Eqs. 5.12, 5.13, 5.14, 5.29 and 5.30 we find that

$$\begin{aligned}
v_{{\rm n}f} &= v_{\rm n}\sin(\theta) = \sqrt{v_{\rm n}^2 - \left(-(v_{{\rm i}x}+v_{{\rm k}x})\sin(f_2) + (v_{{\rm i}y}+v_{{\rm k}y})\cos(f_2)\right)^2} \\
&= \sqrt{(v_{{\rm i}x}+v_{{\rm k}x})^2\cos^2(f_2) + (v_{{\rm i}y}+v_{{\rm k}y})^2\sin^2(f_2) + v_{{\rm k}z}^2 + 2(v_{{\rm i}x}+v_{{\rm k}x})\sin(f_2)(v_{{\rm i}y}+v_{{\rm k}y})\cos(f_2)} \\
&= \sqrt{v_{{\rm k}z}^2 + (v_f + v_{{\rm k}f})^2}.
\end{aligned} \tag{5.31}$$

Using Eqs. 5.27, 5.28 and 5.31 we find that

$$\begin{aligned}
\lambda &= \frac{v_{{\rm n}f}}{v_f} \\
&= \sqrt{\left(\frac{v_{{\rm k}z}}{v_f}\right)^2 + \left(1+\frac{v_{{\rm k}f}}{v_f}\right)^2} \\
&\approx \sqrt{\frac{a_2(1-e_2^2)}{G_N m_3}\frac{v_{{\rm k}z}^2}{(1+e_2\cos(f_2))^2} + \left(1+\sqrt{\frac{a_2(1-e_2^2)}{G_N m_3}}\frac{v_{{\rm k}f}}{(1+e_2\cos(f_2))}\right)^2}.
\end{aligned} \tag{5.32}$$

Hence,

$$\lambda^2 c = \frac{a_2^2(1-e_2^2)^2}{G_N m_3}\frac{v_{\rm kz}^2}{(1+e_2\cos(f_2))^2} + \left(1+\sqrt{\frac{a_2(1-e_2^2)}{G_N m_3}}\frac{v_{\rm kf}}{(1+e_2\cos(f_2))}\right)^2 a_2(1-e_2^2) \tag{5.33}$$

and we obtain the following formula for the changed merger time (Eq. 5.25):

$$\begin{aligned} t_{merge} &\approx C\frac{c'^4}{mm_3(m+m_3)} \\ &\approx \frac{C}{mm_3^2}\left(\frac{a_2^2(1-e_2^2)^2}{G_N m_3}\frac{v_{\rm kz}^2}{(1+e_2\cos(f_2))^2} + \left(1+\sqrt{\frac{a_2(1-e_2^2)}{G_N m_3}}\frac{v_{\rm kf}}{(1+e_2\cos(f_2))}\right)^2 a_2(1-e_2^2)\right)^4 . \end{aligned} \tag{5.34}$$

Note that it does not follow from this formula if or when a system becomes unbound. In the derivation we used the constant c', which is only equal to $a_2'(1-e_2'^2)$ for bound systems.

This derivation is with a few small adaptations also valid if $m \approx m_1+m_2$ (if we not assume that $m < m_1+m_2 \ll m_3$). Eq. 5.34 should be multiplied with a factor $\frac{m_3}{m_1+m_2+m_3}$ and the masses m_3 within the brackets should be replaced by $m_1+m_2+m_3$.

5.2.1 Necessary Velocity Kick for Merger within Time T

To examine what merger times can be reached when the inner binary receives a kick, we consider a system in which, before the merger of the inner binary, $g_2 = \frac{1}{2}\pi + k\pi$ where $k \in \mathbb{Z}$. We also consider a fixed kick velocity $v_{\rm kick}$. We are interested in the value of $v_{\rm kick}$ such that for every value of e_2 and a_2 there is a direction of the kick α and a position in the orbit f_2 such that the merger time is equal to a certain time T.

Let $\alpha = (k+1)\pi$, hence $v_{\rm kz} = 0$. At apastron ($f_2 = \pi$) $v_{\rm kf} = -v_{\rm kick}$. If the expression within the square in Eq. 5.34 is negative for $v_{\rm kz} = 0$ and $v_{\rm kf} = -v_{\rm kick}$, we can choose another f_2 such that $t_{\rm merge} = 0$ (by varying f_2 we can vary $v_{\rm kf}$ between $-v_{\rm kick}$ and $v_{\rm kick}$ while $v_{\rm kz}$ remains zero). Thus, the minimum value of Eq. 5.34 considered as function of α and f_2 is 0 if

$$v_{\rm kick} \geq \sqrt{\frac{G_N m_3}{a_2(1-e_2^2)}}(1-e_2) = \sqrt{\frac{G_N m_3(1-e_2)}{a_2(1+e_2)}}. \tag{5.35}$$

and its minimum value is

$$t_{\rm merge} \approx \frac{C}{mm_3^2}\left(1-\sqrt{\frac{a_2(1+e_2)}{G_N m_3(1-e_2)}}v_{\rm kick}\right)^8 a_2^4(1-e_2^2)^4 = \frac{C}{mm_3^2}\left(\sqrt{a_2(1-e_2^2)} - \frac{a_2(1+e_2)}{\sqrt{G_N m_3}}v_{\rm kick}\right)^8 \tag{5.36}$$

if

$$v_{\rm kick} \leq \sqrt{\frac{G_N m_3(1-e_2)}{a_2(1+e_2)}}. \tag{5.37}$$

Consider the second case. It is clear that the minimum merger time decreases with increasing e_2. This is caused by two mechanisms: first, the merger time without a kick would already be small because a system radiates more gravitational radiation when e_2 is closer to 1, and second, because of the large eccentricity the velocity at apastron is small such that the kick velocity has a greater impact. Thus, the minimum merger time is the largest for $e_2 = 0$; if we want the value of the kick such that for every combination of a_2, e_2 the merger time T can be reached, we should substitute $e_2 = 0$ in Eq. 5.36. Equating Eq. 5.36 with a merger time T gives:

$$\frac{C}{mm_3^2}\left(\sqrt{a_2} - \frac{a_2}{\sqrt{G_N m_3}}v_{\rm kick}\right)^8 = T \tag{5.38}$$

or

$$\sqrt{a_2} - \sqrt{\frac{1}{G_N m_3}}v_{\rm kick}a_2 = \left(\frac{Tmm_3^2}{C}\right)^{1/8}. \tag{5.39}$$

This is a quadratic equation in $\sqrt{a_2}$ and will have 2 solutions as long as the discriminant is larger than zero. The two solutions are the boundary of a range in a_2 where the minimum merger time is larger than T. This happens when

$$1 - 4\sqrt{\frac{1}{G_N m_3}}\left(\frac{Tmm_3^2}{C}\right)^{1/8} v_{\rm kick} > 0. \tag{5.40}$$

It follows that for

$$v_{\rm kick} > \frac{1}{4}\sqrt{G_N m_3}\left(\frac{C}{Tmm_3^2}\right)^{1/8} \tag{5.41}$$

for each possible combination of a_2, e_2 there is a certain combination of α and f_2 such that we have a merger time T.

Note that the situation changes for other values of g_2, because in those cases $v_{{\rm k}f}$ can not reach $-v_{\rm kick}$ at apastron (Eq. 5.30). This causes the derivation above to be not valid anymore.

5.2.2 Change Distribution Merger Times by Kick

The formulas derived above, show that if the kick is larger than a certain value, it is is possible to reach a certain merger time. But the more interesting part is the fraction of systems that merges faster; we would like to see how the distribution of merger times changes when we apply a certain kick. We first examined this for a system with $m_1 = 10^3$ $\mathrm{M_{Sun}}$, $m_2 = 10^4$ $\mathrm{M_{Sun}}$, $m_3 = 10^6$ $\mathrm{M_{Sun}}$, $a_2 = 10^{-3}$ pc, $e_2 = 0.4$, $g_2 = \frac{3}{2}\pi$ and $i_{\rm tot} = 1.1(\approx 63\,\mathrm{deg})$, using a Monte Carlo simulation: from distributions (that are defined below) for the direction of the kick α and the true anomaly f_2 a distribution of the merger time is created. We initiated α and f_2, evaluated Eqs. 5.21 and 5.22 and substituted these values in Eq. 4.1 such that eventually, we found a distribution of the merger time. We took α from a flat distribution between 0 and 2π, because the direction of the kick is random, and for f_2 we used the distribution

$$\frac{1}{2\pi}\frac{(1-e_2^2)^{3/2}}{(1+e_2\cos(f_2))^2}. \tag{5.42}$$

We know that the mean anomaly l_2 is uniformly divided between 0 and 2π. Since Eq. 5.42 is the derivative of the mean anomaly with respect to the true anomaly normalized to 1, this is the distribution for the true anomaly. We created a value for f_2 from this distribution by drawing a value r from a flat distribution between 0 and 1 and using the cumulative function of the distribution of the true anomaly,

$$F(x) = \int_0^x \frac{1}{2\pi}\frac{(1-e_2^2)^{3/2}}{(1+e_2\cos(x))^2}dx, \tag{5.43}$$

where $0 \leq x \leq 2\pi$ to solve for $F^{-1}(f_2) = r$. We solved this equation with the Newton-Raphson method.

In Fig. 5.2 one can find the resulting distributions for 9 different kick velocities: 100, 200, 400, 600, 800, 1000, 2000, 3000 and 4000 km/s. Of course, we find from Eq. 5.1 that for these systems the kick velocity is always 62 km/s if they have zero spin; if we include spin, kick velocities up to 4000 km/s can be reached, however, in such cases the kick can be outside the orbital plane of the inner binary. To show the quantitative effect of the kick we include large kick velocities, although we assume that they are in the orbital plane of the inner binary. For each distribution 200,000 systems are used which are divided into 50 bins. We also calculated what fraction $f_{e\geq 1}$ becomes unbound after applying the kick. In table 5.1 the average values and standard deviations of the distributions can be found and in Fig. 5.3 the cumulative distributions. The merger time of the binary with masses $m_1 + m_2$ and m_3 without a kick is approximately 2 Hubble times, so we see that the average merger time becomes larger because of the kick. We also see that the distribution of merger times becomes broader with increasing kick velocity. We notice that for a kick velocity of 2000 km/s a significant fraction (approximately 10%) of the systems merge in a time smaller than one-hundred-thousandth of the merger time without kick.

We repeat the process we did above, but now we average over all initial parameters m_1, m_2, m_3, a_2, e_2, g_2, $i_{\rm tot}$, f_2, α and $v_{\rm kick}$. All the systems that were initiated to make the distributions above had the same merger time without a kick. Since we now average over all parameters, we have a distribution of the merger times without a kick. We want to compare the distributions of the merger times without the kick and the merger times as result of the velocity kick. Because the distributions of these parameters are unknown we make some assumptions about them.

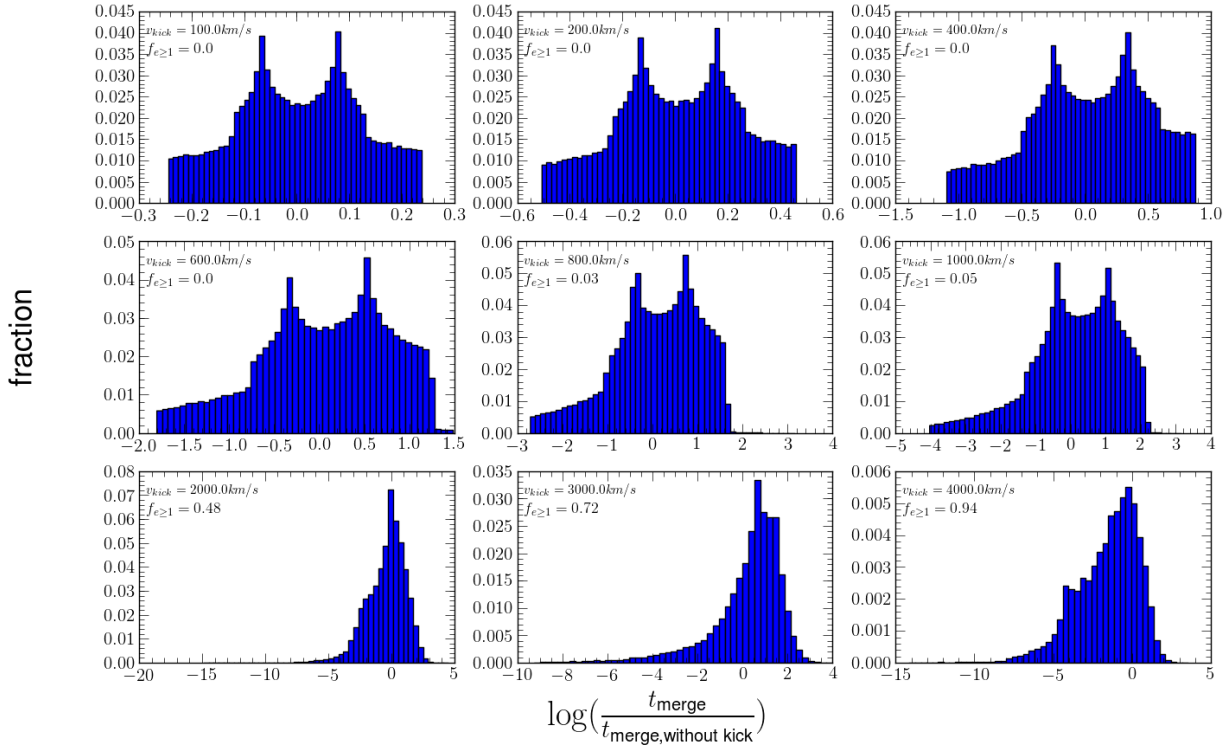

Figure 5.2: Distributions of the change in merger time due to different kick velocities. We used a system with $m_1 = 10^3$ M_{Sun}, $m_2 = 10^4$ M_{Sun}, $m_3 = 10^6$ M_{Sun}, $a_2 = 10^{-3}$ pc, $e_2 = 0.4$, $g_2 = \frac{3}{2}\pi$ and $i_{tot} = 1.1 \approx 63^o$. We used the kick velocities 100, 200, 400, 600, 800, 1000, 2000, 3000, and 4000 km/s and in every histogram we show the fraction of systems that becomes unbound ($e_2' \geq 1$). We used 200,000 points divided into 50 bins for every histogram. Note that the x-axis is logarithmic. One can find the cumulative distributions in Fig. 5.3.

v_{kick}(km/s)	Mean (Myrs)	Standard Deviation (Myrs)
0	27,883	0
100	29,190±18	7,867
200	32,747±38	17,182
400	48,951±106	47,452
600	88,104±261	116,813
800	163,114±635	284,008
1000	351,612±1,579	706,037
2000	365,580±8,399	3,756,178
3000	643,578±6,666	2,981,274
4000	69,936±2,086	932,790

Table 5.1: Mean and standard deviation in Myrs for the distributions of Figs. 5.2 and Fig. 5.3.

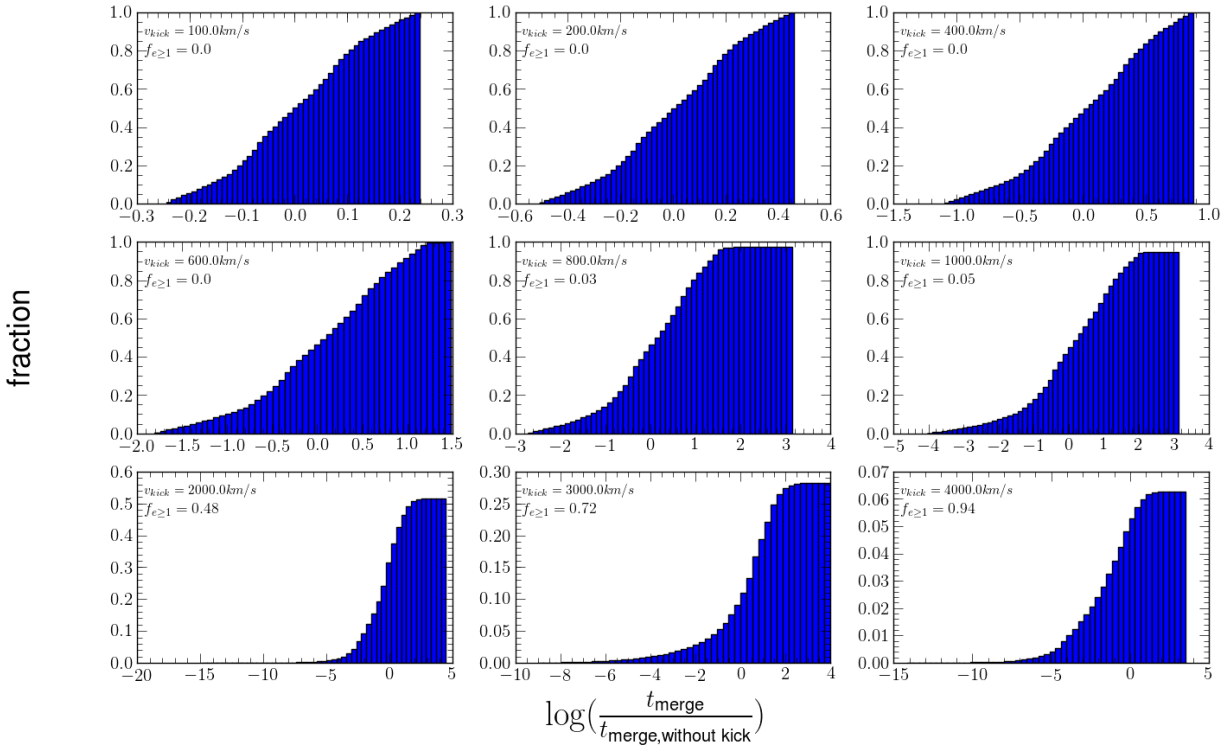

Figure 5.3: Cumulative distributions for the distributions of Fig. 5.2.

We take $m_i = 10^x$ M_{Sun}, where $i \in \{1, 2, 3\}$ and x is drawn from a flat distribution between 0 and 9. For e_2 we use a thermal distribution: $P(e_2) = 2e_2$. g_2 and i_{tot} are drawn from a flat distribution between 0 and 2π, and 0 and π respectively. We use the same distributions as described earlier for f_2 and α. For a_2 and v_{kick} we use different distributions which are defined below. We did three simulations with 2,000,000 systems each, with different v_{kick} and period distributions: Simulation 1) for v_{kick} we use the distribution

$$P(v_{kick}) \propto \frac{v_{kick}}{1000} e^{-(\frac{v_{kick}}{1000}+2)^2}, \tag{5.44}$$

where v_{kick} is in km/s, this distribution is plotted in Fig. 5.4a. Furthermore, we use for a_2 the distribution found by Belczynski et al. (2004). They found an empirical distribution for the periods of black hole binaries in young stellar environments using theoretical models for the black hole population. We have plotted this distribution in Fig. 5.4b. Although in their simulations they only found black hole masses up to 80 M_{Sun}, we use this distribution also for more massive black holes. From this distribution and masses m_1 and m_2 the semi-major axis can be found by using Kepler's third law $T^2 = \frac{4\pi^2}{G_N(m_1+m_2+m_3)} a_2^3$. Simulation 2) We draw v_{kick} from a flat distribution between 0 and 1500 km/s and we use $a_2 = 10^x$ pc where x is drawn from a flat distribution between -6.53 and 0.14. These values give the smallest and largest semi-major axis that we can find from the period distribution we use in simulation 1. Simulation 3) We use for a_2 the same distribution as in simulation 1 and for v_{kick} we use the expression from Eq. 5.1, $v_{kick} = 1.2 \cdot 10^4 \frac{\eta^2(1-q)}{1+q} [1 - 0.93\eta]$ km/s. Note that for simulation 3 the most realistic kick velocities are used, because we assume that we are dealing with black holes that initially have no spin. In simulation 2 and 3 much larger kick velocities are reached, so the effect of the kick should be clearer. In Table 5.2 we show a survey of the distributions used for v_{kick} and a_2 in the different simulations.

Simulation	v_{kick}	a_2
1	Eq. 5.44	(Belczynski et al., 2004)
2	Flat between 0 and 1500 km/s	Flat in logarithmic space
3	Eq. 5.1	(Belczynski et al., 2004)

Table 5.2: Per simulation the distributions that are used for v_{kick} and a_2.

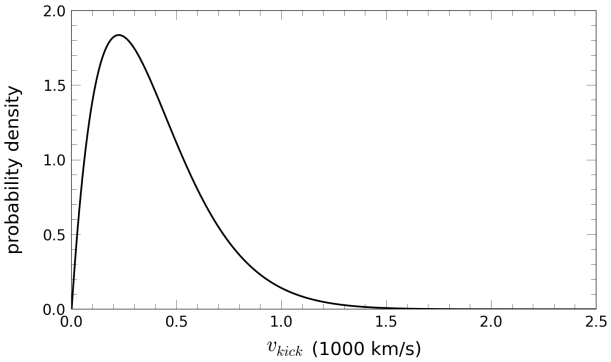

(a) Distribution of the kick velocity that we used for simulation 1.

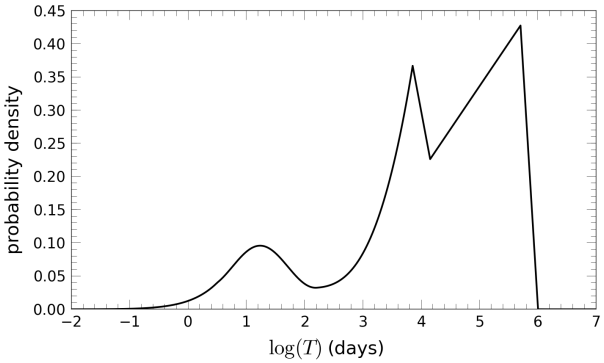

(b) Distribution of the period of the outer binary that we used for simulation 1 and 3 (Belczynski et al., 2004).

Figure 5.4

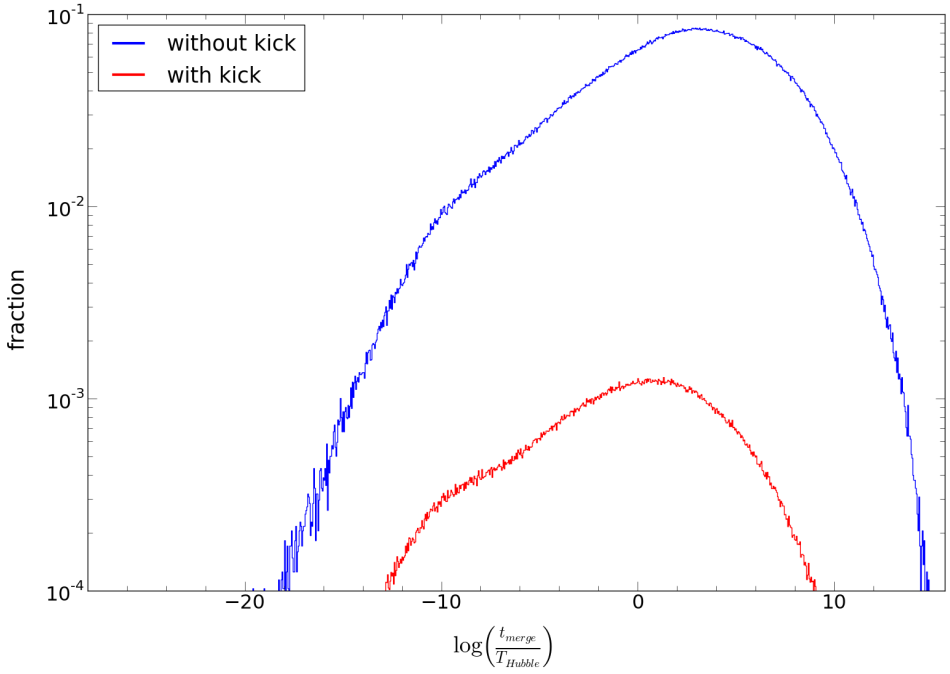

Figure 5.5: Distributions of the merger time resulting from simulation 1, we used 2,000,000 systems for these plots divided over 1000 bins. The blue curve is the distribution of merger times without a kick. The red curve is the distribution for the same systems with a kick. 67% of the systems become unbound by the kick.

5.2.2.1 Simulation 1

In Fig. 5.5 the distributions resulting from simulation 1 can be found. The blue curve is the distribution of the merger times when there is no kick. If we include the kick, we find that 67% of the systems become unbound. The distribution of the merger times of the other systems is the red curve in Fig. 5.5. Due to the kick, many systems become unbound and the distribution of merger times of the remaining systems shifts to shorter times and narrows. The large fraction of the systems that becomes unbound is due to the relatively large kick velocities.

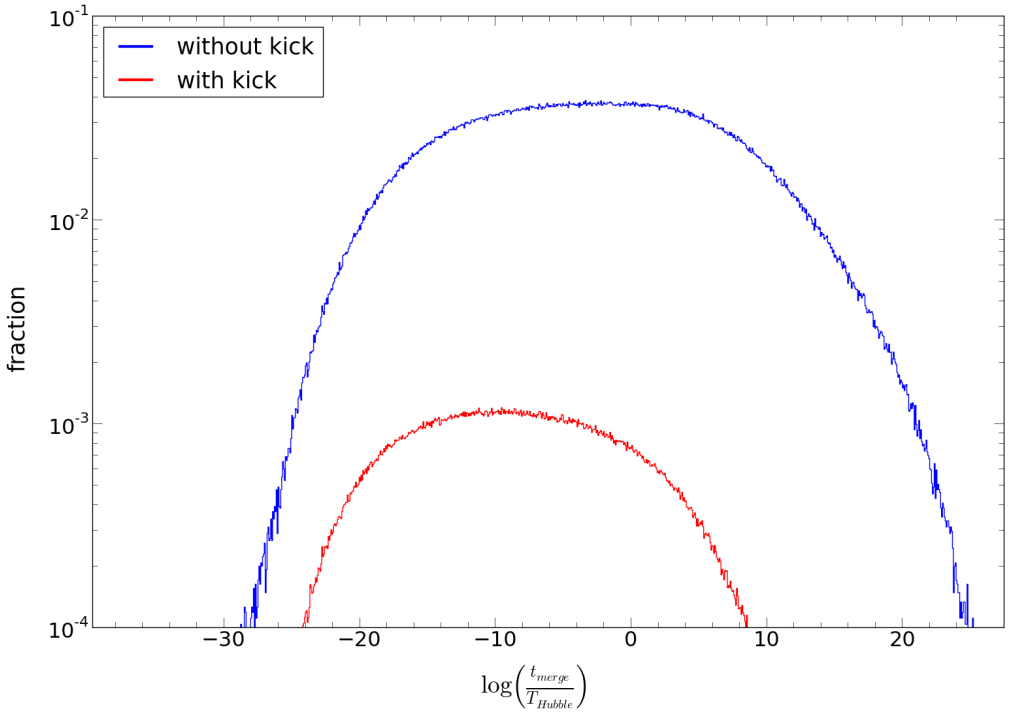

Figure 5.6: Similar plot as Fig. 5.5 but now for simulation 2. 63% of the systems become unbound by the kick.

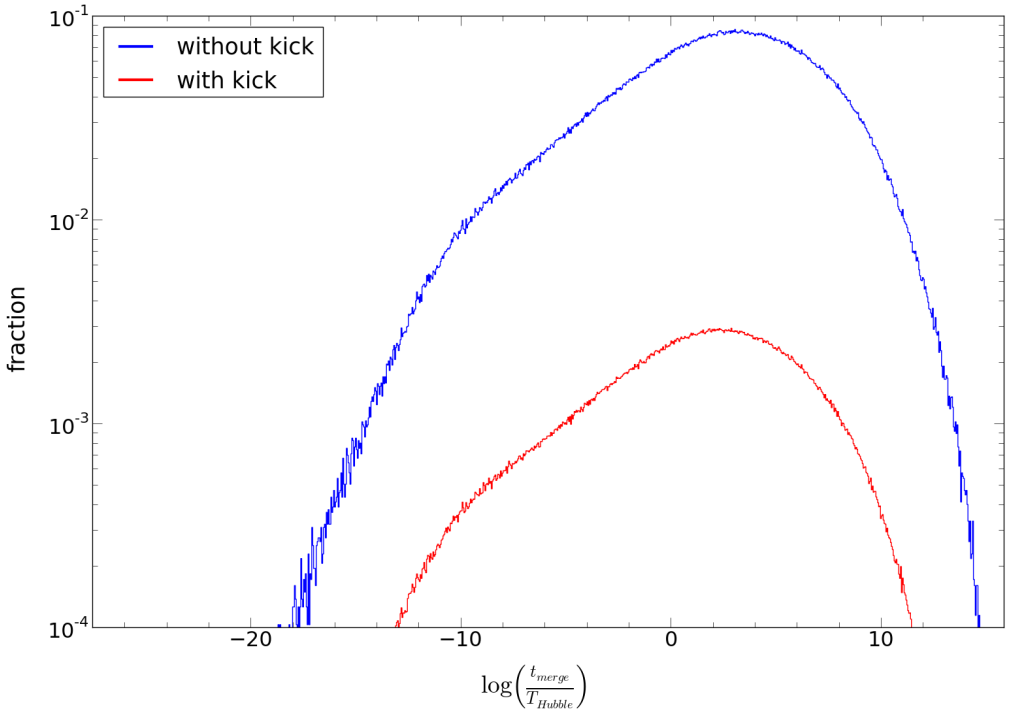

Figure 5.7: Similar plot as Fig. 5.5 but now for simulation 3. 23% of the systems become unbound by the kick.

5.2.2.2 Simulation 2

In Fig. 5.6 the distributions resulting from simulation 2 can be found. Again the blue line is the distribution of the merger times without a kick and the red line is the distribution with velocity kick. The kick causes 63% of the systems to become unbound. We find the same behavior as in simulation 1: due to the kick the distribution shifts to shorter times and narrows. If we compare the distributions of the merger times with no kick resulting from simulation 1 and 2, we see that taking another distribution for the semi-major axes makes a big difference.

5.2.2.3 Simulation 3

In Fig. 5.7 one can find the distributions resulting from simulation 3. The kick causes 23% of the systems to become unbound. We find again the same behavior as in simulation 1. By the kick the average merger time shifts to the left, this is different from what we found for the system in the beginning of this section. Thus, it is possible that for certain systems the average merger time increases due to the kick, but in general the merger time shifts to smaller values.

5.3 Influence of the Kozai Effect on the Velocity Kick

Consider the case in which we have a hierarchical triple in which the merger of the inner binary is accelerated by the Kozai mechanism and the merger time of the remnant of this merger with the tertiary component is decreased by the velocity kick. We want to know what the influence is of the Kozai mechanism on the merger time of the outer binary. First, in our treatment of the Kozai mechanism, we average over l_2, so we assume that this value is random when the inner binary merges. As we discussed at the beginning of this chapter, a_2 and e_2 can be considered constant during the time before the merger of the inner binary. Hence, Kozai can only effect the merger time of the outer binary via the final value of g_2 and $i_{\rm tot}$. In Fig. 5.8a we plotted the final g_2 with respect to the initial g_2 of the systems that we used to find the correction factor in the quadrupole case and to make the plots in the octupole case (Sec. 4.2.7). We find that Fig. 5.8a does not demonstrate a correlation between the initial and final g_2. In Fig. 5.8b we did the same, but now for the final $i_{\rm tot}$ with respect to the initial $i_{\rm tot}$. We find that for prograde orbits the final $i_{\rm tot}$ is smaller than the initial value and for retrogade orbits the final $i_{\rm tot}$ is larger than the initial $i_{\rm tot}$.

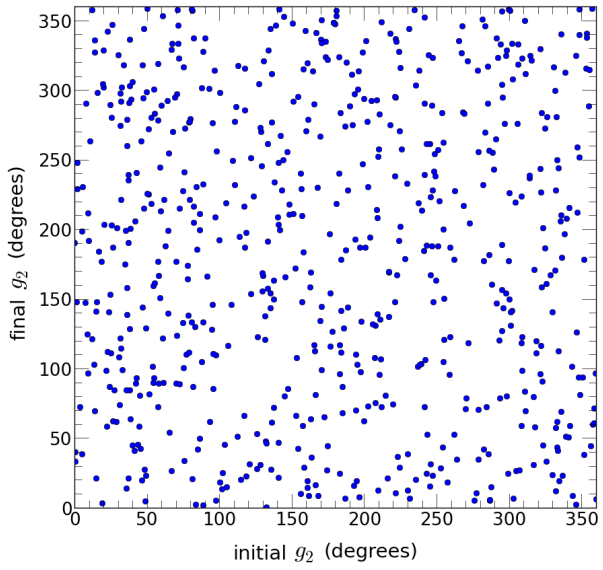

(a) Final g_2 with respect to the initial g_2 of the systems simulated for the quadrupole and octupole case.

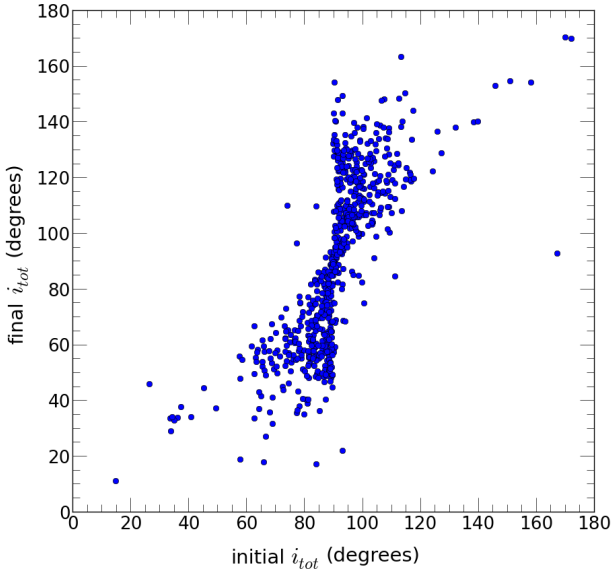

(b) Final $i_{\rm tot}$ with respect to the initial $i_{\rm tot}$ of the systems simulated in the quadrupole and octupole case.

Figure 5.8

Thus, the Kozai effect transforms a certain initial distribution of $i_{\rm tot}$ such that the distribution of $\cos(i_{\rm tot})$ shifts to larger values. This means that the component of the recoil velocity perpendicular to the orbital plane of the outer binary becomes smaller such that less energy is lost in changing the orbital plane and more energy goes into changing the value of the eccentricity and semi-major axis. Thus, due to the Kozai effect, the standard deviation of the distribution of the merger times becomes larger.

Chapter 6

Discussion

In this chapter we discuss the assumptions we made and the possibilities for future work.

6.1 Assumptions

We have made a lot of assumptions in this thesis, some of which we already discussed such as the averaging over the mean anomalies in deriving the secular Hamiltonian.

In Section 5 on the influence of the velocity kick on the merger time of the outer binary, we assumed the kick to be instantaneous. This is a huge oversimplification, as can be found in e.g. Favata et al. (2004): the kick lasts for a finite amount of time and the recoil velocity changes direction during this time. Thus, the calculation of the new orbit becomes much more difficult: at every infinitesimal time step the new orbit should be calculated until the inner binary merges. There are no analytic expressions for the magnitude of the recoil velocity as a function of time, thus it is impossible to calculate the new orbit analytically. It is possible to do this numerically, see for instance Favata et al. (2004); they did it for a binary in which one of the masses had a non-zero spin, but similar calculations can be done for the situation with 2 black holes with no spin.

The kick and other relativistic processes influence the evolution of the triple black hole system, just before the merger. Since the merger has a relatively small timescale compared to the timescale of the total evolution, it was correct to neglect these effects in the integration of the equations of motion of the triple black hole system.

We also made assumptions on the distributions of the kick velocity and the initial parameters of the resulting binary after the inner binary merged. We did three different simulations with different distributions for these parameters. We found the same general behavior in these simulations: the distribution of merger times as result of the kick narrows and shifts to smaller times. There was only a large difference between simulation 1 and 2, and simulation 3 in the fraction of systems that became unbound. This was caused by the large recoil velocities that could be reached in simulation 1 and 2 with respect to simulation 3. That the general behavior was the same suggests that also the 'real' distribution will be of this form and the fraction of systems that become unbound strongly depends on the recoil velocities that can be reached.

6.2 Future Work

During the integration of the equations of motion, we encountered many problems with convergence and snapshot time steps that were too large. We made sure that all systems which had a merger time of the inner binary that deviated more than a factor 2.5 in the quadrupole case and a factor 10 in the octupole case from the estimated value, were integrated correctly. But with more time, we would check the other systems. We do not expect that this will result in other correction factors, because we found in the systems we checked, that the closer their merger time is to the estimated value, the more systems were integrated correctly.

It would also be nice to obtain criteria for the parameters of the triple black holes in which the secular theory is valid. For specific systems comparisons between N-body integration and integration of the secular equations of motion have been made which showed that the secular theory was very good (e.g. Blaes et al. (2002); Naoz et al. (2012)), but this was not done for the whole evolution of the triple. Seto (2013) showed that it is possible that with the secular theory the maximum eccentricity reached in the oscillations can be artificially blocked by the back-reaction of the emission of gravitational waves. Due to this effect the merger time found with secular theory

it too large. Seto suggested to not average over the mean anomaly of the outer orbit such that the influence of the positions of the inner binary and tertiary on the eccentricity evolution would become clear.

In this thesis we found that the octupole term is anti-symmetric under interchanging the inner two masses. This indicates that the secular theory is not valid for triples in which one of the inner masses is much larger than the other mass even if the triple is dynamically stable. It would be nice to find the origin of this anti-symmetry.

In this work we only considered Schwarzschild black holes. Since as far as we know spin has not been considered in previous research it would be interesting to include spin in future work.

Future work can also address the influence of a non-instantaneous kick on the merger time of the outer binary. This will probably result in different distributions of the merger time than we found.

Chapter 7

Conclusion

In this thesis we considered the merger timescales of hierarchical triple black hole systems and we examined the possibility that all three black holes merge on a small timescale with respect to the Hubble time. We found a formula that approximated the merger time of the inner binary in a triple and used this formula to find the influence of the initial conditions of the triple on the merger time of the inner binary. We found that the merger time of the inner binary can be strongly decreased due to the influence of the tertiary if the inclination is close enough to 90^o, the semi-major axis of the outer orbit is small enough and the mass of the tertiary is large enough. We also derived a criterion for the influence of the Kozai effect.

We examined the influence of the kick, that the inner binary receives during the merger, on the merger time of the outer binary. We derived an approximation for this merger time. Also distributions of the merger time were created assuming distributions of the initial parameters of the outer binary and the kick. For a specific system we made distributions for different recoil velocities and assuming the direction of the kick to be random. It was found that the kick broadens the distribution of merger times for a specific system; dependent on the position of the inner binary in the outer orbit and on the direction of the kick, the merger time is increased or decreased. It is possible to obtain every merger time, smaller than the merger time without the kick, if the kick velocity is large enough. In the simulations where we averaged over all initial parameters, we found that the distributions of merger times with kick were narrowed and shifted to smaller times with respect to the distributions without the kick.

We thus conclude that it is possible for the black holes in a hierarchical triple black hole system to all merge on a very small timescale, but that we need the distribution of the initial parameters to calculate the fraction of systems for which this happens.

Acknowledgments I would like to thank Daniel Caputo and Simon Portegies Zwart for their supervision in this project. Especially Daniel has taught me a lot: from improvements on my programming style (which was very bad) to information about the scientific world. I would also like to thank Adrian Hamers that I could use the code he developed for the simulation of triple systems, and for the valuable advise he gave during this project. Finally, I would like to thank Gerard Barkema for being my supervisor in Utrecht.

Bibliography

S. J. Aarseth and R. A. Mardling. The Formation and Evolution of Multiple Star Systems. In P. Podsiadlowski, S. Rappaport, A. R. King, F. D'Antona, and L. Burderi, editors, *Evolution of Binary and Multiple Star Systems*, volume 229 of *Astronomical Society of the Pacific Conference Series*, page 77, 2001.

M. C. Begelman, R. D. Blandford, and M. J. Rees. Massive black hole binaries in active galactic nuclei. *Nature*, 287:307–309, September 1980. doi: 10.1038/287307a0.

J. D. Bekenstein. Gravitational-Radiation Recoil and Runaway Black Holes. *Astrophysical Journal*, 183:657–664, July 1973. doi: 10.1086/152255.

K. Belczynski, A. Sadowski, and F. A. Rasio. A Comprehensive Study of Young Black Hole Populations. *Astrophysical Journal*, 611:1068–1079, August 2004. doi: 10.1086/422191.

O. Blaes, M. H. Lee, and A. Socrates. The Kozai Mechanism and the Evolution of Binary Supermassive Black Holes. *Astrophysical Journal*, 578:775–786, October 2002. doi: 10.1086/342655.

D. Brouwer. Solution of the problem of artificial satellite theory without drag. *Astrophysical Journal*, 64:378, November 1959. doi: 10.1086/107958.

B. W. Carroll and D. A. Ostlie. *An introduction to modern astrophysics and cosmology*. July 2006.

S. Chandrasekhar. *Principles of stellar dynamics*. 1942.

G.E.O. Ciacaglia. *Notes on Von Zeipel's Method*. Goddard Space Flight Center, 1964.

M. Favata, S. A. Hughes, and D. E. Holz. How Black Holes Get Their Kicks: Gravitational Radiation Recoil Revisited. *Astrophysical Journal*, 607:L5–L8, May 2004. doi: 10.1086/421552.

E. B. Ford, B. Kozinsky, and F. A. Rasio. Secular Evolution of Hierarchical Triple Star Systems. *Astrophysical Journal*, 535:385–401, May 2000. doi: 10.1086/308815.

A. S. Hamers. The evolution of coeval stellar hierarchical triple systems, 2012.

R. S. Harrington. *The Dynamical Evolution of Triple-Star Systems*. PhD thesis, THE UNIVERSITY OF TEXAS AT AUSTIN., 1968.

M. Holman, J. Touma, and S. Tremaine. Chaotic variations in the eccentricity of the planet orbiting 16 Cygni B. *Nature*, 386:254–256, March 1997. doi: 10.1038/386254a0.

Y. Kozai. Secular perturbations of asteroids with high inclination and eccentricity. *Astrophysical Journal*, 67:591, November 1962. doi: 10.1086/108790.

C. O. Lousto, M. Campanelli, Y. Zlochower, and H. Nakano. Remnant masses, spins and recoils from the merger of generic black hole binaries. *Classical and Quantum Gravity*, 27(11):114006, June 2010. doi: 10.1088/0264-9381/27/11/114006.

M. C. Miller and D. P. Hamilton. Four-Body Effects in Globular Cluster Black Hole Coalescence. *Astrophysical Journal*, 576:894–898, September 2002. doi: 10.1086/341788.

S. Naoz, W. M. Farr, Y. Lithwick, F. A. Rasio, and J. Teyssandier. Secular Dynamics in Hierarchical Three-Body Systems. *ArXiv e-prints*, July 2011.

S. Naoz, B. Kocsis, A. Loeb, and N. Yunes. Resonant Post-Newtonian Eccentricity Excitation in Hierarchical Three-body Systems. *ArXiv e-prints*, June 2012.

R. Penrose. Gravitational Collapse and Space-Time Singularities. *Physical Review Letters*, 14:57–59, January 1965. doi: 10.1103/PhysRevLett.14.57.

P. C. Peters. Gravitational radiation and the motion of two point masses. *Phys. Rev.*, 136:B1224–B1232, Nov 1964. doi: 10.1103/PhysRev.136.B1224. URL `http://link.aps.org/doi/10.1103/PhysRev.136.B1224`.

S. Portegies Zwart, S. McMillan, S. Harfst, D. Groen, M. Fujii, B. Ó. Nualláin, E. Glebbeek, D. Heggie, J. Lombardi, P. Hut, V. Angelou, S. Banerjee, H. Belkus, T. Fragos, J. Fregeau, E. Gaburov, R. Izzard, M. Jurić, S. Justham, A. Sottoriva, P. Teuben, J. van Bever, O. Yaron, and M. Zemp. A multiphysics and multiscale software environment for modeling astrophysical systems. *New Astronomy*, 14:369–378, May 2009. doi: 10.1016/j.newast.2008.10.006.

S. Portegies Zwart, S. L. W. McMillan, E. van Elteren, I. Pelupessy, and N. de Vries. Multi-physics simulations using a hierarchical interchangeable software interface. *Computer Physics Communications*, 183:456–468, March 2013. doi: 10.1016/j.cpc.2012.09.024.

D. Richstone, E. A. Ajhar, R. Bender, G. Bower, A. Dressler, S. M. Faber, A. V. Filippenko, K. Gebhardt, R. Green, L. C. Ho, J. Kormendy, T. R. Lauer, J. Magorrian, and S. Tremaine. Supermassive black holes and the evolution of galaxies. *Nature*, 395:A14, October 1998.

G. Schäfer. Three-body hamiltonian in general relativity. *Physics Letters A*, 123:336–339, August 1987. doi: 10.1016/0375-9601(87)90389-6.

N. Seto. Highly Eccentric Kozai Mechanism and GW Observation for Neutron Star Binaries. *ArXiv e-prints*, April 2013.

T. A. Thompson. Accelerating Compact Object Mergers in Triple Systems with the Kozai Resonance: A Mechanism for "Prompt" Type Ia Supernovae, Gamma-Ray Bursts, and Other Exotica. *Astrophysical Journal*, 741:82, November 2011. doi: 10.1088/0004-637X/741/2/82.

M. Valtonen and H. Karttunen. *The Three-Body Problem*. March 2006.

L. Wen. On the Eccentricity Distribution of Coalescing Black Hole Binaries Driven by the Kozai Mechanism in Globular Clusters. *Astrophysical Journal*, 598:419–430, November 2003. doi: 10.1086/378794.

Appendices

Appendix A

Derivation Octupole Term Averaged over l_1

In this section we will derive Eq. 2.96. We start from Eqs. 2.92 and 2.95 and substitute the relations 2.85. This gives

$$\begin{aligned}
\mathcal{H}_{\rm oct}(\mathbf{q}',\mathbf{p}')\epsilon^3 &= \frac{1}{2\pi}\int_0^{2\pi}\frac{16}{15}C_{\rm oct}\left(\frac{r_1}{a_1}\right)^3\Big[10A_1^3-6A_1+\frac{1}{2}\Big(15A_1A_2^2-5A_1^3\Big)\Big]e_2dl_1\\
&= \frac{4e_2}{\pi}C_{\rm oct}\int_0^{2\pi}\left(\frac{r_1}{a_1}\right)^3\Big[\Big(B_1\cos(f_1)+B_2\sin(f_1)\Big)^3-\frac{4}{5}\Big(B_1\cos(f_1)+B_2\sin(f_1)\Big)\\
&\quad+\Big(B_1\cos(f_1)+B_2\sin(f_1)\Big)\Big(B_3\cos(f_1)+B_4\sin(f_1)\Big)^2\Big]dl_1\\
&= \frac{4e_2}{\pi}C_{\rm oct}\int_0^{2\pi}\left(\frac{r_1}{a_1}\right)^3\Big[\Big(B_1^3+B_1B_3^2\Big)\cos^3(f_1)+\Big(3B_1^2B_2+2B_1B_3B_4+B_2B_3^2\Big)\cos^2(f_1)\sin(f_1)\\
&\quad+\Big(3B_1B_2^2+B_1B_4^2+2B_2B_3B_4\Big)\cos(f_1)\sin^2(f_1)+\Big(B_2^3+B_2B_4^2\Big)\sin^3(f_1)\\
&\quad-\frac{4}{5}B_1\cos(f_1)-\frac{4}{5}B_2\sin(f_1)\Big]dl_1\\
&= \frac{4e_2}{\pi}C_{\rm oct}\int_0^{2\pi}\left(\frac{r_1}{a_1}\right)^3\Big[C_1\cos^3(f_1)+C_2\cos^2(f_1)\sin(f_1)+C_3\cos(f_1)\sin^2(f_1)\\
&\quad+C_4\sin^3(f_1)-\frac{4}{5}B_1\cos(f_1)-\frac{4}{5}B_2\sin(f_1)\Big]dl_1,
\end{aligned}\tag{A.1}$$

where

$$\begin{aligned}
C_1 &= B_1^3+B_1B_3^2;\\
C_2 &= 3B_1^2B_2+2B_1B_3B_4+B_2B_3^2;\\
C_3 &= 3B_1B_2^2+B_1B_4^2+2B_2B_3B_4;\\
C_4 &= B_2^3+B_2B_4^2.
\end{aligned}\tag{A.2}$$

Transforming the integral to the eccentric anomaly (using Eq. 2.30 as jacobian) and applying the integrals 2.80 and 2.81 we find that

$$\begin{aligned}
\mathcal{H}_{\rm oct}(\mathbf{q}',\mathbf{p}')\epsilon^3 &= \frac{4e_2}{\pi}C_{\rm oct}\int_0^{2\pi}\big(1-e_1\cos(E_1)\big)\Big[C_1\Big(\cos(E_1)-e_1\Big)^3+C_2\Big(\cos(E_1)-e_1\Big)^2\sin(E_1)\sqrt{1-e_1^2}\\
&\quad +C_3\Big(\cos(E_1)-e_1\Big)\sin^2(E_1)(1-e_1^2)+C_4\sin^3(E_1)(1-e_1^2)^{3/2}\\
&\quad -\Big(1-e_1\cos(E_1)\Big)^2\Big(\frac{4}{5}B_1(\cos(E_1)-e_1)+\frac{4}{5}B_2\sin(E_1)\sqrt{1-e_1^2}\Big)\Big]dE_1\\
&= \frac{4e_2}{\pi}C_{\rm oct}\int_0^{2\pi}\Big[-e_1C_1\cos^4(E_1)-C_1e_1^3-3e_1C_1\cos^2(E_1)-3e_1^3C_1\cos^2(E_1)+C_3\Big(1-e_1^2\Big)\Big(-e_1\cos^2(E_1)\\
&\quad -e_1\Big)\sin^2(E_1)+\frac{4}{5}B_1\cos(E_1)\Big(3e_1\cos(E_1)+e_1^3\cos^3(E_1)\Big)+\frac{4}{5}B_1e_1\Big(1+3e_1^2\cos^2(E_1)\Big)\Big]dE_1\\
&= \frac{4e_2}{\pi}C_{\rm oct}\Big[-\frac{3}{4}e_1C_1\pi-2\pi C_1e_1^3-3\pi e_1C_1-3\pi e_1^3C_1-\frac{5}{4}\pi C_3e_1(1-e_1^2)\\
&\quad +\frac{12}{5}B_1e_1\pi+\frac{3}{5}B_1e_1^3\pi+\frac{8}{5}\pi B_1e_1+\frac{12}{5}B_1e_1^3\pi\Big]\\
&= e_2C_{\rm oct}\Big[-15e_1C_1-20C_1e_1^3-5C_3e_1(1-e_1^2)+12B_1e_1^3+16B_1e_1\Big]. \qquad (A.3)
\end{aligned}$$

If we substitute C_1 and C_3 we find that

$$\begin{aligned}
\mathcal{H}_{\rm oct}(\mathbf{q}',\mathbf{p}')\epsilon^3 &= e_2C_{\rm oct}\Big[\Big(-15e_1-20e_1^3\Big)\Big(B_1^3+B_1B_3^2\Big)-5\Big(3B_1B_2^2+B_1B_4^2+2B_2B_3B_4\Big)e_1(1-e_1^2)\\
&\quad +12B_1e_1^3+16B_1e_1\Big]\\
&= 5e_1e_2C_{\rm oct}\Big[\Big((-3-4e_1^2)(B_1^2+B_3^2)-(1-e_1^2)(3B_2^2+B_4^2)\Big)B_1 \qquad (A.4)\\
&\quad -2B_2B_3B_4(1-e_1^2)+\frac{12}{5}B_1e_1^2+\frac{16}{5}B_1\Big].
\end{aligned}$$

The next step is to calculate the constants. We will use the trigonometric relations from Sec. 2.2. First of all, notice that $B_2B_3 = B_1B_4 - \cos(i_{\rm tot})$ such that $B_2B_3B_4 = B_4^2B_1 - \cos(i_{\rm tot})B_4$, hence,

$$\begin{aligned}
\mathcal{H}_{\rm oct}(\mathbf{q}',\mathbf{p}')\epsilon^3 &= 5e_1e_2C_{\rm oct}\Big[\Big((-3-4e_1^2)(B_1^2+B_3^2)-(1-e_1^2)(3B_2^2+B_4^2)\Big)B_1\\
&\quad -2(1-e_1^2)\Big(B_4^2B_1-\cos(i_{\rm tot})B_4\Big)+\frac{12}{5}B_1e_1^2+\frac{16}{5}B_1\Big]\\
&= 5e_1e_2C_{\rm oct}\Big[\Big((-3-4e_1^2)(B_1^2+B_3^2)-3(1-e_1^2)(B_2^2+B_4^2) \qquad (A.5)\\
&\quad +\frac{12}{5}e_1^2+\frac{16}{5}\Big)B_1+2(1-e_1^2)\cos(i_{\rm tot})B_4\Big].
\end{aligned}$$

Then using Eqs. 2.85:

$$\begin{aligned}
B_1^2+B_3^2 &= \Big(-\cos(g_1)\cos(g_2)-\sin(g_1)\sin(g_2)\cos(i_{\rm tot})\Big)^2+\Big(\cos(g_1)\sin(g_2)-\sin(g_1)\cos(g_2)\cos(i_{\rm tot})\Big)^2\\
&= \cos^2(g_1)+\sin^2(g_1)\cos^2(i_{\rm tot})\\
&= 1-\sin^2(g_1)\sin^2(i_{\rm tot}); \qquad (A.6)\\
B_2^2+B_4^2 &= \Big(\sin(g_1)\cos(g_2)-\cos(g_1)\sin(g_2)\cos(i_{\rm tot})\Big)^2+\Big(-\sin(g_1)\sin(g_2)-\cos(g_1)\cos(g_2)\cos(i_{\rm tot})\Big)^2\\
&= \sin^2(g_1)+\cos^2(g_1)\cos^2(i_{\rm tot})\\
&= 1-\cos^2(g_1)\sin^2(i_{\rm tot}). \qquad (A.7)
\end{aligned}$$

We collect the terms in Eq. A.5 with $\sin^2(i_{\rm tot})B_1$ as a factor:

$$
\begin{aligned}
& (-3-4e_1^2)\cdot -\sin^2(g_1) - 3(1-e_1^2)\cdot -\cos^2(g_1) \\
= \; & -(-3-4e_1^2)\sin^2(g_1) + (1-e_1^2)\cos^2(g_1) - 2(1-e_1^2)\sin^2(g_1) + 2(1-e_1^2) \\
= \; & 1 + 6e_1^2\sin^2(g_1) - e_1^2\cos^2(g_1) + 2(1-e_1^2) \\
= \; & e_1^2\Big[5\big(\frac{1}{2} - \frac{1}{2}\cos(2g_1)\big) - \cos(2g_1)\Big] + 1 + 2(1-e_1^2) \\
= \; & \frac{1}{2}B + 2(1-e_1^2), \qquad \text{(A.8)}
\end{aligned}
$$

where

$$
B = 2 + 5e_1^2 - 7e_1^2\cos(2g_1). \qquad \text{(A.9)}
$$

Finally, we collect all the remaining terms with B_1 as a factor:

$$
\begin{aligned}
& (-3-4e_1^2) - 3(1-e_1^2) + \frac{12}{5}e_1^2 + \frac{16}{5} \\
= & \frac{7}{5}e_1^2 - \frac{14}{5}. \qquad \text{(A.10)}
\end{aligned}
$$

Using the expressions found above, we find that

$$
\begin{aligned}
\mathcal{H}_{\rm oct}(\mathbf{q}',\mathbf{p}')\epsilon^3 \; &= \; 5e_1e_2C_{\rm oct}\Big[\Big(\frac{7}{5}e_1^2 - \frac{14}{5} + \big(\frac{1}{2}B + 2(1-e_1^2)\big)\sin^2(i_{\rm tot})\Big)B_1 + 2(1-e_1^2)\cos(i_{\rm tot})B_4\Big] \\
&= \; e_1e_2C_{\rm oct}\Big[\Big(7e_1^2 - 14 + \big(\frac{5}{2}B + 10(1-e_1^2)\big)\sin^2(i_{\rm tot})\Big)B_1 + 10(1-e_1^2)\cos(i_{\rm tot})B_4\Big]. \qquad \text{(A.11)}
\end{aligned}
$$

We then calculate:

$$
\begin{aligned}
& 10(1-e_1^2)\sin^2(i_{\rm tot})B_1 + 10(1-e_1^2)\cos(i_{\rm tot})B_4 \\
= \; & 10(1-e_1^2)\sin^2(i_{\rm tot})\Big(-\cos(g_1)\cos(g_2) - \sin(g_1)\sin(g_2)\cos(i_{\rm tot})\Big) \\
& +10(1-e_1^2)\cos(i_{\rm tot})\Big(-\sin(g_1)\sin(g_2) - \cos(g_1)\cos(g_2)\cos(i_{\rm tot})\Big) \\
= \; & -10(1-e_1^2)\sin(g_1)\sin(g_2)\cos(i_{\rm tot})\sin^2(i_{\rm tot}) - 10(1-e_1^2)\sin^2(i_{\rm tot})\cos(g_1)\cos(g_2) \\
& -10(1-e_1^2)\sin(g_1)\sin(g_2)\cos(i_{\rm tot}) - 10(1-e_1^2)\cos(g_1)\cos(g_2)\cos^2(i_{\rm tot}) \\
= \; & -10(1-e_1^2)\sin(g_1)\sin(g_2)\cos(i_{\rm tot})\sin^2(i_{\rm tot}) - 10(1-e_1^2)\cos(g_1)\cos(g_2) \\
& -10(1-e_1^2)\sin(g_1)\sin(g_2)\cos(i_{\rm tot}) \\
= \; & -10(1-e_1^2)\sin(g_1)\sin(g_2)\cos(i_{\rm tot})\sin^2(i_{\rm tot}) + 10(1-e_1^2)B_1. \qquad \text{(A.12)}
\end{aligned}
$$

If we further define:

$$
A = -3e_1^2 - 4 + \frac{5}{2}B\sin^2(i_{\rm tot}), \qquad \text{(A.13)}
$$

we find that

$$
\mathcal{H}_{\rm oct}(\mathbf{q}',\mathbf{p}')\epsilon^3 \; = \; e_1e_2C_{\rm oct}\Big[AB_1 - 10(1-e_1^2)\sin(g_1)\sin(g_2)\cos(i_{\rm tot})\sin^2(i_{\rm tot})\Big] \qquad \text{(A.14)}
$$

and this is Eq. (2.96).

Appendix B

Octupole Equations of Motion

We will now do the same process as we did in Sec. 2.6, but now for the octupole part of the equations of motion. We again have that

$$\dot{g}_{1,\mathrm{oct}} = \frac{\partial \mathcal{H}_{\mathrm{oct}}}{\partial G_1} = \frac{\partial \mathcal{H}_{\mathrm{oct}}}{\partial e_1}\frac{\partial e_1}{\partial G_1} + \frac{\partial \mathcal{H}_{\mathrm{oct}}}{\partial i_{\mathrm{tot}}}\frac{\partial i_{\mathrm{tot}}}{\partial G_1}. \tag{B.1}$$

Using Eqs. 2.101, A.9, A.13 and A.14, one finds:

$$\begin{aligned}
\frac{\partial \mathcal{H}_{\mathrm{oct}}}{\partial e_1}\frac{\partial e_1}{\partial G_1} &= \Big\{ e_2 C_{\mathrm{oct}} \Big[AB_1 - 10(1-e_1^2)\sin(g_1)\sin(g_2)\cos(i_{\mathrm{tot}})\sin^2(i_{\mathrm{tot}}) \Big] + e_1 e_2 C_{\mathrm{oct}} \\
&\quad \times \Big[\Big(-6e_1 + \frac{5}{2}\cdot(10e_1 - 14e_1\cos(2g_1))\sin^2(i_{\mathrm{tot}}) \Big) B_1 + 20 e_1 \sin(g_1)\sin(g_2)\cos(i_{\mathrm{tot}})\sin^2(i_{\mathrm{tot}}) \Big] \Big\} \cdot \frac{e_1^2-1}{e_1 G_1} \\
&= \frac{e_1^2-1}{e_1 G_1} e_2 C_{\mathrm{oct}} \Big\{ AB_1 - 10(1-e_1^2)\sin(g_1)\sin(g_2)\cos(i_{\mathrm{tot}})\sin^2(i_{\mathrm{tot}}) + \Big[-6e_1^2 + 25e_1^2\sin^2(i_{\mathrm{tot}}) \\
&\quad -35e_1^2\cos(2g_1)\sin^2(i_{\mathrm{tot}}) \Big] B_1 + 20 e_1^2 \sin(g_1)\sin(g_2)\cos(i_{\mathrm{tot}})\sin^2(i_{\mathrm{tot}}) \Big\} \\
&= \frac{e_1^2-1}{e_1 G_1} e_2 C_{\mathrm{oct}} \Big\{ B_1 \Big[3A + 6e_1^2 + 8 - 5\left(2 + 5e_1^2 - 7e_1^2\cos(2g_1)\right)\sin^2(i_{\mathrm{tot}}) - 6e_1^2 + 25e_1^2\sin^2(i_{\mathrm{tot}}) \\
&\quad -35e_1^2\cos(2g_1)\sin^2(i_{\mathrm{tot}}) \Big] - 10(1-3e_1^2)\sin(g_1)\sin(g_2)\cos(i_{\mathrm{tot}})\sin^2(i_{\mathrm{tot}}) \Big\} \\
&= \frac{e_1^2-1}{e_1 G_1} e_2 C_{\mathrm{oct}} \Big\{ B_1 \Big[3A - 2 + 10\cos^2(i_{\mathrm{tot}}) \Big] - 10(1-3e_1^2)\sin(g_1)\sin(g_2)\cos(i_{\mathrm{tot}})\sin^2(i_{\mathrm{tot}}) \Big\}.
\end{aligned} \tag{B.2}$$

From Eq. 2.106 and the definition of B_1 in Eqs. 2.85, we obtain:

$$\begin{aligned}
\frac{\partial \mathcal{H}_{\mathrm{oct}}}{\partial i_{\mathrm{tot}}}\frac{\partial i_{\mathrm{tot}}}{\partial G_1} &= e_1 e_2 C_{\mathrm{oct}} \Big[5B\sin(i_{\mathrm{tot}})\cos(i_{\mathrm{tot}})B_1 + A\sin(g_1)\sin(g_2)\sin(i_{\mathrm{tot}}) - 20(1-e_1^2)\sin(g_1)\sin(g_2) \\
&\quad \times \cos^2(i_{\mathrm{tot}})\sin(i_{\mathrm{tot}}) + 10(1-e_1^2)\sin(g_1)\sin(g_2)\sin^3(i_{\mathrm{tot}}) \Big] \cdot \frac{1}{\sin(i_{\mathrm{tot}})}\left(\frac{1}{G_2} + \frac{\cos(i_{\mathrm{tot}})}{G_1}\right) \\
&= e_1 e_2 C_{\mathrm{oct}} \Big[5B\cos(i_{\mathrm{tot}})B_1 + A\sin(g_1)\sin(g_2) - 30(1-e_1^2)\sin(g_1)\sin(g_2)\cos^2(i_{\mathrm{tot}}) \\
&\quad + 10(1-e_1^2)\sin(g_1)\sin(g_2) \Big] \cdot \left(\frac{1}{G_2} + \frac{\cos(i_{\mathrm{tot}})}{G_1}\right) \\
&= e_1 e_2 C_{\mathrm{oct}} \Big\{ \sin(g_1)\sin(g_2) \Big[A + 10(1-e_1^2)(1-3\cos^2(i_{\mathrm{tot}})) \Big] + 5BB_1\cos(i_{\mathrm{tot}}) \Big\} \left(\frac{1}{G_2} + \frac{\cos(i_{\mathrm{tot}})}{G_1}\right).
\end{aligned} \tag{B.3}$$

Hence,

$$\begin{aligned}
\dot{g}_{1,\mathrm{oct}} &= -C_{\mathrm{oct}} e_2 \frac{1-e_1^2}{e_1 G_1} \Big\{ B_1 \Big[3A - 2 + 10\cos^2(i_{\mathrm{tot}}) \Big] - 10(1-3e_1^2)\sin(g_1)\sin(g_2)\cos(i_{\mathrm{tot}})\sin^2(i_{\mathrm{tot}}) \Big\} \\
&\quad + e_1 e_2 C_{\mathrm{oct}} \Big\{ \sin(g_1)\sin(g_2) \Big[A + 10\big(1-e_1^2\big)\big(1-3\cos^2(i_{\mathrm{tot}})\big) \Big] + 5BB_1\cos(i_{\mathrm{tot}}) \Big\} \cdot \left(\frac{1}{G_2} + \frac{\cos(i_{\mathrm{tot}})}{G_1}\right)
\end{aligned} \tag{B.4}$$

The octupole part of the argument of periastron of the outer binary is:

$$\dot{g}_{2,\mathrm{oct}} = \frac{\partial \mathcal{H}_{\mathrm{oct}}}{\partial G_2} = \frac{\partial \mathcal{H}_{\mathrm{oct}}}{\partial e_2}\frac{\partial e_2}{\partial G_2} + \frac{\partial \mathcal{H}_{\mathrm{oct}}}{\partial i_{\mathrm{tot}}}\frac{\partial i_{\mathrm{tot}}}{\partial G_2}. \tag{B.5}$$

Using Eqs. 2.101, A.9, A.13 and A.14, and the definition of $C_{\rm oct}$ in Eq. 2.100, we find that

$$\begin{aligned}\frac{\partial \mathcal{H}_{\rm oct}}{\partial e_2}\frac{\partial e_2}{\partial G_2} &= e_1\left(1+5\frac{e_2^2}{1-e_2^2}\right)C_{\rm oct}\Big[AB_1-10(1-e_1^2)\sin(g_1)\sin(g_2)\cos(i_{\rm tot})\sin^2(i_{\rm tot})\Big]\frac{e_2^2-1}{e_2G_2}\\ &= e_1\left(-\frac{1+4e_2^2}{e_2G_2}\right)C_{\rm oct}\Big[AB_1-10(1-e_1^2)\sin(g_1)\sin(g_2)\cos(i_{\rm tot})\sin^2(i_{\rm tot})\Big]. \qquad \text{(B.6)}\end{aligned}$$

From Eq. 2.106 (symmetry) we find that

$$\begin{aligned}\frac{\partial \mathcal{H}_{\rm oct}}{\partial i_{\rm tot}}\frac{\partial i_{\rm tot}}{\partial G_2} &= e_1e_2C_{\rm oct}\Big\{\sin(g_1)\sin(g_2)\Big[A+10\big(1-e_1^2\big)\big(1-3\cos^2(i_{\rm tot})\big)\Big] \qquad \text{(B.7)}\\ &\quad +5B\cos(i_{\rm tot})B_1\Big\}\left(\frac{1}{G_1}+\frac{\cos(i_{\rm tot})}{G_2}\right).\end{aligned}$$

Thus,

$$\begin{aligned}\dot{g}_{2,\rm oct} &= C_{\rm oct}e_1\left(-\frac{1+4e_2^2}{e_2G_2}\right)\Big[AB_1-10(1-e_1^2)\sin(g_1)\sin(g_2)\cos(i_{tot})\sin^2(i_{\rm tot})\Big] \qquad \text{(B.8)}\\ &\quad +e_1e_2C_{\rm oct}\Big\{\sin(g_1)\sin(g_2)\Big[A+10\big(1-e_1^2\big)\big(1-3\cos^2(i_{\rm tot})\big)\Big]+5BB_1\cos(i_{\rm tot})\Big\}\left(\frac{1}{G_1}+\frac{\cos(i_{\rm tot})}{G_2}\right).\end{aligned}$$

For $\dot{e}_{1,\rm oct}$ one finds the following equation (using Eq. 2.101):

$$\begin{aligned}\dot{e}_{1,\rm oct} &= \frac{1-e_1^2}{e_1G_1}\frac{\partial \mathcal{H}_{\rm oct}}{\partial g_1}\\ &= C_{\rm oct}e_2\frac{1-e_1^2}{G_1}\Big\{A\Big(\sin(g_1)\cos(g_2)-\cos(g_1)\sin(g_2)\cos(i_{\rm tot})\Big) \qquad \text{(B.9)}\\ &\quad +35B_1e_1^2\sin(2g_1)\sin^2(i_{\rm tot})-10(1-e_1^2)\cos(g_1)\sin(g_2)\cos(i_{\rm tot})\sin^2(i_{\rm tot})\Big\}.\end{aligned}$$

We find the following equation for $\dot{e}_{2,\rm oct}$:

$$\begin{aligned}\dot{e}_{2,\rm oct} &= \frac{1-e_2^2}{e_2G_2}\frac{\partial \mathcal{H}_{\rm oct}}{\partial g_2}\\ &= C_{\rm oct}e_1\frac{1-e_2^2}{G_2}\Big\{A\Big(\cos(g_1)\sin(g_2)-\sin(g_1)\cos(g_2)\cos(i_{\rm tot})\Big) \qquad \text{(B.10)}\\ &\quad -10(1-e_1^2)\sin(g_1)\cos(g_2)\cos(i_{\rm tot})\sin^2(i_{\rm tot})\Big\}.\end{aligned}$$